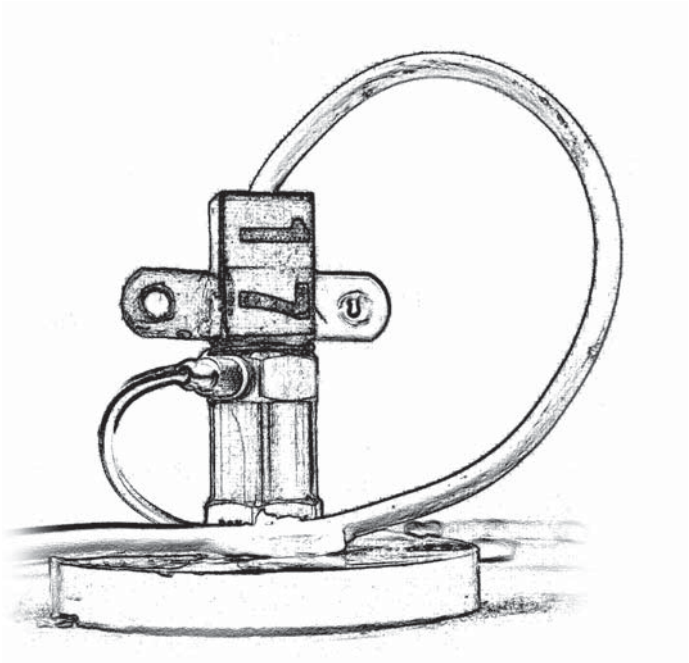

CONSTRUCTION AND IN-HOUSE CALIBRATION OF MEMS-BASED VIBRATION TRANSDUCERS

R. DARULA, A. SJÖSTRÖM, J. NEGREIRA and D. BARD

Engineering Acoustics

Measurement Report

DEPARTMENT OF CONSTRUCTION SCIENCES

DIVISION OF ENGINEERING ACOUSTICS

ISRN LUTVDG/TVBA--16/3131--SE (1-77) | ISSN 0281-8477

CONSTRUCTION AND IN-HOUSE CALIBRATION OF MEMS-BASED VIBRATION TRANSDUCERS

R. DARULA, A. SJÖSTRÖM, J. NEGREIRA and D. BARD

Online version available at: http://bit.ly/1WghuDr

Printed by Media-Tryck LU, Lund, Sweden, February 2016 *(Pl)*.

For information, address:

Div. of Engineering Acoustics, LTH, Lund University, Box 118, SE-221 00 Lund, Sweden.
Homepage: http://www.akustik.lth.se

Acknowledgements

The research reported on here was funded by the Silent Spaces project, a part of the EU program Interreg IV-A. The authors highly appreciate the financial support provided.

The authors would like to thank all people who helped to clarify the concepts of calibration or signal processing as such. Especially and firstly, we would like to thank Dr.Tom Sørensen from Bruel&Kjaer for his help, support and advices in tuning the methodology and for his help with the B&K PULSE system.

Special thanks as well to Jan Balle Larsen, GRUNDFOS, and Dr. George Juraj Stein for fruitful discussions on calibration procedures for piezo and MEMS devices as well as on signal processing in itself.

Last but not least, a word of thanks to all our project colleagues from the Department of Construction Sciences (Lund) and the Departments of Mechanical and Manufacturing Enginneering and Civil Engineering (Aalborg). It has been a pleasure to collaborate with all of you during the course of the Silent Spaces project.

Thanks to all!

The authors

Table of Contents

Nomenclature **iii**
Acronyms . . . iii

1 Preface **1**
1.1 Motivation . . . 1
1.2 Objective and method . . . 1
1.2.1 Outline . . . 1
1.2.2 Research limitations . . . 2
1.3 Ultimate aim . . . 2

2 Introduction **3**
2.1 Sensors and transducers . . . 3
2.2 Accelerometers . . . 3
2.2.1 Types of accelerometers . . . 3
2.2.2 Parameters of accelerometers . . . 5
2.2.3 Fixation of contact accelerometers . . . 6
2.2.4 Calibration of accelerometers . . . 6
2.2.5 MEMS calibrations methods . . . 9

3 MEMS accelerometers **11**
3.1 Introduction . . . 11
3.2 Description of sensors . . . 11
3.3 Construction . . . 12

4 Apparatus **15**
4.1 Apparatus used . . . 15

5 Calibration using the MTS machine **19**
5.1 MTS Measurements . . . 19
5.1.1 Equipment and measurement set-up . . . 19
5.1.2 Limitations . . . 20
5.2 Discussion on results . . . 20
5.3 Conclusions . . . 21

6 Pre-measurements at AAU **23**
6.1 Verification of the calibration procedure using a shaker . . . 23
6.2 Calibration of the reference accelerometer B&K 8305 . . . 23
6.3 Comparison of pre-amplifiers and calibrators . . . 25
6.3.1 Changing the accelerometer calibrator . . . 25
6.3.2 Comparison of the calibrators . . . 26
6.4 Conclusions . . . 27

7 Steady State Response Measurements **29**
7.1 Multi-buffer vs. Steady-State Response . . . 29
7.2 Tests of MEMS accelerometers . . . 30
7.2.1 Accelerometer type . . . 30
7.2.2 Measurement direction . . . 30
7.2.3 Type of fixation . . . 30
7.2.4 Amount of wax . . . 30

7.2.5 Fixation to reference accelerometer / fixing directly on shaker . . . 34
7.2.6 Relative position of the MEMS with respect to the reference one . . . 36
7.2.7 Influence of vibration amplitude . . . 37
7.3 Calibration of piezo accelerometers . . . 38
7.3.1 Accelerometer B&K 4374 to be calibrated using B&K 8305 as reference . . . 38
7.3.2 Accelerometer B&K 4371 calibrated with B&K 8305 and a mica washer . . . 39
7.3.3 Accelerometer B&K 4374 calibrated using B&K 4371 as reference . . . 40
7.4 Cable fixation . . . 41
7.4.1 Piezo accelerometer . . . 41
7.4.2 MEMS accelerometer . . . 41
7.5 Verification of shakers . . . 41
7.5.1 Shaker's location . . . 42
7.5.2 Shaker used . . . 42
7.6 Signal clipping . . . 43
7.7 Linearity of the MEMS transducer . . . 44
7.8 Reproducibility of measurements . . . 45
7.9 Steady-state response vs. Sine sweep excitation . . . 45
7.9.1 Sine sweep settings . . . 45
7.10 Conclusions . . . 47

8 Sine Sweep Measurements using a vibration controller 49
8.1 Sine sweep settings . . . 49
8.2 Sine sweep vs. single sine excitation . . . 50
8.3 Conclusions . . . 51

9 Sine sweep measurement at LU 53
9.1 Fixation of the shaker . . . 53
9.2 Sweep rate investigation . . . 54
9.3 Comparison of MEMS transducers . . . 56
9.4 MEMS position onto the reference accelerometer . . . 56
9.5 Capsule fixation onto the reference . . . 57
9.6 MEMS vs. piezo accelerometer . . . 57
9.7 Two channel recordings . . . 60
9.8 Conclusions . . . 60

10 Additional characterisations 61
10.1 Gain evaluation . . . 61
10.2 Tilting of the MEMS' chip using a rubber isolator . . . 62
10.2.1 Influence of tilting . . . 62
10.2.2 Using a rubber isolator . . . 64
10.2.3 Influence of beeswax layer . . . 64
10.3 Bandwidth settings by a capacitance value . . . 65
10.4 Sweep parameters . . . 67
10.5 Conclusions . . . 67

11 Conclusions 69
11.1 Guidelines for development of MEMS accelerometers . . . 69

Bibliography 72

Appendices

A Laboratory journals 73

B MATLAB GUI for data comparison 75
B.1 Features . . . 75
B.2 Restrictions . . . 76

Nomenclature

Acronyms

AAU Aalborg University.

B&K Bruel & Kjaer (company).

CCLD Constant Current Linear Drive.

CPB Constant Power Bandwidth.

DAQ Data Acquisition.

DMME Department of Mechanical and Manufacturing Engineering (at AAU).

FE Finite Element.

FFT Fast Fourier Transform.

FRF Freqeuency Response Function.

GUI Graphical User Interface.

LCC Leadless Chip Carrier.

LU Lund University.

MEMS Micro Electro Mechanical System.

MTS Material Testing Machine.

PCB Printed Circuit Board.

RMS Root Mean Square.

SSR Steady State Response.

1 Preface

The report presented here summarises the process of development of Micro Electro Mechanical Systems (MEMS) capacitive accelerometers, from mounting to calibration, to be employed for low frequency vibration testing. This project was carried out within the frame of the Silent Spaces project, a part of the EU program Interreg-IVA, and more specifically in conjunction between the project partners Lund University (LU) in Sweden and Aalborg University (AAU) in Denmark.

1.1 Motivation

Wooden multi-storey buildings have steadily increased their market share in Sweden since 1994, the year in which their construction was reintroduced after a century-old-ban (due to numerous urban fires during the 1800s) was lifted. Ever since, product development has been carried out based on engineers' experience and measurements performed in already existing buildings. Despite of the many advantages that the use of wood as construction material involves, namely sustainability, reduction of the material transportation costs, smaller size of the foundations needed due to wood's light weight, wood being abundant particularly in Sweden, etc. (Negreira, 2013), complaints among residents often arise due to low frequency noise and vibrations, even when those buildings fulfil the standards currently in force (ISO, 2013a,b). It is believed that the main reason for peoples' discontent in their apartments is low frequency sound and vibrations below 50 Hz. Analyses below 50 Hz are seldom performed as those frequencies are left outside the scope in the current standards (Ljunggren et al., 2014) and evaluations methods do not yet exist. It is desired, therefore, to develop low frequency numerical prediction tools so as to be able to foresee the vibroacoustic performance of such structures during their design phase, the latter entailing savings in terms of money and time for the industry, as one would avoid the construction of mock-ups and test buildings. Nevertheless, the variability of a natural material such as wood, the complexity of the junctions between structural parts involved and external factors such as workmanship, makes it difficult to accurately predict the behaviour of wood. Hence, a significant part of the research in the field currently aims at gaining knowledge of such types of structures, its enabling the development of numerical prediction tools (most often by means of finite element (FE) models). The calibration of the aforementioned vibroacoustic prediction tools is carried out using measurement data as calibration input for the models. In line with the latter, having numerous transducers facilitates the acquisition of data as well as improves the richness of it and hence the quality of the predictions.

1.2 Objective and method

A hindrance in having such an extensive measurement equipment with many transducers is the price of the apparatus involved. Thus, the idea of this project was to develop accelerometers from scratch, by buying MEMS capacitive sensors (i.e. the inner-chip), mount the components and perform the calibration ourselves.

1.2.1 Outline

In the report, a theoretical background about accelerometers as well calibration methods found in the literature is given first. Subsequently, the mounting of the accelerometers is described step by step (i.e. soldering of the inner-chip, casing and cabling). Finally, the calibration procedure is presented. Special attention is paid to the description of all the tests performed in order to keep track of all that was tested

and which approach leads to a more precise calibration. After discussion with Dr. Tom Sørensen from Bruel & Kjaer (Sørensen, T., 2011), the back-to-back calibration procedure using an electrodynamic shaker as a source of vibration controlled via feedback loop in order to ensure a constant excitation level, was chosen.

1.2.2 Research limitations

The calibration described in this report is not an accredited one, but rather an unofficial in-house calibration, without any calibration certificate provided. However, the methods employed involve the usage and comparison with a calibrated reference accelerometer, the precision obtained hence being more than sufficient for academic purposes as the ones dealt with in our research.

1.3 Ultimate aim

The ultimate aim of this report is to increase the accuracy and reliability of the measurements carried out using these MEMS capacitive accelerometers and eventually thus have calibration input of better quality for the low frequency vibroacoustic prediction tools that are to be developed.

The authors

2 Introduction

In this chapter, the aim is to provide a background to the topic dealt with in the report. More specifically, concepts about accelerometers, namely different types, their parameters, fixation methods and calibration procedures will be presented.

2.1 Sensors and transducers

According to (Bishop, 2002), a sensor can be defined as "a device, that when exposed to a physical phenomenon (temperature, displacement, force, etc.) produces a proportional output signal (electrical, mechanical, magnetic, etc.)", i.e. a device that responds to a change in a measurand[1]. In contrast, a transducer is "a device that converts one form of energy to another". In other words, a sensor detects a change in a physical quantity that varies due to some type of excitation, whereas a transducer is also capable (apart from the detection) of communicating the measurand, i.e. it has a signal conditioning involved as well. All in all, every transducer is also in itself (or has inside it) a sensor, but the opposite is not always true (cf. Fig. 2.1).

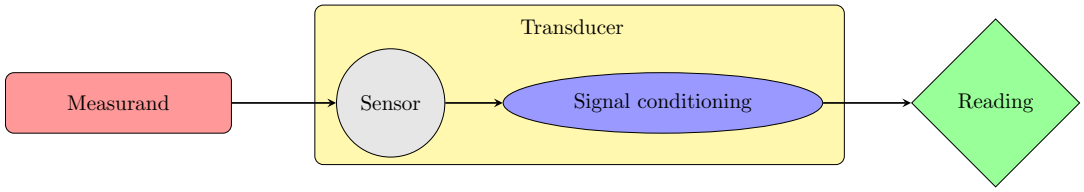

Fig. 2.1: Schematic drawing of a sensor and a transducer.

As stated in (Bishop, 2002), the sensors can be classified as passive or self-powered if the the power is provided by a sensed physical phenomenon (e.g. thermometer); or active, when external power is necessary for operation. Depending on the output signal, they can also be classified as analog, when the output signal is continuous; or digital when it is discretised. Likewise, according to (ISO, 1998), transducers can be classified as non-contact transducers, if they are located in a close vicinity of the structure to be measured (e.g. eddy-current, optical proximity); or contact, if mechanical contact between the transducer and the structure exists (e.g. piezoelectric, piezoresistive).

2.2 Accelerometers

The report presented here focuses in a special category of transducers: accelerometers, being defined as transducers which produce an output signal proportional to the acceleration sensed (Randall, 2011). More specifically, the report summarises the process of development of MEMS capacitive accelerometers, from mounting to calibration, to be employed for low frequency vibration testing.

2.2.1 Types of accelerometers

There are many types of accelerometers, the most common ones being the following (Negreira, 2013; Bishop, 2002):

[1] The physical phenomenon that is to be measured.

- **Capacitive:** a typical capacitive sensor (the MEMS accelerometers studied here are of this type) is composed of a movable proof mass provided with a plate (representing a capacitor) that is attached to a reference frame by a mechanical suspension system, as shown in Fig. 2.2a. The deflection of the suspended mass with respect to the suspension frame attached to the vibrating structure, causes a change of capacitance between the outer plates and the plates attached to the mass and thus in the output voltage, which is proportional to the sensed acceleration. In other words, the variation in the output signal is produced by sensing changes in capacitance when the geometry of the capacitor inside the sensor is changing due to the acceleration sensed (due either to the change of area of the electrodes, the distance between them or the permittivity of the material separating them).
- **Piezoelectric:** a piezoelectric accelerometer uses the piezoelectric effect of quartz or ceramic crystals to provide an electrical output which is proportional to the sensed acceleration. The piezoelectric effect produces a charge which is emitted by the crystal when it is subjected to a compressive force. A force applied to a quartz crystal lattice structure alters the alignment of the positive and the negative ions, which results in an accumulation of these charged ions on the opposing surfaces. These charged ions accumulate on an electrode that is ultimately conditioned by transistor microelectronics and designed to measure the acceleration. The piezoelectric crystal is normally bonded to a mass such that when the accelerometer is subjected to a force, the mass in question compresses the crystal, which produces an electric signal proportional to the acceleration; see Fig. 2.2b, (Negreira, 2013). Piezoelectric accelerometers can be used over a wide range of frequencies, showing an excellent linearity over a broad dynamic range. The measurements they provide are attainable with excellent accuracy for a large variety of environmental conditions. They require no power supply, are extremely durable since they contain no movable parts, are extremely compact and have a high sensitivity-to-mass ratio (Bruel&Kjaer, 1978). Their price is one of their main disadvantages, as they are much more expensive than MEMS accelerometers.

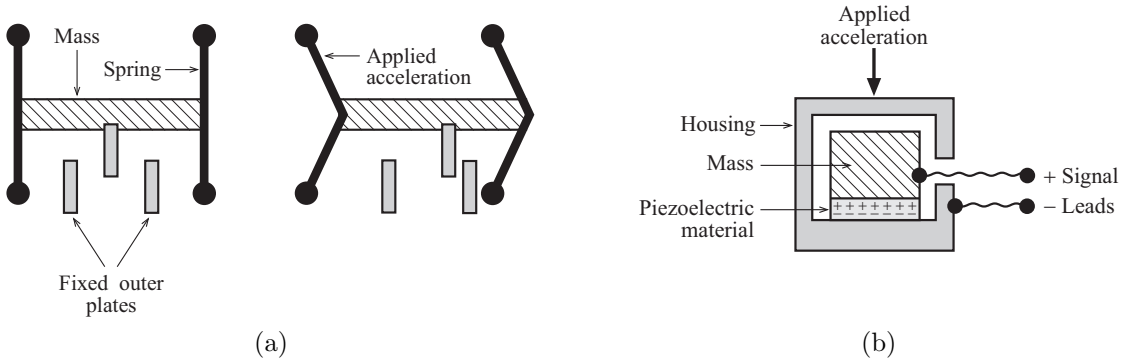

Fig. 2.2: Scheme of a MEMS accelerometer (a) and of piezoelectric accelerometer (b), (Negreira, 2013).

- **Piezoresistive:** also called strain gauge accelerometers. This type of accelerometers takes advantage of the resistance change of piezoresistive materials to covert mechanical strain to a DC output voltage. The resistors are normally configured into a Wheatstone bridge circuit, which provides a change in output voltage that is proportional to acceleration. They are often used for shock applications. They can sense accelerations down to 0 Hz; however, they are not very accurate for high frequencies.
- **Hall effect:** a magnet and a Hall effect sensor detecting changes in magnetic field values are placed in the seismic mass (proofmass) of the sensor. The output voltage sent by the Hall effect sensor is proportional to the acceleration the transducer is exposed to.
- **Heat transfer:** heat transfer accelerometers measure internal changes in heat transfer due to acceleration, and use thermoresistors to send out an electrical signal proportional to the acceleration detected.

Note that MEMS denotes the technology of very small devices, i.e. a technology that in its most general form can be defined as miniaturised mechanical and electro-mechanical elements (i.e., devices and structures) that are made using the techniques of microfabrication. Therefore, MEMS is not just associated to the capacitive accelerometers under investigation in this report, but also there can be MEMS piezoresistive accelerometers, for example, if this manufacturing technology is employed.

2.2.2 Parameters of accelerometers

The main parameters defining an accelerometer (and that could also be generalised for any type of transducer) are (Bishop, 2002; Bruel&Kjaer, 1978):

- **Sensitivity:** ratio of the accelerometer's electrical output to the mechanical input, expressed in terms of voltage per physical unit (e.g. $\mathrm{mV/ms^{-2}}$). In analog sensors, the sensitivity is given as the slope of the output and input signals. A special case (and also important in measurements) is the so-called transverse sensitivity, defined as the sensitivity to an acceleration applied at right angles to its main geometric axis.
- **Frequency response:** dependence of the charge or voltage sensitivity with frequency. It defines the useful frequency range with linear sensitivity. The upper frequency limit depends primarily upon the mounting resonance, whereas the bottom one is restricted mainly by the pre-amplifier used (Bruel&Kjaer, 1978). Accelerometers exposed to temperature variations will generate a low frequency response. Therefore, the pre-amplifiers can be set to have some cut-off frequency in the lower region to avoid it.
- **Phase response:** time delay between the mechanical input and the resulting electrical output. In general, this delay is not constant for all frequencies.
- **Transient response:** for shocks and transient vibrations. Two types can be distinguished:
  1. Zero shift: presence of phase non-linearities in the preamplifier, or accelerometers.
  2. Ringing: the transient contains high frequencies so that the resonance of the accelerometer is excited. It can be reduced by setting the mounting resonance to not less than 10/T, where T is the duration of the transient in seconds.
- **Resolution:** the smallest increment of input that can be reliably detected. In digitally operated sensors, the resolution is determined as the number of pulses per physical quantity. The analog sensors have, on the contrary, a resolution limit characterised by low-level electrical noise.
- **Weight:** in general, one could adhere to the following rule of thumb: the weight of the accelerometer should be at least ten times less than the effective weight of the vibration test specimen. A more precise relationship can also be calculated depending on the impedances and the so-called an added mass effect discussed in (Hopkins, 2007), according to:

$$v_m = v_a \frac{Z_{dp}}{Z_{dp} + i\omega m_{acc}}, \tag{2.1}$$

  with v_m and v_a being the measured and actual velocities respectively, Z_{dp} the driving point impedance of the structure and m_{acc} the mass of the transducer.
- **Dynamic range:** range over which the electrical output of the accelerometer is directly proportional to the acceleration at its base. The lower limit is a practical issue and is determined by the noise level of the measuring system. In general, the upper limit is higher with decreasing size of the accelerometer. The upper limit is of special interest for shock measurements.
- **Environmental characteristics:** the sensitivity of an accelerometer is influenced also by the environmental conditions, especially temperature, humidity, acoustic field, magnetic field or radiation. If measurements in severe conditions are to be performed, special accelerometers should be used.
- **Repeatability (reproducibility):** defined as the ability of the transducer to give identical outputs for the same input. The repeatability is influenced by e.g. electrical noise and hysteresis. To increase repeatability, averaging techniques or low-pass filtering can be used.
- **Linearity and accuracy:** ability to provide a direct (linear) relationship between the input and the output with minimal fluctuations. It is expressed as percentage of the full-scale.
- **Impedance:** ratio of the voltage and the current flow through the sensor. In general, a high input impedance is required to reduce current flowing from the source. As for output impedance, it is required to be low, as they behave as a source of current.
- **Eccentricity:** geometrical non-linearity.
- **Saturation:** defines the maximum output capability. When a sensor is saturated, its output remains constant even with increasing input signal.
- **Deadband:** a region of the input close to zero at which the output remains also zero. Once the input travels outside the deadband, then the output varies with the input accordingly. Occurs, for example, in thermostats or joysticks, so as to avoid small fluctuations.

2.2.3 Fixation of contact accelerometers

When performing measurements in general, and vibration measurements in particular, special attention must be paid to the way transducers are attached to the structure under investigation, as the results acquired could depend very much upon these fixations. An analysis prior to the measurements should be carried out to evaluate the most accurate possible way to affix the transducers onto the object to be measured. Typically, 9 types of fixations can be used (Bruel&Kjaer, 1982; ISO, 1998):

1. **Threaded stud:** the best fixation is to attach the accelerometer to the structure using a stud. It is recommended to use a thin layer of grease to increase the contact stiffness between both surfaces. It is necessary to make sure that the hole in the structure is perpendicular and that the contact surface is smooth. A drawback with this type of fixation is that the holes driven into the structure remain there after the measurements are performed, which is not always allowed depending on the object to be measured. Moreover and in particular for thin or fragile structures or materials, structural integrity could be affected when modifying the object to be measured by removing material and screwing studs into it.
2. **Beeswax:** to stick the accelerometer onto the structure, a thin layer of beeswax can also be used. Limitations of this type of attachment are its sensitivity to temperature (not feasible to use it for temperatures above 40°C), and to amplitude levels (when attaching them to clean surfaces, it can be used up to levels of about 100 m/s^2).
3. **Cement:** when drilling holes into the experimental structure is not possible, cement can also be used instead. It is recommended to use epoxy and cyanoacrylate types of cement.
4. **Isolated studs and mica washers:** recommended types of fixations when electrical isolation of the accelerometer from the object is required (i.e. in order to prevent ground loops).
5. **Permanent magnet:** applicable for flat magnetic surfaces. The magnet also electrically isolates the accelerometer. Even though the resonant frequency is reduced when using this type of fixation, it is still reasonably high even for accelerations up to 1000 or 2000 m/s^2.
6. **Hand held:** suitable for quick-look survey work. Due to its low stiffness, it introduces a lot of errors and is just suitable up to 1 kHz. According to (IEEE, 1999), this method is generally not recommended.
7. **Vacuum mounting:** it requires smooth surfaces and an external device to remove the air from the suction cup. Most of the times, it is practically difficult to perform.
8. **Double-sided adhesive disk:** suitable when the thickness as well as the material properties of the tape influence the transducer's operation region.
9. **Quick mount:** when an important issue is to experimentally determine the resonance and amplitude limits for the mount used.

The described mounting methods are shown in Fig. 2.4 and their performance is compared according to (ISO, 1998) in Fig. 2.5.

A discussion on the type and fixation of the transducers' cable is presented in the standard (ISO, 1998). According to the latter source, the cable should:

- Not be stiff, in order to avoid additional (unwanted) strain.
- Be properly fixed (e.g. using tape), since the loose cables may introduce tribo-electric effects (for piezoelectric type transducers), or also contribute to the acceleration recorded due to unwanted rebounds of the wires against the structure. A recommended clamping of the cables is shown in Fig. 2.3.

2.2.4 Calibration of accelerometers

According to the International Bureau of Weights and Measures (BIPM, 2008), calibration is the operation that, under specified conditions, in a first step, establishes a relation between the quantity values with measurement uncertainties provided by measurement standards and corresponding indications with associated measurement uncertainties (of the calibrated instrument or secondary standard) and, in a second step, uses this information to establish a relation for obtaining a measurement result from an indication. A calibration may be expressed by a statement, calibration function, calibration diagram, calibration curve, or calibration table. In some cases, it may consist of an additive or multiplicative correction of the indication with associated measurement uncertainty. It is also stated in the latter reference that calibration should not be confused with adjustment of a measuring system, often mistakenly called self-calibration, nor with verification of calibration. Matters related with calibration can be found in the

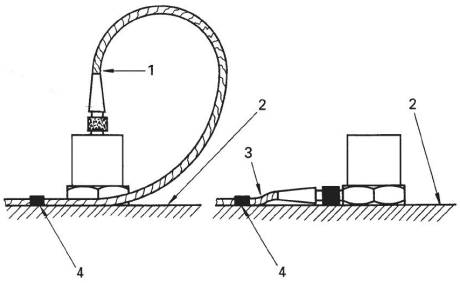

Fig. 2.3: Cable fixation for accelerometers with axial and radial connectors after (ISO, 1998). 1 and 3: transducer cable (not too tight so as to not influence the connection between cable and transducer), 2: structure to be measured, 4: fixation of cable to the surface to avoid rebounds.

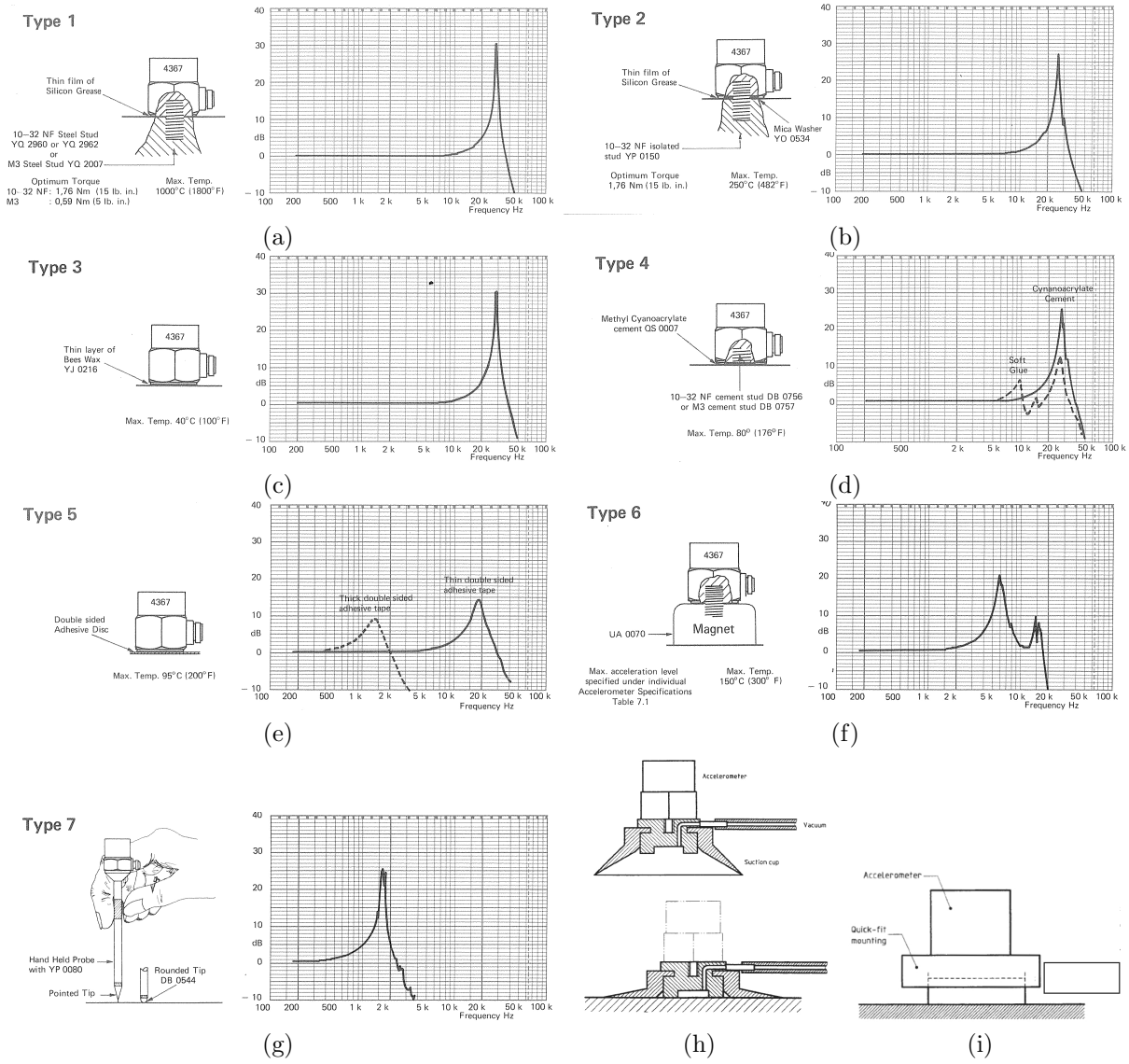

Fig. 2.4: Typical frequency responses for mountings using: (a) a threaded stud; (b) isolated threaded stud and mica washer; (c) thin even layer of bees wax; (d) methyl cyanoacrylate cement; (e) double sided adhesive disc; (f) permanent magnet; (g) hand-held probe (reproduced from (Bruel&Kjaer, 1978)); (h) vacuum mounting; and (i) quick mount discussed in (ISO, 1998).

	Resonance frequency	Temperature	Mass of transducer and stiffness of mounting	Resonance magnification factor Q	Importance of surface preparation
Stud	●	●	●	●	●
Methylcyano acrylate cement	●	●	●	●	◑
Beeswax	◑	○	◑	●	●
Double-sided tape	○	◑	○	○	●
Quick mount	◑	●	◑	◑	◑
Vacuum mounted	◑	●	●	◑	◑
Magnet	◑	●	○	○	●
Hand held	○	○*)	○	○	○

*) Depends entirely on distance between hand and measured surface.
Key: ● high ◑ average ○ poor

Fig. 2.5: Mounting methods criteria according to (ISO, 1998).

international standard (ISO, 2003).

In order words, and referred to the transducers dealt with in this report, calibration is performed in order to determine the correct sensitivity of a particular accelerometer, since, in general, each transducer has its own sensitivity (due to manufacturing, material variabilities, etc.). The sensitivity is normally frequency dependent. According to (Bruel&Kjaer, 1978), the following calibration procedures can be distinguished:

- **Use of calibration chart:** the so-called theoretical calibration, suitable for most general purpose measurements. The sensitivity value in the calibration chart is based on factory calibration. As stated in (Bruel&Kjaer, 1978), the accuracy of the factory calibration is better than ±2% and includes the influence of the connection cable supplied with the accelerometer.
- **Calibration using constant acceleration:** the sensitivity is determined from measurements of the peak output voltage by exciting the transducer with a known value. If an RMS indicating instrument is used, then the overall sensitivity corresponds to the RMS voltage measured multiplied by $\sqrt{2}$ (Bruel&Kjaer, 1978). In general, the input value employed is 10 ms^{-2}, e.g. using an accelerometer calibrator type B&K 4294, providing 10 ms^{-2} RMS at frequency 159.2 Hz (1000 rad/s). As noticed in (Bruel&Kjaer, 1978), the accuracy of the 10 ms^{-2} peak reference level of the B&K 4291 is ±2%.
- **Back-to-back calibration:** the method can be described as a comparative method. It involves coupling the accelerometer to be calibrated as close as possible to a double-ended standard accelerometer for which its sensitivity over the frequency range in known; and driving the coupled pair with a shaker, carrying out a frequency sweep for the whole frequency response. Since they are tightly coupled together, they will both experience the same motion, thus the calibration being done by comparing both responses by measuring the output voltage and also taking into account that the ratio between their sensitivities is known:

$$S(f)_{\text{unknown}} = S(f)_{\text{ref}} \frac{V(f)_{\text{unknown}}}{V(f)_{\text{ref}}}, \tag{2.2}$$

  where $S(f)$ is the frequency-dependent sensitivity and $V(f)$ the output voltage for each frequency of the accelerometer in question (unknown or reference). The calibration accuracy achieved can well be better than 2%. The method is described in (ISO, 2003). A discussion on uncertainties involved is presented in the standard as well. This is the method that was chosen to carry out the

calibration of the MEMS capacitive accelerometers developed in this report, thus a more precise description of it taken up later on.

The calibration process can also be classified according to the following criteria (Bruel&Kjaer, 1978):

- **Comparison method:** for example, the back-to-back calibration, where an unknown accelerometer is mounted as close as possible to a reference one, the vibration generator being carefully controlled. Accuracies better than 2% can be obtained.
- **Absolute method:** two methods can be distinguished, both having an accuracy of about 0.5% (Bruel&Kjaer, 1978):
  - Reciprocity calibration method: is based on the principle that reciprocal correspondence exists between transducers which are reversible, passive and linear.
  - Interference method: it uses laser interferometry, where the interference between two laser beams is used to determine the acceleration level. It is considered as a rapid and accurate calibration method (Bruel&Kjaer, 1978).

It must be noted that the accelerometer calibration should be done together with the pre-amplifier to be used. Although it is true that the pre-amplifier's uncertainty is usually low enough to not alter too much practical measurements, it has also its own uncertainty and should therefore be accounted for in order to increase accuracy.

2.2.5 MEMS calibrations methods

Some standardised ways to calibrate the MEMS accelerometers are presented in (IEEE, 1999) (Annex K and L) and in its updated version (IEEE, 2008). In general terms, two different methods for calibrating MEMS can be distinguished; one static and one dynamic.

Calibration using acceleration due to gravity

The widely applied method for MEMS calibration is to use gravitational acceleration. This method is also proposed by the manufacturers (Analog Devices, 2000, 2010).

Apart from some basic knowledge about calibration, acceleration due to gravity is also dealt with in (Carver and Looney, 2008). There, a two-axial sensor is fixed vertically and rotated $90°, 180°$ and $270°$ respectively, while recording the accelerations produced (Fig. 2.6a). When rotating, the output is sinusoidal with regard to the angle (Fig. 2.6b). In the figure, the ideal signal is shown with zero off-set and amplitude equal to 1 g. Comparing both measured and ideal results, the gain (sensitivity) and off-set (bias) can be determined. This method, however, is static and no frequency dependence is investigated (read-outs of the g-values are done after rotation at angles $90°, 180°$ and $270°$). As noticed in (Carver and Looney, 2008), perfect vertical alignment and precision in initial angle estimation is crucial to get correct results of sensitivity. A similar procedure to this one was used also in (Stein et al., 2007), where a tri-axial MEMS accelerometer was used instead. Discussions on this so-called "tumble test" are presented in (IEEE, 1999) (Annex K).

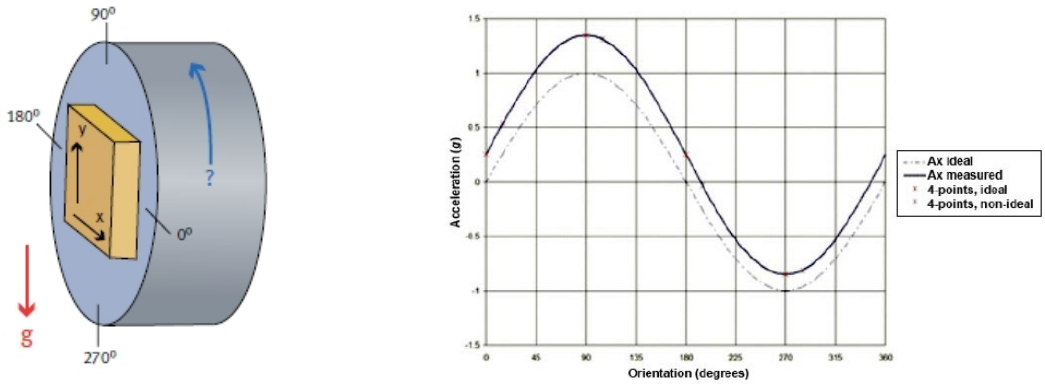

(a) (b)

Fig. 2.6: (a) Set-up used for calibration; (b) sinusoid (ideal and measured) fitted from 4 points measured (Carver and Looney, 2008).

Calibration in the frequency domain

Calibration in the frequency domain is analysed in e.g. (Badri et al., 2010), Fig. 2.7. In there, the back-to-back calibration (using a PCB integrated circuit piezoelectric accelerometer) is presented. An electrodynamic shaker was employed, with a sweep signal of rate 2.5 kHz/s. For verification, a pure sine signal was used as well (testing frequencies 20 Hz, 145 Hz and 377 Hz).

Some notes to frequency domain calibration of MEMS devices are summarised also in (IEEE, 1999) (Annex L), where the recommended sweep-rate to be used is 4 Hz/s.

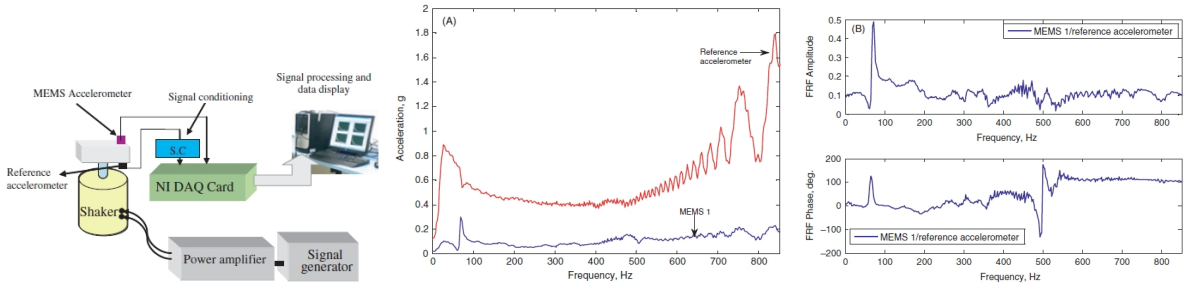

(a) (b) (c)

Fig. 2.7: (a) Set-up used for calibration; (b) acceleration measured; (c) corresponding frequency response function and phase plot (Badri et al., 2010).

3 MEMS accelerometers

In this chapter, an overview of the construction of the MEMS accelerometers developed is presented and the issues related to it discussed. Moreover, the principle and procedure of calibration is presented.

3.1 Introduction

In Fig. 3.1, a general capacitive accelerometer structure and its corresponding lumped mass model can be seen. Capacitive acceleration sensors have several attractive features: they have excellent sensitivity, the transduction mechanism is intrinsically insensitive to temperature and also independent of the base material. The lumped mass model in Fig. 3.1 depicts a typical MEMS accelerometer composed of a movable proof mass M with plates attached through a mechanical suspension system with stiffness K and damping D to a reference frame. As the external acceleration displaces the supporting frame, the internal stress in the suspension spring changes. The relative displacement $(y - z)$ can be measured as a change in capacitance (i.e. a change in the output voltage), giving a measure of the external acceleration.

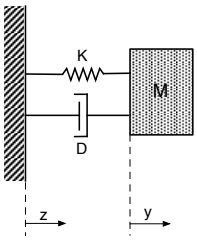

Fig. 3.1: General capacitive accelerometer structure and its corresponding lumped mass model.

3.2 Description of sensors

The MEMS accelerometers chosen for this study are the ADXL-202 and the ADXL-203 (Analog Devices, 2000, 2010). The sensor used in both types of MEMS is a dual-axis accelerometer with signal conditioned voltage outputs; the operating principle is capacitive measurement with a moving mass. A connection circuit diagram for the accelerometer ADXL-203 can be seen in Fig. 3.2. As aforementioned, the sensor measures acceleration by sensing changes in capacitance when the geometry of the capacitor is changing (either the area of the electrodes, the distance between them or the permittivity of the separating material) (Lyshevski, 2002). Table 3.1 shows some of the specifications of the two types of MEMS accelerometers utilised. Some additional notes on the accelerometers used are:

- The output signal is an analogue voltage signal (i.e. not a digital one).
- All the necessary electronics (condenser and the like) are packed within a small plastic casing.
- The power supply is 5 V DC, provided by an in-house built connection box (cf. Fig. 4.1r).
- For matters of fixation, two legs are built-in. In this way, the accelerometer can be attached to the host structure using screws. Also, wax can be used instead as mentioned in Section 2.2.3 if the structure to be measured cannot be damaged.
- The cable is rather thick as it needs to have 4 channels: two devoted to the $x-$ and $y-$signals and two for power supply.
- The cut-off frequency is determined by the choice of capacitor (C_X for measurement in the $x-$direction and C_Y in the $y-$direction), see Fig. 3.2.

Table 3.1: Specifications of the ADXL-202 and 203 accelerometers (Analog Devices, 2000, 2010).

	ADXL-202	**ADXL-203**
Measurement range	±2 g	±1.7 g
Sensitivity	312 mV/g	1000 mV/g
Noise density	500 $\mu g/\sqrt{Hz}$	110 $\mu g/\sqrt{Hz}$
Sensor resonant frequency	10 kHz	5.5 kHz

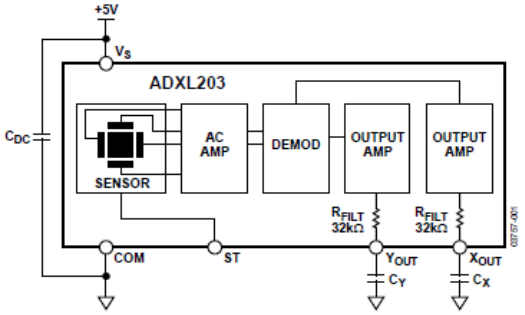

Fig. 3.2: Connection circuit diagram for MEMS accelerometer ADXL-203 (Analog Devices, 2010). The ADXL-202 has exactly the same layout and components, a different chip being used instead.

3.3 Construction

The ADXL-203 is factory packaged in a Ceramic Leadless Chip Carrier (LCC) package of size 5×5×2 mm^3. The package is mounted to a printed circuit board (PCB) as shown in Fig. 3.3b. On the PCB, capacitors determining the bandwidth of each channel are mounted. To amplify the signals, channels are connected to an STMicroelectronics TS922IN operational amplifier. A 4-lead cable is attached to the PCB and the complete setup is mounted in a casing which is filled with epoxy. The finished system can be seen in Fig. 3.3a, where also the mounting clips on each side of the capsule are shown. The PCB with the accelerometer chip is mounted sideways in the capsule; this way the orientation of the sensor will be x in the in-plane direction and y in the out-of-plane direction, as observed in Fig. 3.4a. The bandwidth selection, i.e. the capacitance of the capacitors C_x and C_y, influences the RMS noise of the transducer as shown in Fig. 3.4b. Note that to avoid aliasing effects, the maximum bandwidth is 2.5 kHz. To decouple the sensor from noise from the power supply, a 0.1 μF capacitor C_{DC} is mounted, as shown in Fig. 3.2.

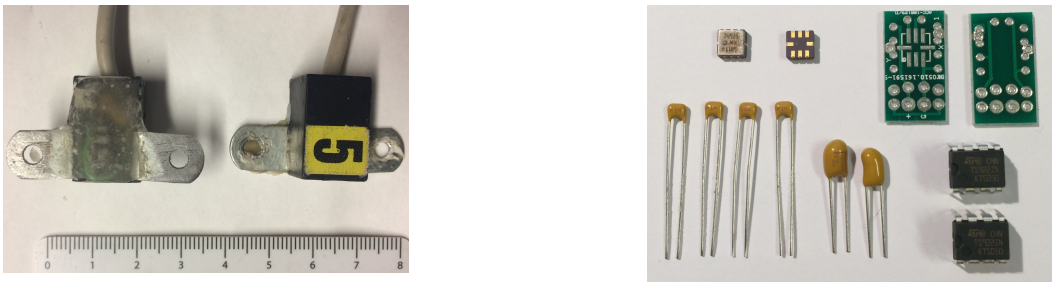

(a) (b)

Fig. 3.3: (a) Finished sensors. left: bottom side, right: top side. Note the PCB visible from the bottom; (b) parts required for building two sensors.

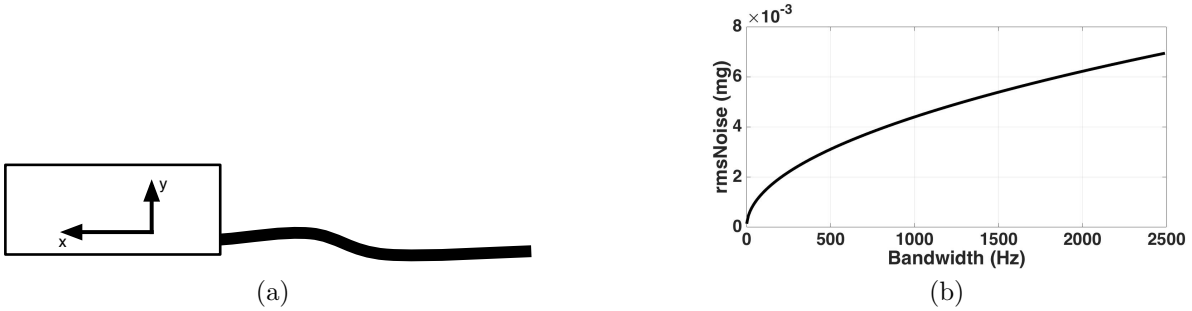

(a) (b)

Fig. 3.4: (a) Orientation of the sensor directions; (b) RMS noise as function of selected bandwidth for the ADXL-203.

4 Apparatus

During the report, different equipment (namely sensors, power supply, excitation sources, etc.) will be referred to. In this chapter, all the apparatus employed during the course of this work are listed below.

4.1 Apparatus used

The laboratory equipment used in the calibration process described in this report is:

MTS 810 (Fig. 4.1a): material testing machine used at LU.
- Versatile, multi-purpose servo-hydraulic testing system.
- Both for static and dynamic material and component testing.
- Waveforms available are: sine, square, triangle, ramp, or user-defined.
- The upper frequency limit is 50 Hz.
- A typical response curve is shown in Fig. 4.2a.

Spectrum computing M2i (Fig. 5.1b): data acquisition system.
- Input: only analog signals.
- 16 channels 250 kSamples/s 16-bit 125 kHz max bandwidth.
- Control and post processing is done in SBench 6 (Spectrum, 2015) with export possibilities into MATLAB.

Bruel & Kjaer PULSE (Fig. 4.1b): data acquisition system.
- Input: only analog signals (voltage signals up to 7 V peak input).
- Limit of PULSE license used at DMME AAU: 4 input and 2 output channels, FFT, CPB, Time data recorder.
- Control and post-processing of measurements can be done either in B&K PULSE LabShop or B&K PULSE REFLEX.
- Both LabShop and REFLEX allow to do post-processing/export also into MATLAB.

Bruel & Kjaer 7541 (Fig. 4.1c): vibration controller.
- Input: only analog signals (voltage signals up to 20 V peak).
- Limit of PULSE license used at DMME AAU: 2 input and 1 output channels.
- The PC interface using B&K Vibration control software.
- Random noise and sine/sweeped sine control up to 2 kHz.

Bruel & Kjaer 4809 (Fig. 4.1d): electrodynamic shaker at DMME AAU.
- Bottom frequency: 20 Hz.
- Maximum force: 44.5 N.
- Maximum acceleration: 75 g.
- Maximum displacement: 8 mm (peak-to-peak).
- Very low cross-motion (below 1% throughout the frequency range (Bruel&Kjaer, 1972)).
- A frequency response function (for a constant feeding voltage) is shown in Fig. 4.2f and load rating curves are presented in Fig. 4.2g.

Bruel & Kjaer 4808 (Fig. 4.1e): electrodynamic shaker at LU.
- Bottom frequency: 5 Hz.
- Maximum force: 112 N.
- Maximum acceleration: 71 g.
- Maximum displacement: 12.7 mm (peak-to-peak).

Bruel & Kjaer 4824 (Fig. 4.1f): electrodynamic shaker at LU.

- Bottom frequency: 2 Hz.
- Maximum force: 100 N.
- Maximum acceleration: 44 g.
- Maximum displacement: 25.4 mm (peak-to-peak).

Bruel & Kjaer 4291: vibration calibrator.

- Horizontal operating position.
- A correct weight of the calibrated transducer needs to be adjusted.
- Excitation with a single sine acceleration of frequency 79.4 Hz and amplitude 1 g.

Bruel & Kjaer 4294: vibration calibrator.

- Vertical operating position.
- No transducer weight adjustment is required (it is done automatically).
- Excitation with a single sine acceleration of frequency 159.2 Hz and RMS value 10 m/s^2.

Bruel & Kjaer 8305 (Fig. 4.1g): reference accelerometer.

- Flat frequency response (Fig. 4.2b).
- Not calibrated with a pre-amplifier (calibration just of the accelerometer). For more precise calibrations, it needs to be calibrated together with the pre-amplifier it is to be used with.

Bruel & Kjaer 4371 (Fig. 4.1j): a general purpose DeltaShear, uni-gain piezoelectric accelerometer.

- Its typical charge sensitivity is 1 pC/m s^{-2}.
- Side connector, i.e. another accelerometer can be attached on the top flat surface using e.g. glue or wax.
- A typical calibration curve is presented in Fig. 4.2c.

Bruel & Kjaer 4384V (Fig. 4.1k): a general purpose DeltaShear, Unigain piezoelectric accelerometer.

- Its typical charge sensitivity is 1 pC/m s^{-2}.
- Top connector.
- A typical calibration curve is presented in Fig. 4.2d.

Bruel & Kjaer 4374 (Fig. 4.1l): miniature charge accelerometer.

- The cable is permanently attached.
- Typical charge sensitivity is 0.15 pC/m s^{-2}.
- A typical calibration curve is presented in Fig. 4.2e.

Bruel & Kjaer 4507 001 (Fig. 4.1m): piezoelectric CCLD accelerometer.

- Built-in pre-amplifier.
- Typical sensitivity is 10 mV/g.

Bruel & Kjaer 4332 (Fig. 4.1n): charge accelerometer.

- Its typical charge sensitivity is 50 pC/g.
- Side connector.

Bruel & Kjaer 4524 B (Fig. 4.1o): triaxial CCLD accelerometer.

- Triaxial accelerometer with a built-in pre-amplifier.
- Typical sensitivity is 100 mV/g.

Bruel & Kjaer 2647A (Fig. 4.1h): charge to DeltaTron converter.

- Simple use (no settings required, just connected between the accelerometer and DAQ).
- CCLD: power supply provided directly from the B&K PULSE.
- Gain: 1 mV/pC.

Bruel & Kjaer 2626 (Fig. 4.1i): charge amplifier.

- Alternative to Bruel & Kjaer 2647A.
- The sensitivity is set in the amplifier, i.e. the output is unit voltage (or its multiples).
- In the past, the B&K 8305 was calibrated together with 2626 as a part of calibration set-up.
- The calibration sheet of B&K 8305 provides sensitivity without amplifier, so for more precise measurements, calibration of the reference accelerometer with the pre-amplifier is required.

Bruel & Kjaer 2706 (Fig. 4.1p): power amplifier for electrodynamic shaker Bruel & Kjaer 4809.

- Amplitude, damping control.
- Clipping (visualisation of distorted signal).

Bruel & Kjaer 2734 (Fig. 4.1q): power amplifier used at LU.

- A power amplifier used with shakers Bruel & Kjaer 4808 and 4824.

Connection box (Fig. 4.1r): in-house power supply/connection box built at LU.

- 5V DC supply to each accelerometer.
- 16 channels for dual axial accelerometers (32 channels).

(a) (b) (c)

(d) (e) (f)

(g) (h) (i)

(j) (k) (l) (m) (n) (o)

(p) (q) (r)

Fig. 4.1: (a) Material testing system MTS 810; (b) Data acquisition system B&K PULSE; (c) Vibration controller B&K 7541; (d) Electrodynamic shaker B&K 4809; (e) Electrodynamic shaker B&K 4808; (f) Electrodynamic shaker B&K 4824; (g) Reference accelerometer B&K 8305; (h) Charge-to-DeltaTron Converter B&K 2647A; (i) Charge amplifier B&K 2626; (j) Accelerometer B&K 4371; (k) Accelerometer B&K 4384V; (l) Accelerometer B&K 4374; (m) Accelerometer B&K 4507 001; (n) Accelerometer B&K 4332; (o) Accelerometer B&K 4524B; (p) Power Amplifier B&K 2706; (q) Power Amplifier B&K 2734; (r) in-house made connection box for MEMS accelerometers (with built-in power supply).

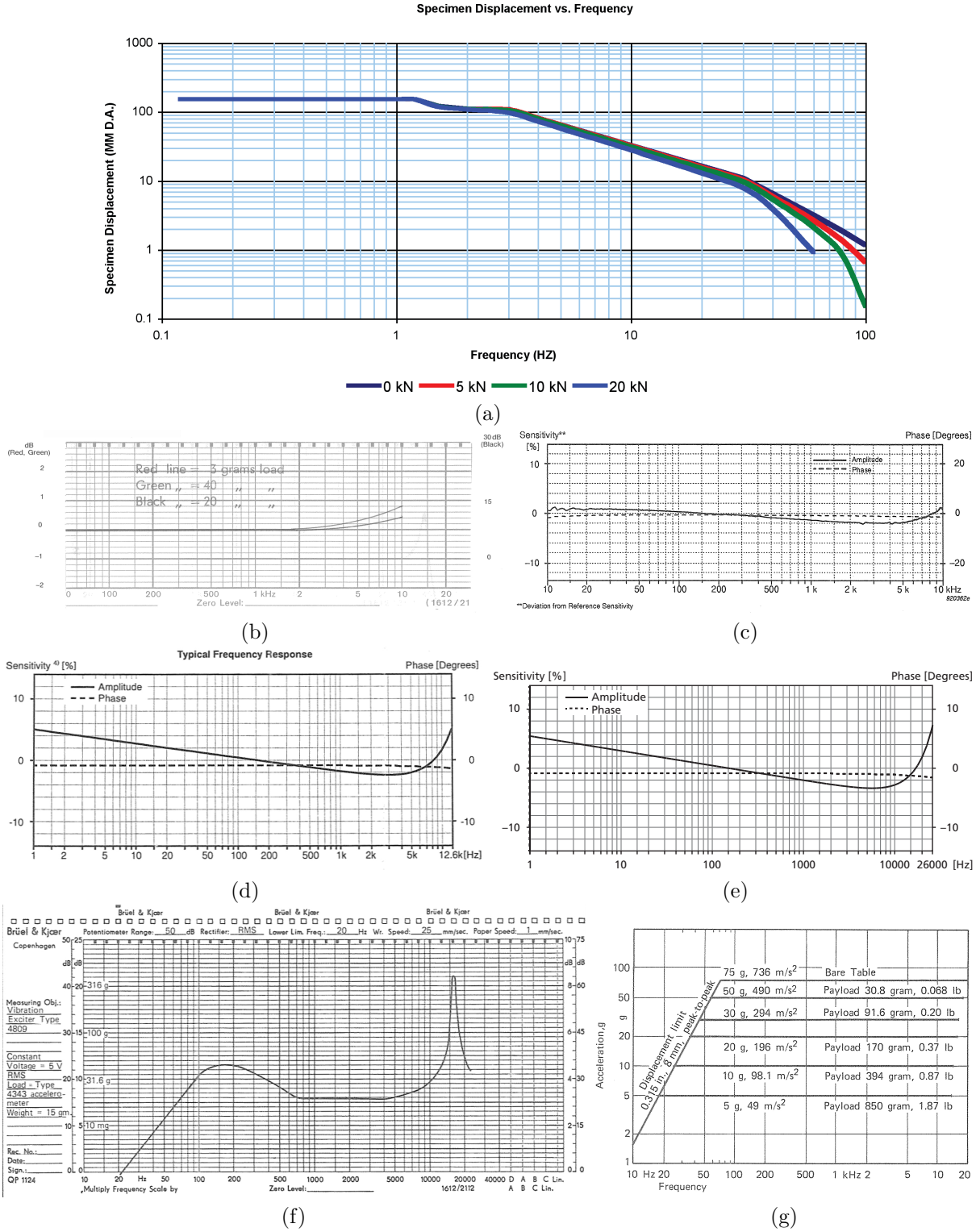

Fig. 4.2: (a) Frequency response curves of MTS 810 (MTS, 2006); Calibration curves for: (b) reference accelerometer B&K 8305; (c) multi-purpose accelerometer B&K 4371 and (d) B&K 4384V; (e) a miniature accelerometer B&K 4374; (f) and (g) a frequency response and load rating curves for a shaker B&K 4809 (Bruel&Kjaer, 1972).

5 Calibration using the MTS machine

The Material Testing System (MTS) is a versatile, calibrated multipurpose servo-hydraulic testing system for both static and dynamic material and component testing. The MTS 810, used in the first steps of these calibrations experiments, can be seen in Fig. 5.1a. The machine can easily be set up to perform any material test needed. Different materials such as plastic, aluminum, composites and even steel can be tested in different ways, namely tension, compression, fatigue, mechanical fracture and durability tests, for example (MTS, 2006).

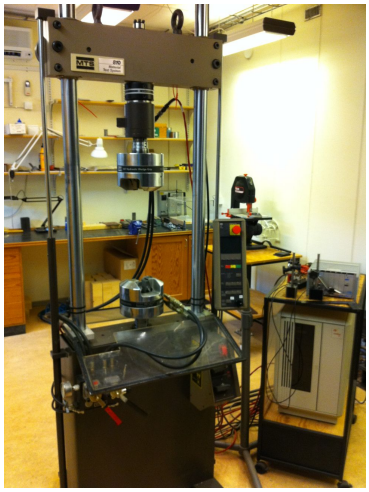

(a)

(b)

Fig. 5.1: (a) MTS 810 used at LU; (b) M2i4711 DAQ Card.

5.1 MTS Measurements

After the mounting of the transducers, the MTS was used to perform the very first calibration steps of the MEMS accelerometers under investigation here. The MTS machine, as a calibration device, is a very accurate but also a time consuming method, as the calibration has to be made with a constant sine excitation, which in turn needs to be repeated for various frequency values to obtain a frequency dependent calibration curve.

5.1.1 Equipment and measurement set-up

The equipment used for these first tests was the MTS 810 machine and the Spectrum computing M2i data acquisition card (DAQ) (see Section 4.1). A 20 mm thick steel plate was attached to the wedges of the MTS machine, which was driven vertically at a single (constant) frequency. The displacement of the plate is measured by the sensors built into the MTS machine. An array of 10 accelerometers was attached onto the aforementioned steel plate using nuts and bolts to ensure a fixed connection, all of them were connected to a computer with a DAQ (cf. Fig. 5.1b). The acceleration acquired by each accelerometer when driving the plate with the MTS machine were saved as MATLAB (.mat) files for post-analysis. As

the time history of the movement is registered by the MTS machine, the acceleration measured by the accelerometers can be calibrated against the movement as measured by the calibrated MTS machine. The software used for the acquisition was Spectrum SBench 6.1 from Spectrum computing (Spectrum, 2015). The acceleration and movement was recorded for 11 seconds with a sampling frequency of 5 kHz. A schematic of the setup can be seen in Fig. 5.2.

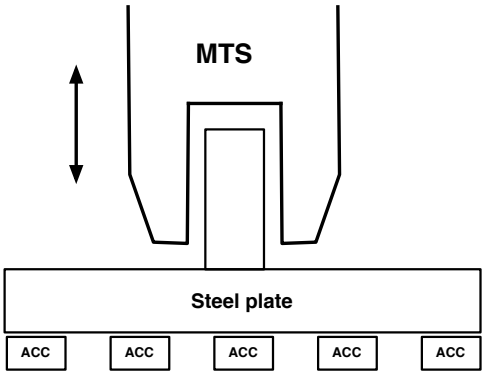

Fig. 5.2: Schematic of the measurement setup, the double arrow indicates the direction of travel.

5.1.2 Limitations

Using the MTS machine to perform calibrations proved to be a fairly accurate method. However, there are some drawbacks. The MTS machine can not be run above 50 Hz due to mechanical limitations in the system. This means that the calibration can only be performed for the very lowest frequencies. Moreover, the calibration is also very time consuming in the set-up of the accelerometers and the fact that the calibration must be performed for a single frequency per time.

5.2 Discussion on results

The signal-to-noise ratio of the data recorded was low. Thus, some sort of filtering was needed to reduce the amount of noise in the signals. The measured data were exported from MATLAB as `.wav` files (using the command `wavwrite(AI_Ch00,fs,'AI_Ch00');` f_s being the sampling frequency, 5 kHz in this case) and imported into B&K PULSE REFLEX to enable easy application of a filter. There, the simple band-pass filter was used setting the cut-off frequencies as close to the excitation frequency as possible, i.e. $f_{cL} = 9.99$ Hz and $f_{cH} = 10.01$ Hz for data measured at $f_e = 10$ Hz (cf. Fig. 5.3).

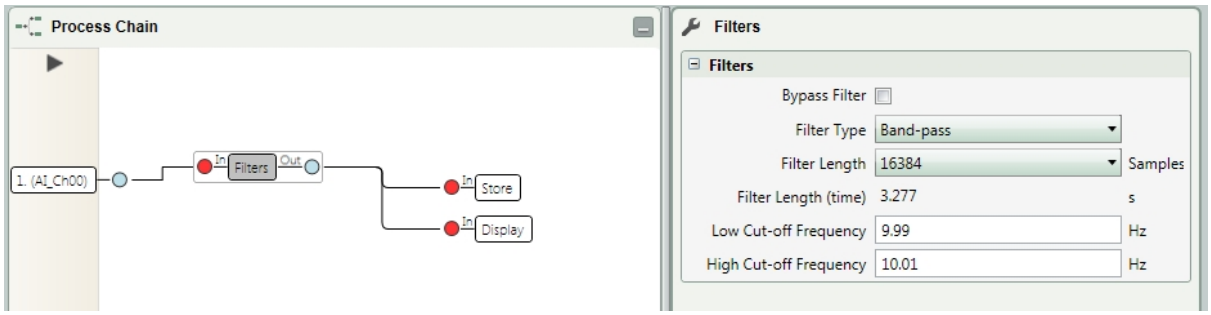

Fig. 5.3: Filter used in B&K PUSLE REFLEX environment.

The filtered data were processed back into MATLAB. As a first step, the amplitude at the excitation frequency (in the presented case 10 Hz) had to be found. This can be done in two principal ways:

- Analysis of peak-to-peak value: basically, minimum and maximum values are found in MATLAB and the amplitude is re-calculated. This method is not recommended, as small ripples (modulation of frequencies or filter error) are present in the signal even after filtering.

- Analysis of the amplitude in the FFT of the filtered signal: a crucial point in the FFT is the choice of the sample width and weighting (windowing) function. But when correct parameters are chosen, the FFT can be more precise and therefore decouple the ripples from the analysed signal.

The idea was to apply a rectangular window to the "ideal" signal, for which no distortion (attenuation) is introduced. However, as discussed in (Quach, 2011) and shown in Fig. 5.4, it is important that the sine wave analysed starts and ends in the same point, i.e. no discontinuities are introduced.

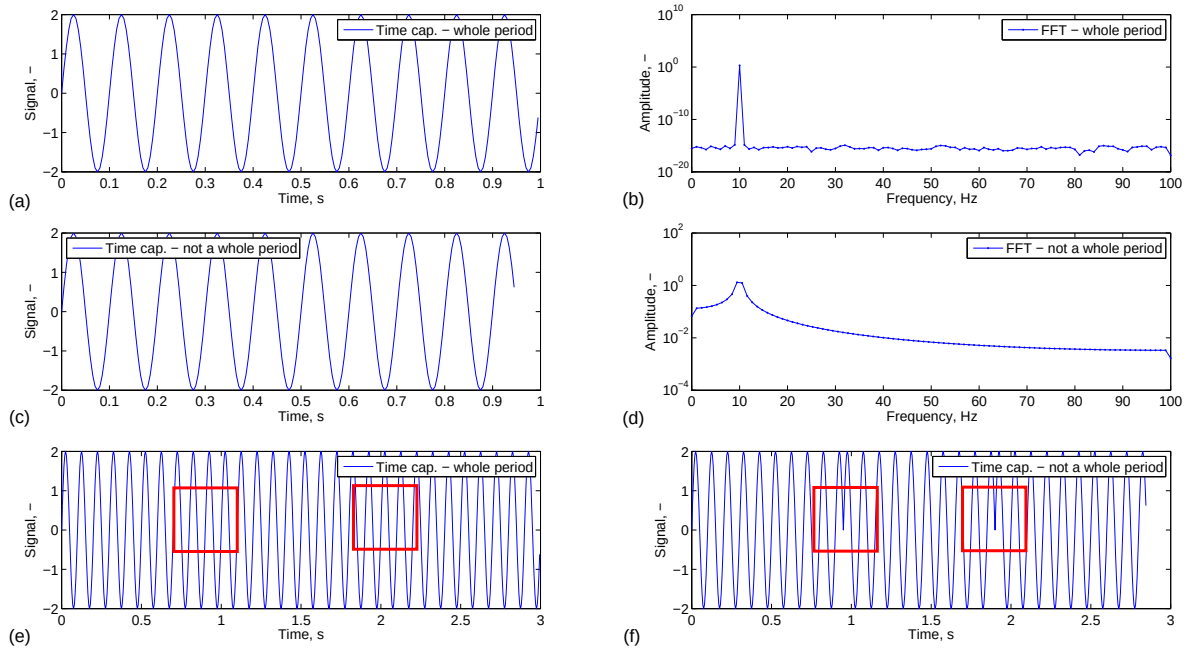

Fig. 5.4: Example of spectral leakage: (a)-(b) ideal sinusoid signal - whole period; (c)-(d) non-ideal sinusoid end (some delay); (e)-(f) comparison of three signals in a row, the rectangles show points where signals are merged. In the case (e) (ideal - whole period) no discontinuity is noticeable, but in (f) the discontinuity is obvious.

When analysing the filtered data, the signal was properly cropped in MATLAB so that a multiple number of periods were captured. Thus, ideally, no spectral leakage would occur after applying the rectangular window. As presented in Fig. 5.5, the FFT shows a purely tonal frequency at 10 Hz with minimal leakage around for a given analysed frequency, although some small ripples can, nevertheless, be noticed when zooming into the filtered signal. Comparing the maximum amplitude and the amplitude at 10 Hz of the FFT spectra:

- Peak value from the time signal: $A = 2.9063 \times 10^{-4}$.
- Amplitude from the FFT signal: $A = 2.884 \times 10^{-4}$.[1]

The error when comparing both methods is about 0.77%. To increase the accuracy of the FFT, one could possibly make the time signal longer, or also more samples of signal one on top of another could be stacked.

5.3 Conclusions

It can be concluded that even if accurate calibration results using the MTS could be achieved, it is not a practical method due to mainly four reasons:

- The MTS is a slow machine and can therefore not excite frequencies above 50 Hz. Even though the applications the MEMS are intended for will be low frequency vibrations in wood buildings (cf. Chapter 1) it is of interest that the upper frequency limit lies somewhere around 200 Hz to increase the reliability of the data acquired.

[1] When exporting into *.wav*-file, it was necessary to scale the measured data by 10^{-5}. The limitation of the *wavwrite()* function can be found in the MATLAB help (MathWorks, 2010).

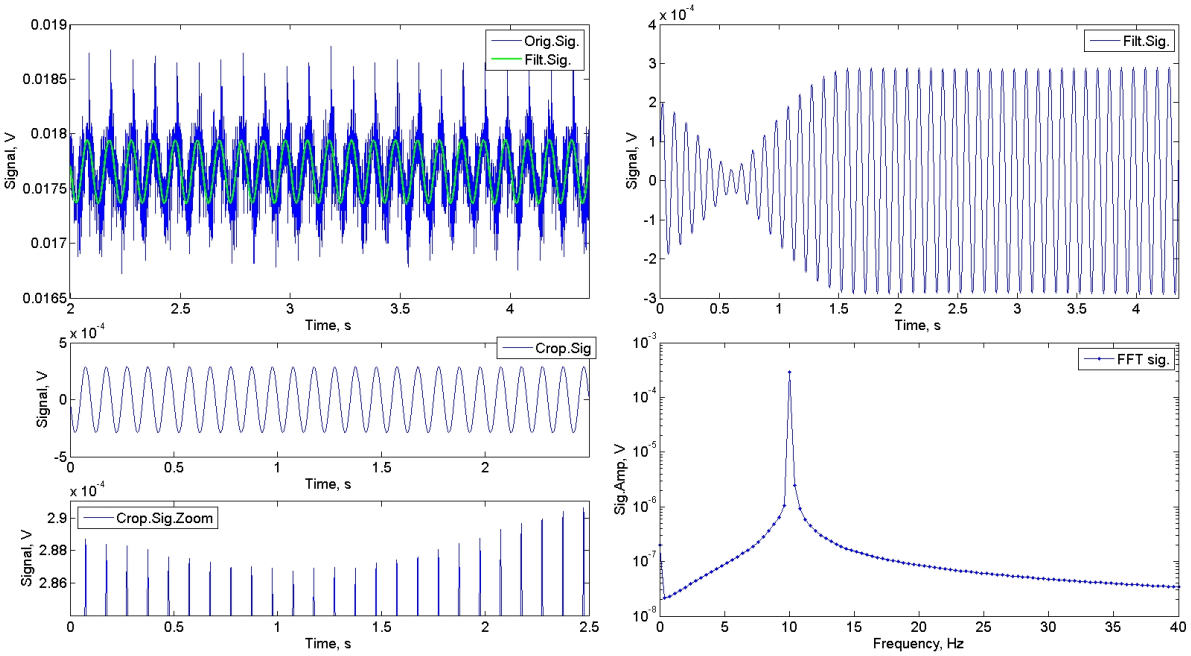

Fig. 5.5: Signal before and after filtration (Orig.Sig and Filt.Sig., respectively), cropped signal (Crop.Sig.) and zoom (Crop.Sig.Zoom) to show the ripples in amplitude and the FFT of the filtrated and cropped signal (FFT sig.).

- Furthermore, the method is not practical, since calibration based on single frequencies must be carried out.
- Filtration of signals is required due to the low signal-to-noise ratio of the data acquired, hence making the method even more time consuming.
- Lastly, one should perform some calculations addressing structural dynamic issues about the characteristics of the plate the array of accelerometers is attached to when performing the calibration. It should be assured that the fundamental mode of vibration of the plate is much higher than the upper frequency limit of calibration allowed by the MTS. Otherwise, the results could be affected by this dynamic unwanted behaviour.

6 Pre-measurements at AAU

In order to test the equipment at AAU and verify the settings of the apparatus involved, a set of preliminary measurements was carried out as described in this chapter.

6.1 Verification of the calibration procedure using a shaker

The aim here was to verify the methodology involved when using a swept sine excitation for the back-to-back calibration. Thus, no MEMS are being analysed thus far, but rather accredited calibrated accelerometers. A sweep sine signal from 50 Hz up to 1.6 kHz with a sweep rate of 4 Hz/s and linear variation was first applied to the electrodynamic shaker B&K 4809.

In Fig. 6.1, the results in form of an autospectra of both signals (the one from the reference accelerometer B&K 8305 and the one to be calibrated B&K 4371) are plotted. Moreover, the bottom plot in Fig. 6.1 presents the ratio between the two latter signals. Only the FFT license was used at this stage in B&K PULSE, i.e. no feedback loop control of the shaker was done. Therefore, the autospectra measured when the electrodynamic shaker was fed with a constant voltage (Fig. 6.1 up) follows the frequency response of the shaker provided by B&K (Fig. 4.2f). Since the response is not flat, the difference between the signals is not constant (Fig. 6.1 down). Hence, it is recommended to use some feedback loop control in order to idealise the excitation.

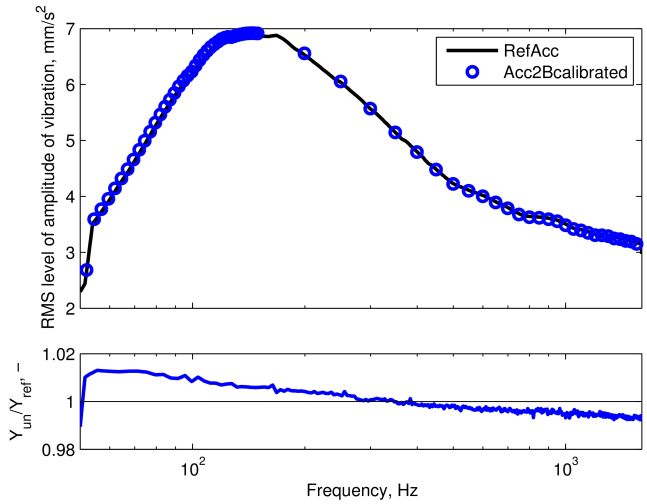

Fig. 6.1: Preliminary results measured with open-loop control (i.e. constant excitation voltage).

6.2 Calibration of the reference accelerometer B&K 8305

In order to see if the sensitivity of the accelerometer B&K 8305 (which will eventually be used as reference for the MEMS calibration using the back-to-back method) provided by the manufacturer in the calibration sheet had remained constant since it was performed, the accelerometer was calibrated using the accelerometer calibrator B&K 4291 (Fig. 6.2a-b). The operating position of this calibrator

(a) (b)

Fig. 6.2: (a) Set-up with B&K 4291 used for the B&K 8305 test calibration; (b) the calibrator B&K 4291.

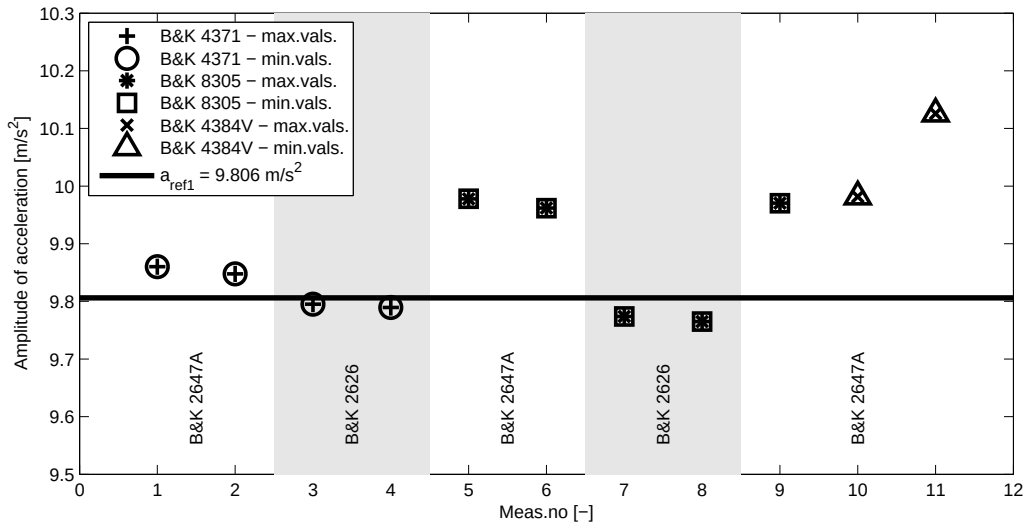

Fig. 6.3: Comparison of all amplitudes of the filtered signal measured for each combination of accelerometer/pre-amplifier. The accelerometer calibrator B&K 4291 was used.

is horizontal and it excites the accelerometer with a peak acceleration level of 1 g, i.e. 9.806 m/s^2, at 79.4 Hz. It is very important to adjust the weight of the accelerometer in the calibrator correctly to be sure that the reference level is indeed 1 g, since otherwise this could lead to additional errors.

The signal from the accelerometer was recorded in the time domain. To estimate the amplitude, minimum and maximum values of the waveform of the filtered signal are used for the calibration, as presented in Fig. 6.3. For the measurement procedure verification, two additional piezoelectric accelerometers (B&K 4371 and B&K 4384V) were used as well. The accelerometers were connected either to the Charge-to-DeltaTron Converters B&K 2647A (Fig. 4.1h), or to a Charge Amplifier B&K 2626 (Fig. 4.1i).

The results obtained and presented in Fig. 6.3 are not very consistent as well as are dependent on the accelerometer used (e.g. on the mass settings of the calibrator B&K 4291). Moreover, the B&K 4291 operates in a horizontal way, i.e. for heavier/larger accelerometers the influence of gravity could also be a reason for calibration errors. Instead, a calibrator with automatic adjustments would be preferred, i.e. one for which is not necessary to do the mass settings and hence subjective (i.e. human) errors when setting the mass scale (cf. Fig. 6.2b) would be removed. Along those lines, an accelerometer calibrator B&K 4294 could be used, for example.

6.3 Comparison of pre-amplifiers and calibrators

The influence of the pre-amplifier employed when calibrating the accelerometer B&K 8305 was also checked in this first studies in order to avoid potential errors stemming from this source. In Fig. 6.4, it can be seen that before filtering (solid lines), the signal is noisier and high frequency components are superimposed, especially when using the Charge-to-DeltaTron Converter B&K 2647A. However, after filtering using a band-pass filter with centre frequency 79.6 Hz and width 1 Hz, those high frequency components are successfully removed. Therefore, it is more recommended to use the Charge Pre-amplifier B&K 2626 in subsequent calibrations, due to the reason that it is more stable and does not introduce that much noise.

The latter statement is also strengthened if one looks back at the previous section. The accelerometers compared in Fig. 6.3 were connected there to two different pre-amplifiers, where, as indicated in the plot:

- A Charge-to-DeltaTron Converter B&K 2647A was used for measurements no. 1, 2, 5, 6, 9-11.
- The charge pre-amplifier B&K 2626 was employed for measurements no. 3, 4, 7, 8.

The results compared in that figure reveal that more consistent and precise data are obtained when the B&K 2626 is used (measurements no. 3, 4, 7, 8). On the other hand, for the accelerometers connected to the B&K 2647A, the amplitude measured was overestimated as the measured values were larger than 1 g, i.e larger than the value applied by the calibrator. Hence, again, the amplifier B&K 2626 seems to perform better and is therefore recommended.

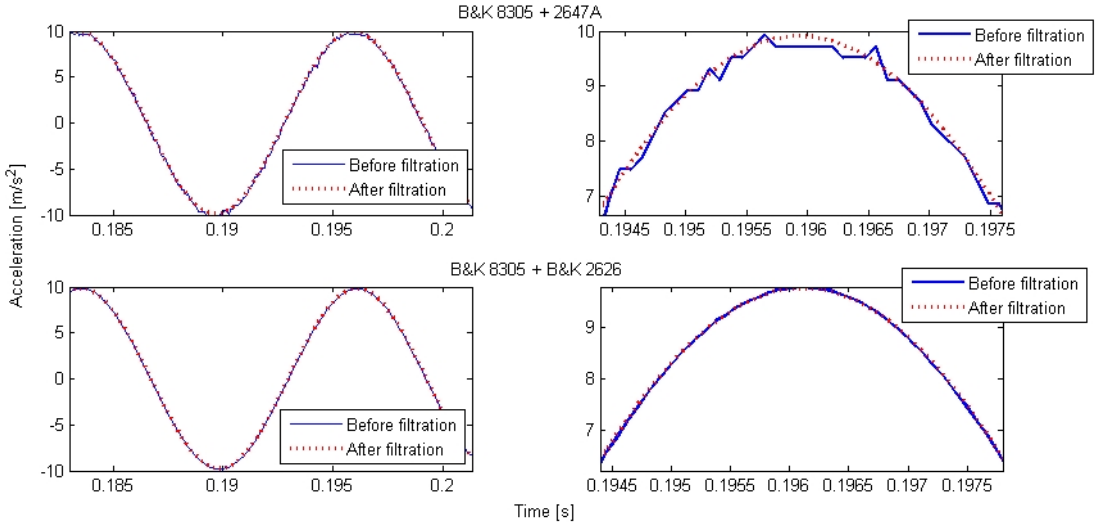

Fig. 6.4: Comparison of the measured and processed time signals using Charge to DeltaTron Converter B&K 2647A (up) and Charge pre-amplifier B&K 2626 (down).

6.3.1 Changing the accelerometer calibrator

To verify, if the calibrator B&K 4291 (cf. Fig. 6.2) works properly, a newer calibrator B&K 4294 (cf. Fig. 6.5a) was borrowed from GRUNDFOS. The advantage in using the B&K 4294 is that it has a built-in control of the vibration level. This means that it is not necessary to set manually the weight of the transducer to get the right level of excitation as well as the fact that it operates in vertical position, i.e. the transversal vibration of large and bulky transducers is minimised.

The previous calibrations using the calibrator B&K 4291 pointed out that the pre-amplifier B&K 2626 seems to be a better option than using the Charge-to-DeltaTron Converter 2647A. Another aim of this set of calibrations was also to double check this assumption and test the two B&K 2626 available at AAU. The results, presented in Fig. 6.6, show that for the calibration of the transducer B&K 8305, more precise measurements were obtained with use of the pre-amplifier B&K 2626_u1 (i.e. the first unit available in the laboratory), while the second B&K 2626 (i.e. the so-called u2) and the B&K 2647A are both at the upper limit of available calibration error. The same measurements as for the B&K 8305 were performed again for a second piezoelectric accelerometer B&K 4371. The difference between the pre-amplifiers is

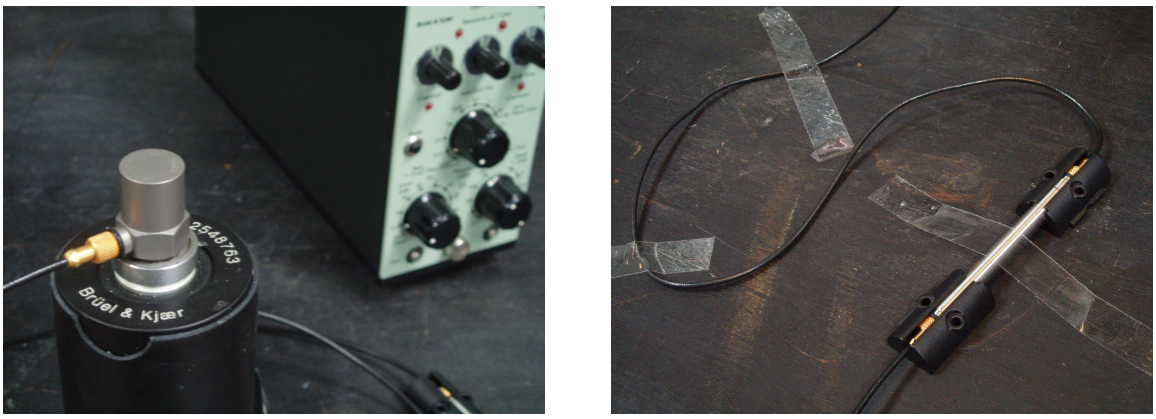

(a) (b)

Fig. 6.5: (a) The accelerometer B&K 4371 fixed onto the calibrator B&K 4294, with the pre-amplifier B&K 2626 shown in the background; (b) the Charge-to-DeltaTron Converter B&K 2647A.

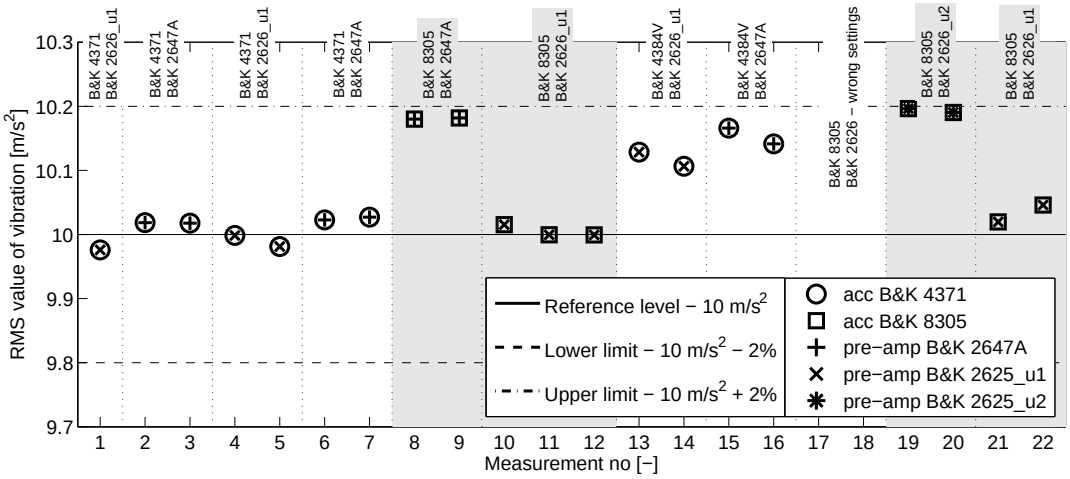

Fig. 6.6: Comparison of the amplitudes measured for each combination of accelerometer/pre-amplifier obtained using a calibrator B&K 4294. Highlighted are measurements using the reference accelerometer B&K 8305 (disregarding the measurements with wrong settings no. 17 and 18). Two pre-amplifiers B&K 2626 (labelled as B&K 2626_u1 and B&K 2626_u2 respectively) are compared as well.

in this case not so dominant. Finally, a last transducer (B&K 4384V) was tested, yielding somewhat imprecise results, i.e. it needs to be properly re-calibrated (i.e. the gain must be adjusted).

The calibrator B&K 4294 was working properly, consistently and the calibration procedure is faster, since no weight adjustments are needed (as required using B&K 4391). Also using the B&K 4294, the tests with the pre-amplifier B&K 2626 were more precise and it is less noisy than the Charge-to-DeltaTron Converter 2647A, which confirms the previous observations.

6.3.2 Comparison of the calibrators

During the tests, one extra B&K 4294 calibrator was found at AAU's laboratory. To verify, that the it still worked properly and to check if the batteries were not dying out[1], new sets of measurements were performed. Thus both the old (B&K 4291) as well as new (B&K 4294) calibrators were compared for a series of calibrations, the results obtained for the B&K 4294 being shown in Fig. 6.7a and for the B&K 4291 in Fig. 6.7b.

[1]As discussed with Dr. Sørensen (Sørensen, T., 2011), the level of acceleration should be constant even when the batteries are dying out. The only thing that could be affected is the time the calibrator is operated after switching it on. Therefore, one can rely on the data measured for all times.

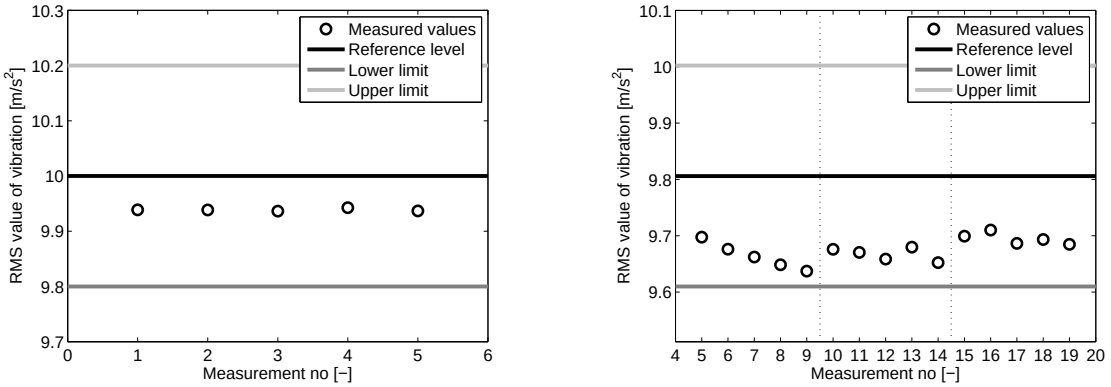

Fig. 6.7: Calibration using (a) B&K 4294 (with fixed accelerometer at all times); (b) using B&K 4291 twice adjusted the mass of accelerometer (some drifting analysed).

It can be seen that the amplitudes obtained are within the limits prescribed by B&K, i.e. they fall within the tolerances marked as upper and lower limits in Fig. 6.7. The gain analysed from B&K 4294 is 1.0061, whereas the one from B&K 4291 is 1.0099. Using the default PULSE LabShop calibration for the B&K 4291, the gain obtained was 1.007 instead.

As already stressed, before each calibration, the B&K 4291 requires to set the correct weight of the accelerometer, which introduces a potential source for additional errors. This can be observed in Fig. 6.7b, where the results have larger variation than the ones obtained for the B&K 4294 (Fig. 6.7a) and even some drifting of the weight set was observed in the first 5 measurements (no. 5-9). After those measurements, the weight value was re-adjusted. Due to this potential additional sources of errors, it is recommended to use the calibrator B&K 4294 instead of the B&K 4291 in subsequent measurements.

6.4 Conclusions

From the preliminary measurements described in the chapter, it can be concluded that the reference accelerometer B&K 8305 can be used for calibration and, together with the pre-amplifier B&K 2626, promising results are obtained, i.e. the amplitudes measured were very close to the one provided by the calibrator. Moreover, there were some inconsistency using the horizontally operated calibrator (B&K 4291), thus the vertically operated one (B&K 4294) should be used instead in subsequent calibrations.

7

Steady State Response Measurements

In order to solve the problem with having a frequency dependent excitation level when the shaker is supplied with a constant voltage input signal (i.e. open-loop control strategy), a license for Steady State Response (SSR) Analysis Type 7772 was used. The SSR analyser uses stepped sine excitation to measure steady state response. The response can be measured as a function of the excitation frequency or excitation level. The measurement system can use an adaptive scan algorithm or linear averaging, ensuring that the steady state response is measured to a user-specified accuracy in the minimum possible time (Bruel&Kjaer, 2015). All the measurements performed with the SSR license were performed using an electrodynamic shaker B&K 4809 with various SSR settings.

7.1 Multi-buffer vs. Steady-State Response

For measurements using a sine sweep type of signal as excitation, the frequency response functions (FRF) were obtained using a multi-buffer to continuously record the responses. The contour plot of such measurements, where each slice represents the frequency response at certain time period defined by multi-buffer, is shown in Fig. 7.1a. The diagonal lines represent the excitation frequency (and its harmonics/orders), from which the total frequency response was extracted. The response measured was extracted exporting contour plots to MATLAB and picking up the amplitudes of the main diagonal (the one with the largest amplitudes). The precision of the method was dependent on the time the slices were saved and sweep rate used. It was not the most ideal approach, but it provided the data needed.

The latter a approach is not very precise and thus after some discussions (Sørensen, T., 2011), an SSR license was used instead and series of measurements were carried out. SSR is used in electroacoustics; and with a stepped sine as excitation, the steady state response is measured (Fig. 7.1b). It provides relatively precise response functions. However, a full feedback loop control would still be more beneficial, since the SSR does not provide the "true" control loop function. Instead, an inverse of the frequency response measured during equalisation is used to provide the signal to the vibration exciter. The latter implies that any random external vibration which was not captured during the equalisation process, can still influence the measurements. On the other hand, in the case of full feedback control, the controller

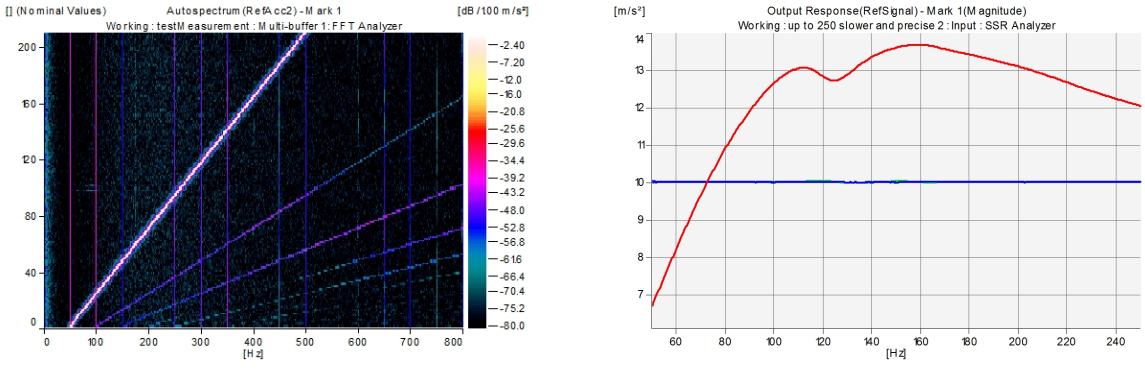

(a) (b)

Fig. 7.1: (a) The FFT analysis using a multi-buffer; (b) Frequency response obtained using SSR.

senses the current vibration of the exciter and adjusts it on-line according to the requirement. Thus it is capable (up to the limits of the control theory used) to handle also the random external vibration and so the measurements are more idealised.

7.2 Tests of MEMS accelerometers

7.2.1 Accelerometer type

In the preliminary tests presented here, two types of MEMS accelerometers, each with different typical sensitivity (namely ADXL-202 and 203, described in Table 3.1), were assessed seeking for differences in their performances. For the measurements, both of the tested accelerometers were glued to the reference accelerometer B&K 8305, which was, in turn, connected to the pre-amplifier B&K 2626 (keeping in mind that back-to-back calibration method was decided to be used, see Section 2.2.4). The coupled pair of transducers was driven by the shaker B&K 4809 (with a power amplifier B&K 2706) fed with a stepped sine excitation up to 500 Hz and a excitation level of 4.4 m/s^2. The response functions from the tests are plotted in Fig. 7.2.

The responses for both MEMS accelerometers (no.8 using an ADXL-202 chip and no.40 with an ADXL-203) are similar in any direction measured ($x-$ as shown in Fig. 7.2a,c,e,g or $y-$ presented in Fig. 7.2b,d,f,h). From the zoomed plots (Fig. 7.2c-h) it can be noticed, that their responses are just being shifted in the frequency domain. Also, as shown in Fig. 7.2h, the transducer no.40 seems to be more sensitive to the excitation at 280 Hz, which will be analysed more thoroughly later on in the report.

7.2.2 Measurement direction

Both MEMS ADXL-202 and 203 were excited in both y- and $x-$directions (cf. Fig. 7.3), the responses being compared for both accelerometers (no.8 and no.40) as shown in the results presented in Fig. 7.4. It can be seen that the behaviour at 280 Hz occurs regardless of the measurement direction. Therefore, it is not linked to the measurement direction and needs, still, to be further analysed to understand its origin.

From Fig. 7.4, it can also be noticed that the MEMS no.8 (the one with an ADXL-202 chip, i.e. with lower characteristic sensitivity) seems to have different sensitivities in the x- and y-directions (i.e. the responses, shown in Fig. 7.4e, do not overlap each other), whereas for the MEMS no.40 (ADXL-203, with higher sensitivity) the sensitivities are fairly similar (Fig. 7.4f). On the other hand, the change of sensitivities can also be caused by a not correct alignment of the chip inside of the capsule. It hence needs to be eventually analysed.

7.2.3 Type of fixation

Another thing that could have an influence in the measurements when performing the back-to-back calibrations was that of the type of fixation of the MEMS accelerometer to the reference one. Hence, investigations aiming at clarify this were performed; the out-of plane direction (i.e. y-direction) being excited according to Fig. 7.5.

Two types of fixations were studied (cf. Fig. 7.5): wax and glue, whose results are plotted in Fig. 7.6. Again, a level of 4.4 m/s^2 was used as excitation for the stepped sine excitation up to 500 Hz employed. Since only a single equalisation procedure of SSR was done, the output response is not perfectly flat. However, the FRFs seem to be sufficiently smooth.

As can be seen from Fig. 7.6, there is a small change in behaviour at around 280 Hz between the two analysed cases (wax and glue) for the directly excited signal (i.e. in the y-direction), which is dependent on the fixation type. As discussed (Larsen, J.B., 2011), the excitation of both x- and y-directions (Fig. 7.6c-d), especially around 280 Hz, could be caused also due to fixation onto the shaker as such. All in all, these strange resonant phenomena should be analysed deeper to get to the cause of it.

7.2.4 Amount of wax

As discussed in Section 7.2.3, the type of fixation of the MEMS to the reference accelerometer on top of the shaker could have an influence when performing measurements. In order to further investigate the

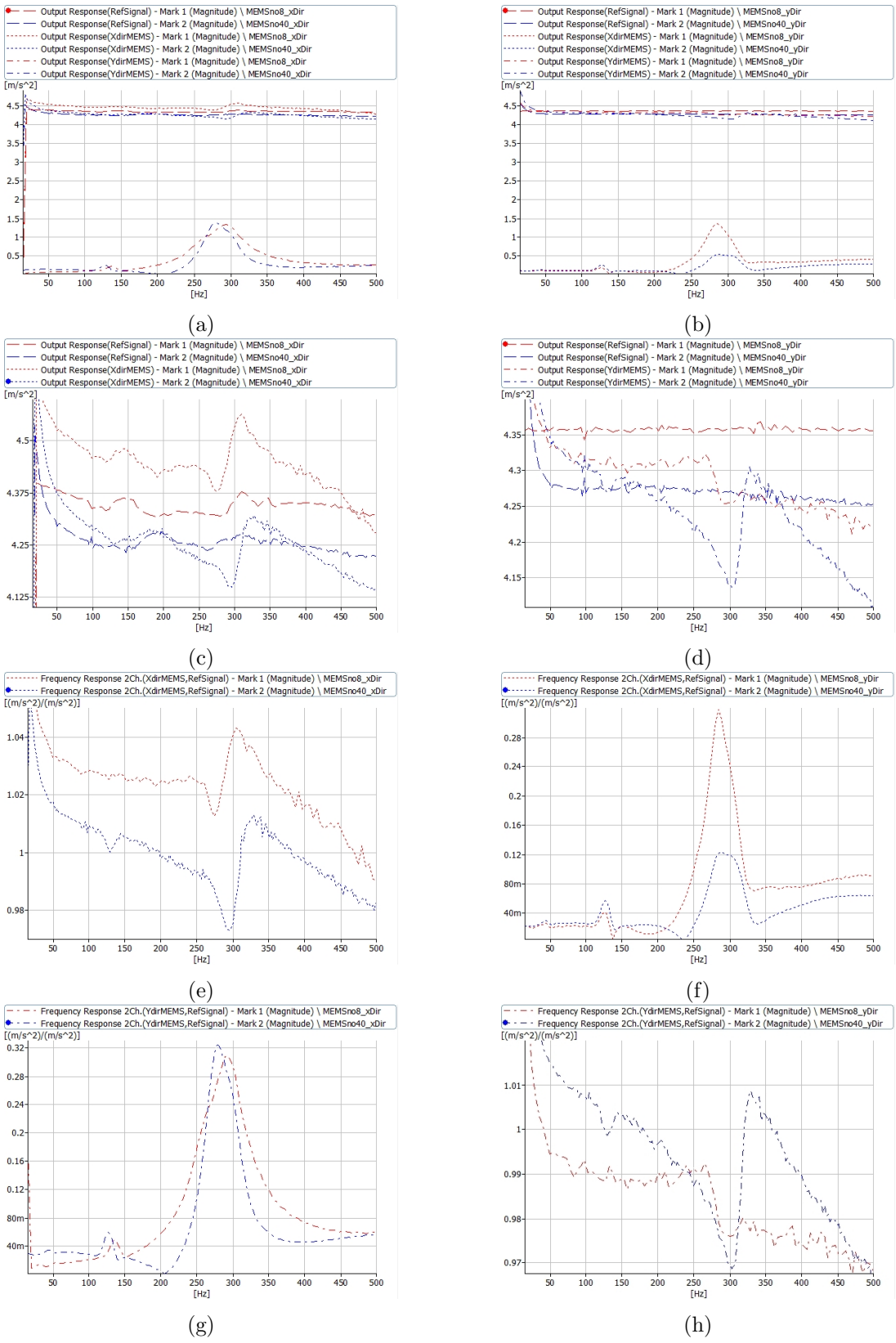

Fig. 7.2: Comparison of the ADXL-202 (MEMS no.8) and ADXL-203 (MEMS no.40) measured either for excitation in x-direction -(a),(c),(e),(g)- and y-direction -(b),(d),(f),(h). In (a)-(b), the output responses are plotted, their zoomed-in version into the excitation level being shown in (c)-(d). In (e)-(h) the FRFs are presented. Colour plots online.

latter statement, studies aiming at determining if the amount of wax (beeswax was used) can influence the response of the accelerometers, were performed. Three different cases were compared (cf. Table. 7.1). It should be noted that the exact amount of wax (defined in here as "normal", "minimum" and "much") was difficult to quantify thoroughly. The purpose of this study was, however, to check whether the wax layer thickness influences the response seen in the previous subsections, where "normal" amount of was was used. Wax behaves as a spring (a non-ideal one, and sometimes even as a damper), so it was our belief that the amount of wax could have some impact on the dynamical response measured. In general, it is recommended to use just a "thin evenly distributed layer" of wax for fixation (Bruel&Kjaer, 1978). The MEMS accelerometer no.40 (the one with higher sensitivity) was used for this set of measurements.

In the previous tests the level of acceleration was taken as 4.4 m/s^2. However, to replicate the calibration used for piezo accelerometers, the amplitude was increased to 10 m/s^2.

The results are presented in Fig. 7.7. Again, it can be seen that the problem with the resonant behaviour at 280 Hz is still not solved, hence the amount of wax not being responsible for that. Further-

(a) (b)

Fig. 7.3: Fixation of the MEMS accelerometer in (a) $y-$ and (b) $x-$direction.

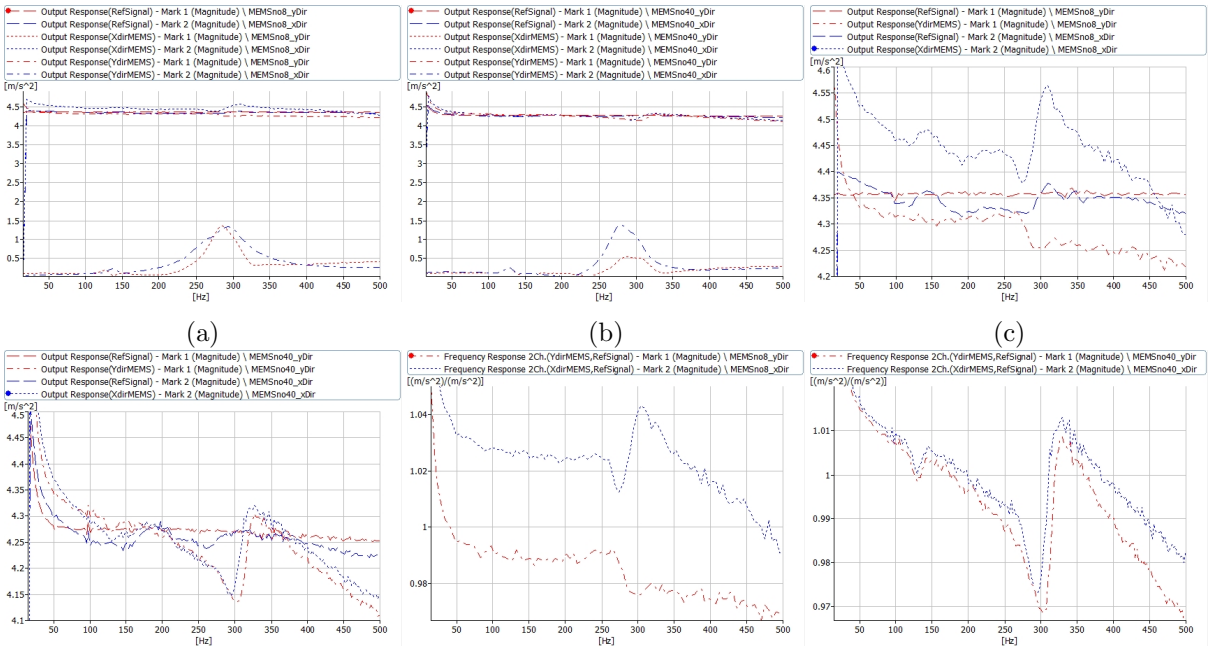

(a) (b) (c)

(d) (e) (f)

Fig. 7.4: Comparison of the measurement directions for ADXL-202 (MEMS no.8) -(a),(c),(e)-, and ADXL-203 (MEMS no.40) -(b),(d),(f). In (a)-(b), the output responses of all signals are plotted with (c)-(d) zoomed into only the excitation direction. The corresponding FRFs are presented in (e)-(f). Colour plots online.

(a) (b)

Fig. 7.5: Fixation of accelerometer: (a) using wax; (b) using cyanoacrylate glue.

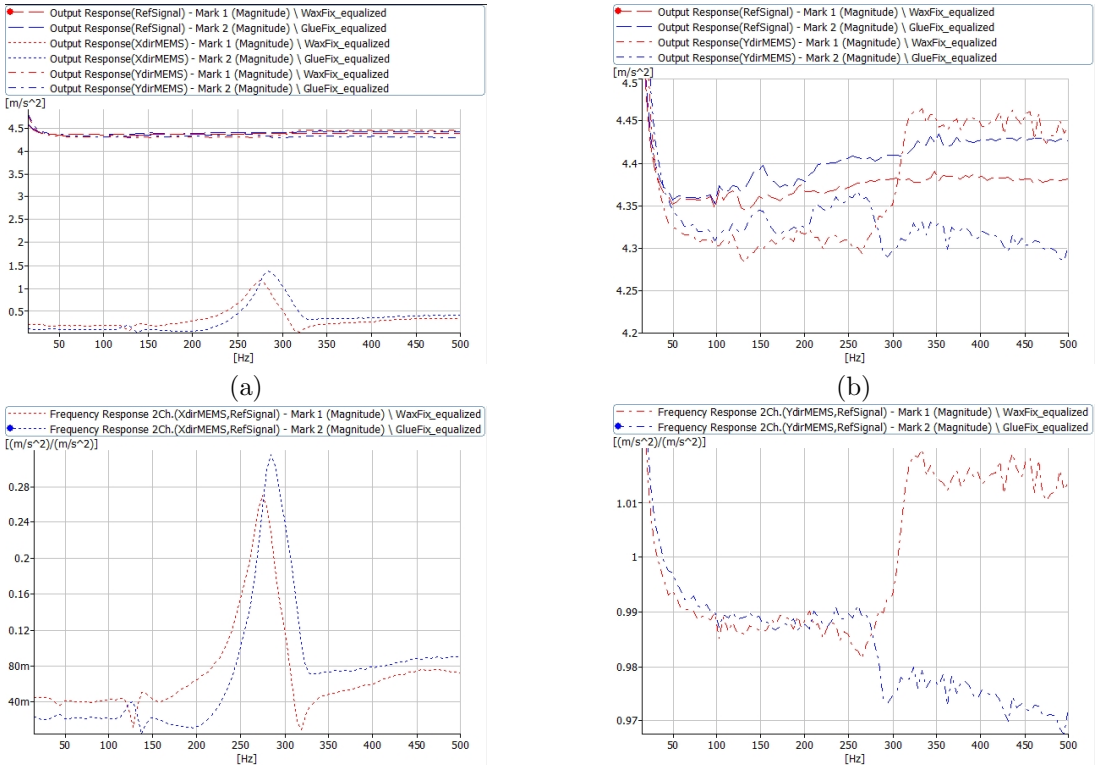

Fig. 7.6: (a) Output response for all the measured signals; (b) zoom of the output response on the excitation level; (c) frequency response of the signal measured in the MEMS' x-direction; (d) frequency response of the signal measured in the MEMS' y-direction. Red curves corresponds to wax fixation whereas blue represent the glued connection. Colour plots online.

Table 7.1: List of set-ups studied to verify the influence of the amount of wax employed.

Case	Fixation of Ref. Acc.	Acc. to be calibrated	Fixation of MEMS
MEMS with normal wax on B&K 8305	Screwed to shaker	MEMS no.40	Normal wax onto 8305
MEMS with minimum wax on B&K 8305	Screwed to shaker	MEMS no.40	Minimum wax onto 8305
MEMS with much wax on B&K 8305	Screwed to shaker	MEMS no.40	Much wax onto 8305

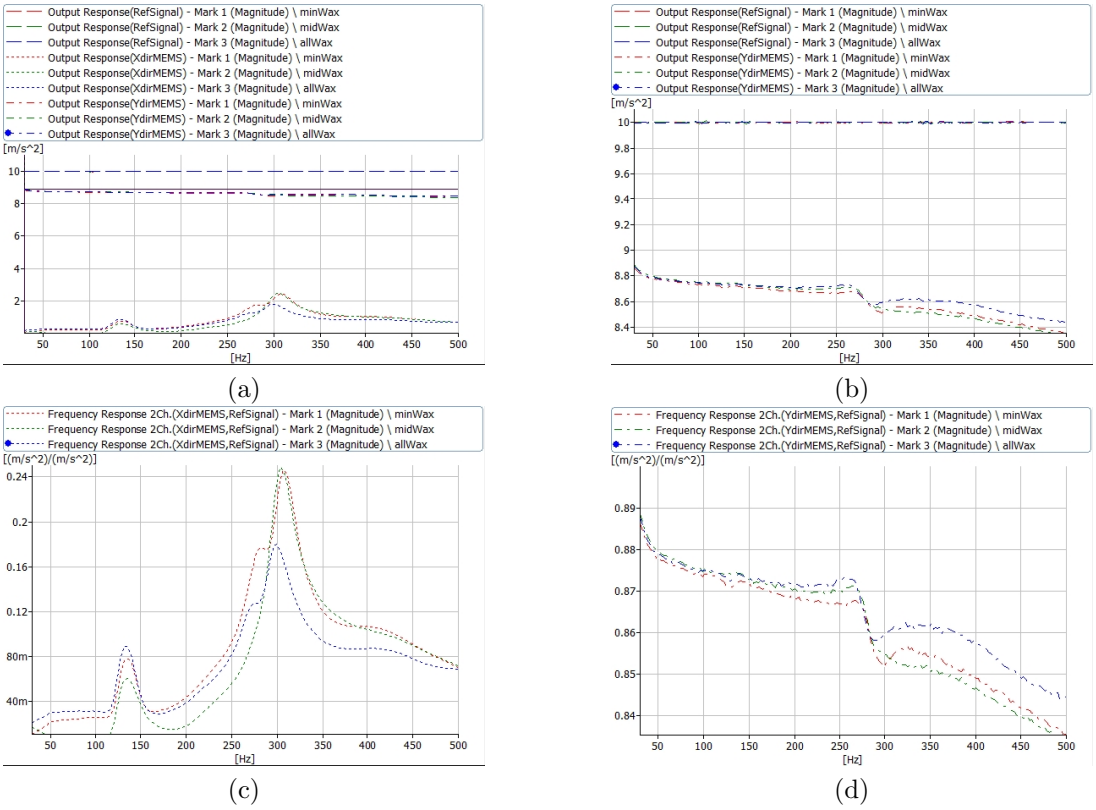

Fig. 7.7: (a) Output response for all the measured signals; (b) zoom of output response on excitation level; (c) frequency response of measured signals in the MEMS' x-direction; (d) frequency response of measured signals measured in the MEMS' y-direction. Red curves corresponds to thin ("minimum") wax layer thickness, green to medium ("normal") and blue to thick ("much") layer. Colour plots online.

more, assuming that wax behaves as a spring element, modifying the amount of wax should modify the local resonance (since the stiffness is changed). However, as it can be seen from Fig. 7.7d, the position of that local resonance is not detuned for the various wax layer thicknesses investigated.

7.2.5 Fixation to reference accelerometer / fixing directly on shaker

After observing that the local resonant behaviour remained the same despite of the type of fixation (glue and wax) and the amount of wax used between the reference and the MEMS accelerometer, it was decided to check whether or not this response came from the fixation of the B&K 8305 reference accelerometer to the vibration exciter as such. To that end, the MEMS was attached directly to the shaker using wax and analysed by comparing its response to the one of a smaller accelerometer B&K 4374. As a reference, the B&K 4374 was taken instead of the so far used B&K 8305 in order to check if its bulky shape and high weight could have been the reason for that local resonance at 280 Hz. The case just described where the MEMS accelerometer was attached directly onto the shaker and compared with a smaller reference accelerometer was also correlated with two already investigated cases (where the MEMS was attached either using wax or glue to the B&K 8305 reference accelerometer), see Fig. 7.8. The coupled pair of transducers was driven by a sine excitation up to 500 Hz and a excitation level of 10 m/s^2. The results obtained are shown in Fig. 7.9. The responses measured for MEMS waxed/glued onto the reference B&K 8305 showed again the local resonance occurring at around 280 Hz, as analysed in the previous measurements. Likewise, the some resonant behaviour is observed even for the small accelerometer B&K 4374 used instead of the B&K 8305, however it is shifted to frequencies above 500 Hz (i.e. out of measurement range).

From the shaker's data sheet (Bruel&Kjaer, 1972) (Fig. 4.2f), one can see that the shaker should have a resonance at around 160 Hz, which should not be responsible for the problems occurring at 280 Hz. For the cases where the MEMS accelerometer was fixed (using wax) directly on the shaker (Fig. 7.8b), one

(a) (b)

Fig. 7.8: Fixation of MEMS and small B&K 4374 on (a) reference one 8305; (b) directly on shaker.

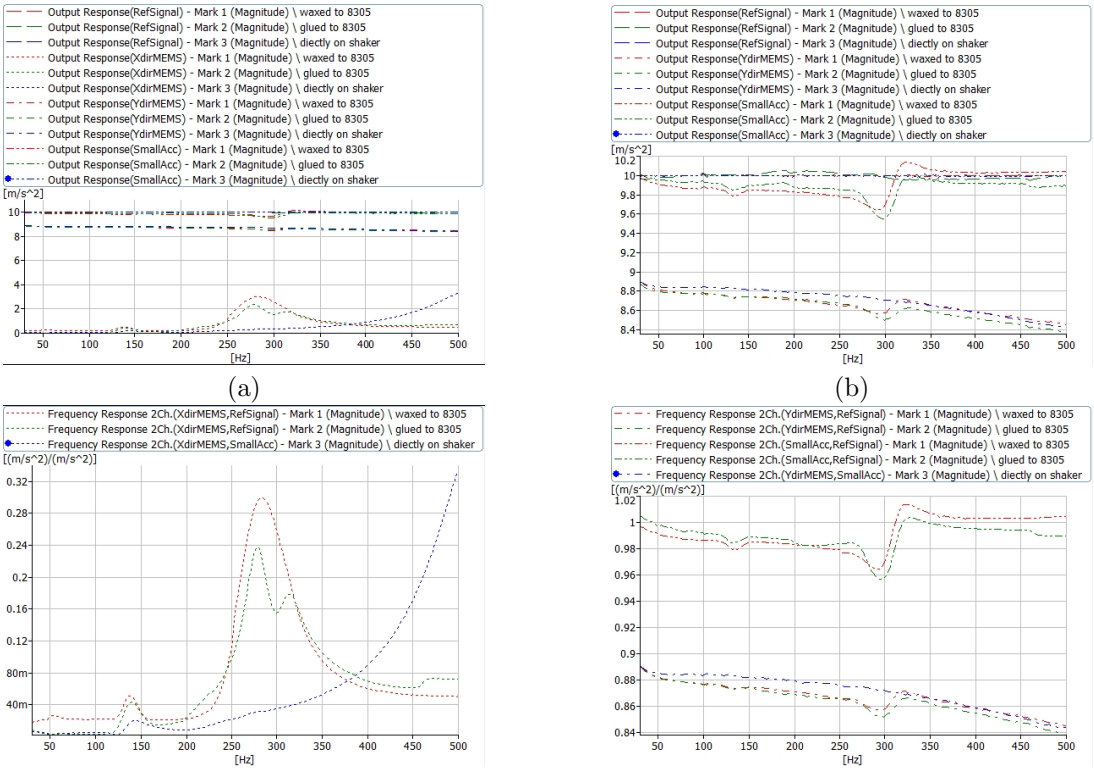

Fig. 7.9: (a) Output response for all the signals measured; (b) zoom of output response on excitation level; (c) frequency response of measured signals in the MEMS' x-direction; (d) frequency response of measured signals in the MEMS' y-direction. Red curves correspond to measurement with the MEMS waxed onto the B&K 8305, green ones to the glued MEMS onto the B&K 8305 and blue lines depict the response of the MEMS directly fixated onto the shaker (wax being used). Colour plots online.

can see that the resultant response (blue curves in Fig. 7.9b and d) are smooth up to 500 Hz. However, looking into the response in the $x-$direction (Fig. 7.9c), it seems that the local resonance is just detuned to the region above 500 Hz. This could point out at a problem having to do with the cable, since fixing the MEMS directly on the shaker made us change the cable fixation. Nevertheless, this needs to be investigated further[1].

All in all and at this stage, if calibration of the MEMS up to just 500 Hz is of interest, then fixation of the MEMS accelerometer directly onto the shaker could solve the problem with the resonant behaviour

[1] Actually, the "detuning of the local resonance" to 500 Hz can be partially observed in Fig. 7.12, where the local resonance is noticeable especially in the x-direction (non-directly excited). In the y-direction, there is some change in response noticeable around 500 Hz, but it is not so significant as for the measurements using the B&K 8305. In fact, it could be caused by also the cable of the MEMS. When the MEMS is fixed to the B&K 8305, the influence of the cable (which could also behave as a stiffness element) is larger. On the other hand, it does not answer the question of why the same behaviour is observed for the small accelerometer B&K 4374.

at 280 Hz. On the other hand, knowledge of what exactly causes this problem to assure why it happens would be beneficial so as to not run into such phenomena when eventually performing measurements.

7.2.6 Relative position of the MEMS with respect to the reference one

In order to investigate if the position of the centre of gravity of the MEMS accelerometer with respect to the reference accelerometer's position can have an influence on the resonant behaviour at 280 Hz, its location was varied, as shown in Fig. 7.10. Wax was used for fixation, as it was faster and simpler in order modify the set-up. The electrodynamic shaker was used for excitation in form of a stepped sine up to 500 Hz.

As shown in the results of Fig. 7.11b, i.e. for the position 3, (Fig. 7.10c), the amplitude at 280 Hz is the largest. All in all and comparing all results in Fig. 7.11, the behaviour at 280 Hz is still present for all cases. The resonant behaviour is lessened for position 1, where the MEMS chip should be aligned with the axis of the B&K 8305 (Fig. 7.10a). Nevertheless, it can be concluded that the location of the MEMS accelerometer with respect to the reference accelerometer is not directly responsible for the resonant behaviour at 280 Hz either. However, it does to some extent affect the response of the MEMS transducer, position 1 being the recommended option.

(a) (b) (c)

Fig. 7.10: Relative position of the MEMS accelerometer with respect to the reference one (B&K 8305): (a) position 1; (b) position 2; (c) position 3.

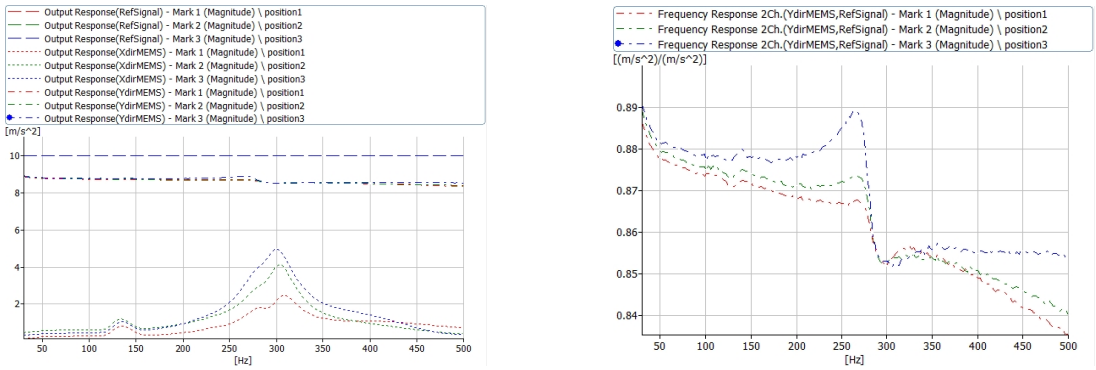

(a) (b)

Fig. 7.11: (a) Output response of all 3 channels (reference signal, MEMS' x- and MEMS' y-direction) and (b) frequency response in the y-direction for the three different positions shown in Fig 7.10. Colour plots online.

7.2.7 Influence of vibration amplitude

The aim of the studies presented in this section is to see to which extent the response of the MEMS transducers is linear. To that end, the variation on vibration amplitudes was assessed. The excitation levels coming out from the shaker were varied from 1 m/s^2 to 10 m/s^2 (set as the "calibration level") in steps of 1 m/s^2. The bandwidth was increased from 50 Hz to 1.5 kHz in order to see the behaviour also at higher frequencies.

The results for the MEMS transducer no.40 are shown in Fig. 7.12, the reference accelerometer used being the B&K 4374. In an ideal case (a linear behaviour of the transducers), the FRFs would be independent of the "calibration level". However, as seen from Fig. 7.12, this is not the case here, i.e. there is some source of this non-linear behaviour present in the measurement chain. According to the data sheet (Analog Devices, 2010), the measuring range is up to 1.7 g (i.e. approx. 16.7 m/s^2), which is way above the maximum level used in tests presented here (10 m/s^2). Thus, the fixation of the MEMS transducer, the casing or cabling could possibly be the responsible for these variations. On the other hand, as discussed earlier, the MEMS' fixation could be ruled-out, since neither the type (wax/glue) nor their amount or a position of the transducer would indicate that is responsible for the local resonance.

From the results obtained for the indirectly excited direction (Fig. 7.12b), a resonant behaviour can still be noticed at around 550 Hz. This could be explained by the stiffness of the support being modified.

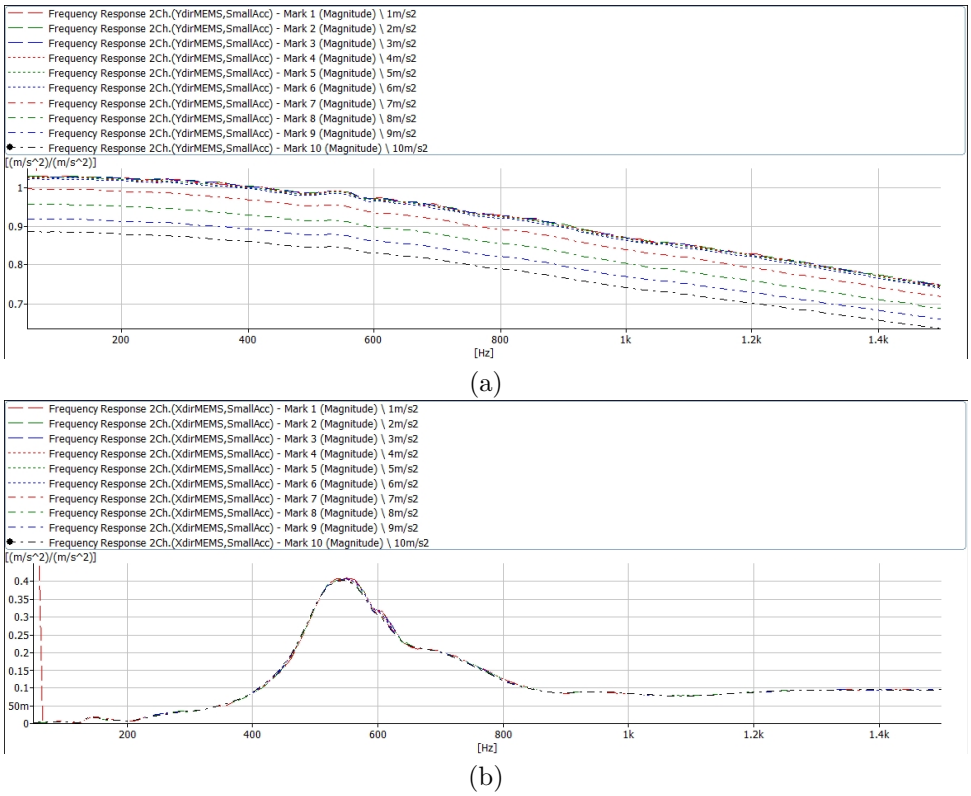

Fig. 7.12: Frequency response of the signal measured in the MEMS' y-direction, where a small accelerometer B&K 4374 is taken as reference: (a) for $y-$direction (excitation direction); (b) for $x-$direction. Colour plots online.

7.3 Calibration of piezo accelerometers

In order to figure out if the problem with the local resonance at 280 Hz is related to the MEMS accelerometer or to other apparatus used, piezoelectric sensors were used instead of the MEMS in this section; the back-to-back calibration being carried out in the same fashion as in the previous tests between combinations of reference and test accelerometers as explained in the subsequent sections.

7.3.1 Accelerometer B&K 4374 to be calibrated using B&K 8305 as reference

First, a small accelerometer B&K 4374 is studied as the accelerometer to be calibrated. As shown in Fig. 7.13 and listed in Table 7.2, three different arrangements are compared. The results are presented in Fig. 7.14. The FRFs (Fig. 7.14b) reveal that at around 280 Hz there is still a significant change of the response, i.e. the curve is not smooth throughout the whole frequency bandwidth analysed. It seems that the fixation is not stiff enough to avoid problems at 280 Hz, even when not using the MEMS accelerometer. Furthermore, the wax seems to perform worse, which could turn into fixation problems.

Table 7.2: List of compared set-ups with B&K 4374.

Case	Fixation of Ref. Acc.	Acc. to be calibrated	Fixation of acc.
B&K 4374 waxed to B&K 8305	screwed to shaker	B&K 4374	Waxed to B&K 8305
B&K 4374 glued to B&K 8305's stud	screwed to shaker	B&K 4374	Glued to stud B&K 8305
B&K 4374 glued to B&K 8305's washer	screwed to shaker	B&K 4374	Waxed to B&K 8305

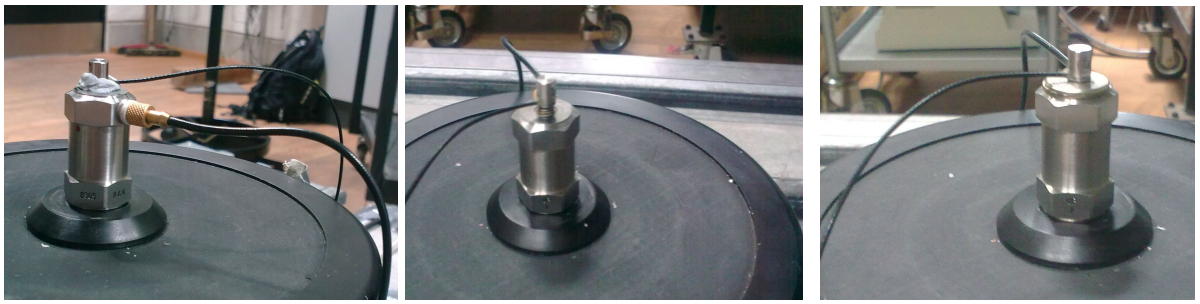

(a) (b) (c)

Fig. 7.13: Fixation of the B&K 4374 to B&K 8305 using: (a) wax; (b) glued to stud; (c) glued to plate.

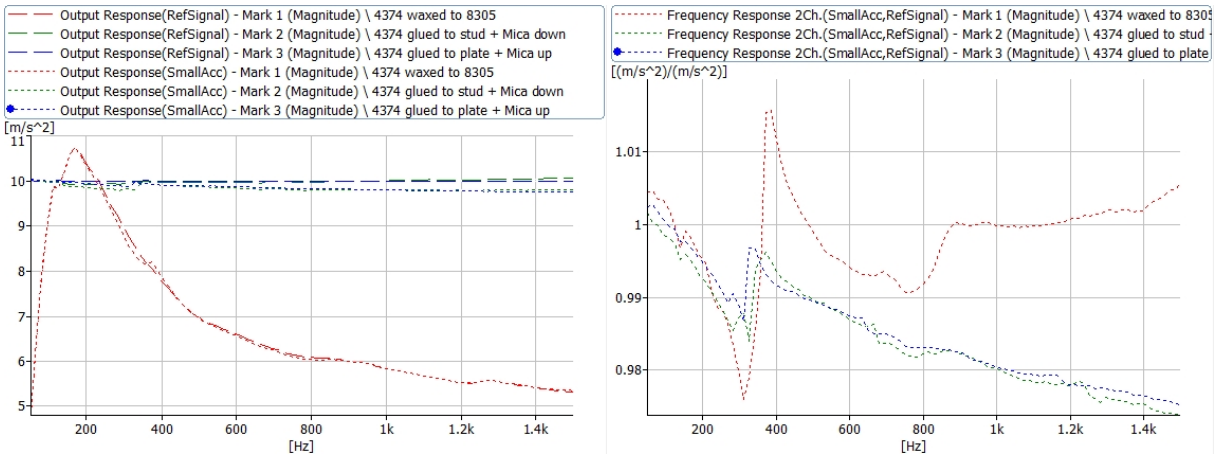

(a) (b)

Fig. 7.14: Output response (a) and FRF (b) measured for the B&K 4374, waxed or glued to the B&K 8305.

7.3.2 Accelerometer B&K 4371 calibrated with B&K 8305 and a mica washer

In order to check if any difference in the behaviours could be detected, the accelerometer B&K 4371 was attached to the reference one (B&K 8305 in this case). Furthermore, a different contact type between the reference and the investigated accelerometer was checked to see if it does influences the response. To that end, a mica washer was introduced in between both transducers (Fig. 7.15a). In Table 7.3, the different measurements performed are listed.

The results presented in Fig. 7.16 depict that the mica washer is not helping to solve the problem with the response at 280 Hz. In fact, its influence is counterproductive, i.e. it introduces a non-ideal surface and thus the problem at 280 Hz is enhanced. Thus, the use of mica washers is not recommended at all to perform this type of calibrations.

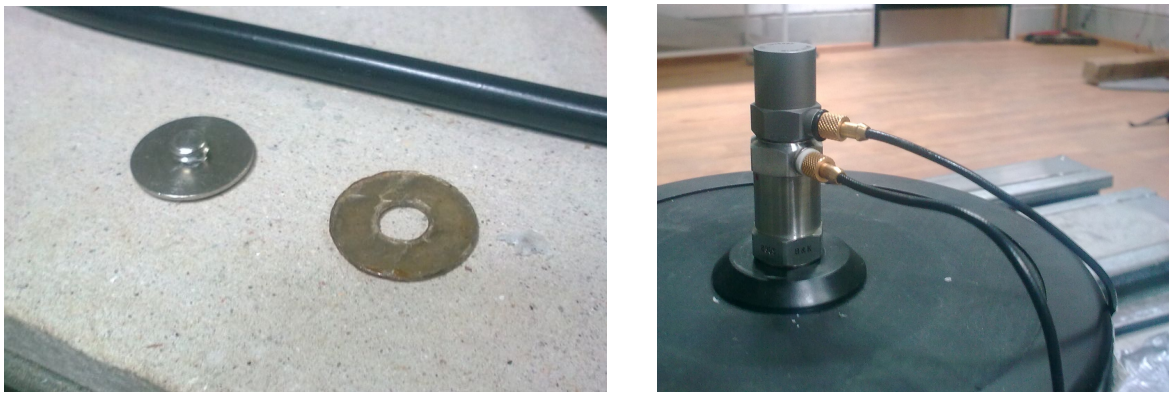

(a) (b)

Fig. 7.15: (a) Disk plate and a mica washer; (b) B&K 4371 on the top of B&K 8305.

Table 7.3: List of set-ups with the accelerometer B&K 4371 and a mica washer.

Case	Fixation of Ref. Acc.	Acc. to be calibrated	Fixation of acc.
B&K 4371 screwed to B&K 8305	screwed to shaker	B&K 4371	Waxed to B&K8305
B&K 4371 screwed to B&K 8305 one mica washer	screwed to shaker (mica washer in-between)	B&K 4371	Screwed to B&K 8305
B&K4371 screwed to 8305 two mica washers	screwed to shaker (mica washer in-between)	B&K 4371	Screwed to B&K 8305 (mica washer in-between)

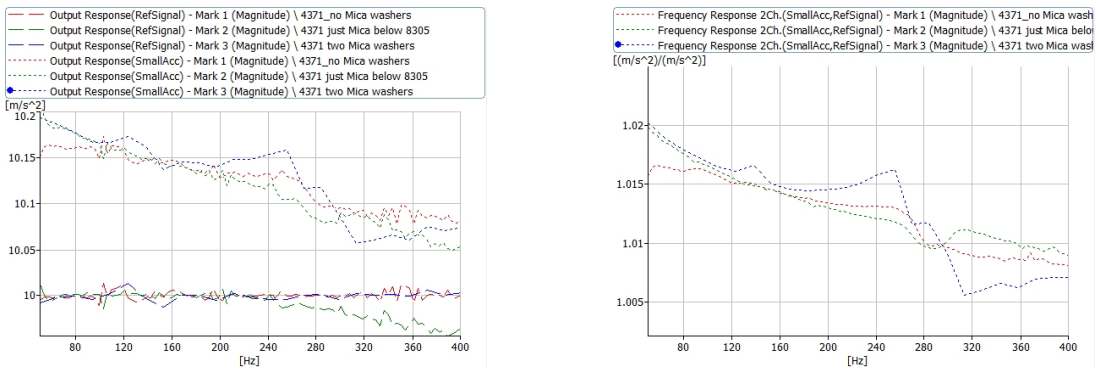

(a) (b)

Fig. 7.16: Output function (a) and frequency response (b) measured for the B&K 4371 and the B&K 8305, with or without mica washers. Colour plots online.

7.3.3 Accelerometer B&K 4374 calibrated using B&K 4371 as reference

Further tests were performed to analyse if the fixation of the accelerometer to the previously used as reference B&K 8305 is the cause of the local resonance. In the test performed here, the B&K 4371 was used as reference against the B&K 4374, two fixation types being compared: (a) using wax and (b) employing glue (cf. Fig. 7.17 and Table 7.4).

The results are presented in Fig. 7.18. It can be seen, that the local resonance around 280 Hz is still present (similarly as when the B&K 8305 was used as the reference accelerometer); the latter implying that the issue investigated here is not the cause of it.

Table 7.4: Studied set-ups with the accelerometer B&K 4371 as a reference.

Case	Fixation of Ref. Acc.	Acc. to be calibrated	Fixation of acc.
B&K 4374 waxed to B&K 4371	screwed to shaker	B&K 4374	Waxed to B&K 4371
B&K 4374 glued to B&K 4371	screwed to shaker	B&K 4374	Glued to B&K 4371

(a) (b)

Fig. 7.17: A small accelerometer B&K 4374 attached to B&K 4371, used as reference, with: (a) wax; (b) glue.

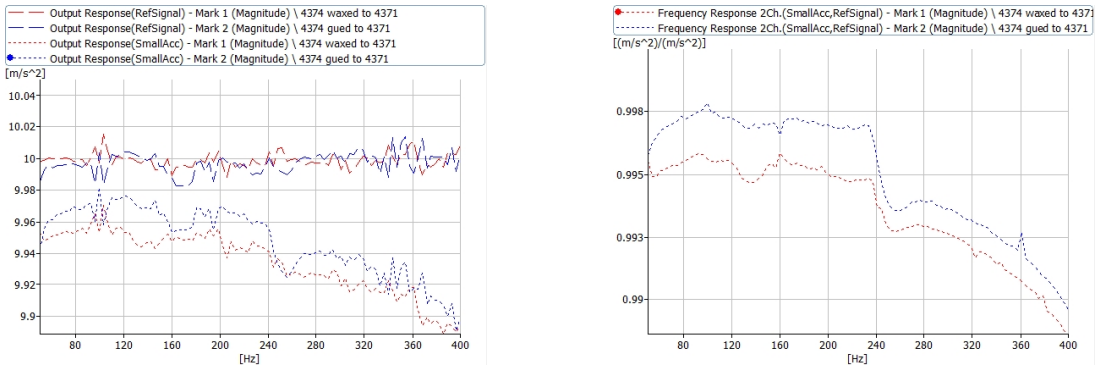

(a) (b)

Fig. 7.18: Output function (a) and frequency response (b) measured for wax (red) and glue (blue) fixation. Colour plots online.

7.4 Cable fixation

As noted in Section 2.2.3, the cable should be correctly attached to the shaker in order to avoid unwanted influences on the measurements. Thus various arrangements were tested, the results being summarised in the subsequent sections.

7.4.1 Piezo accelerometer

With the piezo accelerometer B&K 4371 fixed on the reference one (B&K 8305), three cases are compared Fig. 7.19: (a) old measurement set-up with free attachment of the cables and location of the shaker on the concrete block; (b) cables fixed using a wax and (c) cable fixations performed using a hot glue gun, which should ensure firm attachment. As can be seen in Fig. 7.19b, the fixation type of cables as such does not have any marked influence on the outputs recorded. On the other hand, together with the different fixation, the shaker as such was moved between the measurements from the concrete block to the floor. And the latter alternation does have a bigger impact, as will be discussed later in Section 7.5.1.

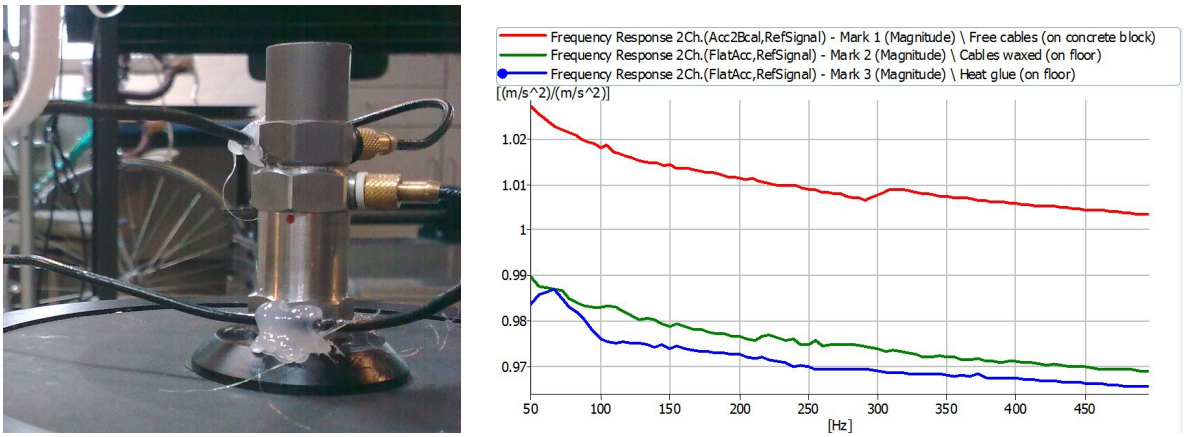

(a) (b)

Fig. 7.19: (a) Fixation of cables using a hot glue gun; (b) measured FRFs. Colour plots online.

7.4.2 MEMS accelerometer

The same type of tests as in the previous section were performed, this time attaching the MEMS accelerometer instead of the piezo on top of the reference one (B&K 8305). Again, three cases are compared (Fig. 7.20): (a) cables are hanging freely; (b) cables being taped to the reference accelerometer using a duct tape and (c) cables glued (as recommended in the standard (ISO, 1998)), hot glue being used.

The results (cf. Fig. 7.21) point out that the problem could lie in the balancing of the MEMS accelerometer and/or in the thickness of the cable involved, since neither of the cable fixation methods used is solving the problem with the unwanted response around 280 Hz. Even the firmer attachment did not help to solve the problem. Therefore, it could be interesting to test the MEMS with a thin cable in order to lessen the effect of the cable thickness (i.e. cable stiffness).

7.5 Verification of shakers

It was our belief that the measurement results can be influenced also by the electrodynamic shaker involved in the tests, and especially by its inherent dynamic characteristics or location during the test. The aim here is to investigate issues related to the shakers used.

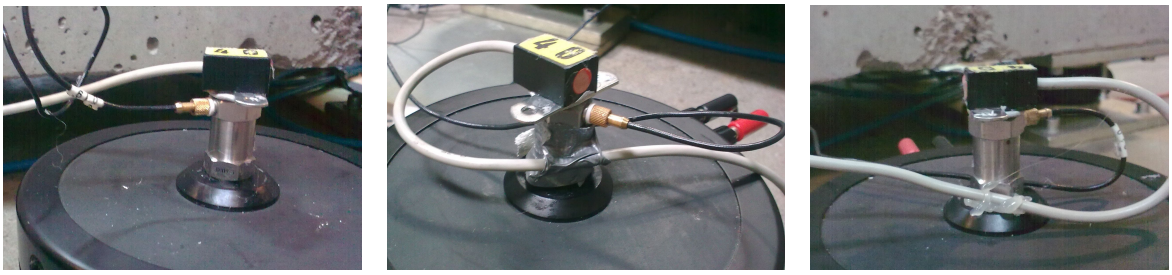

(a) (b) (c)

Fig. 7.20: (a) Cables freely hanging; (b) cables taped using duct tape; (c) cables glued using a hot glue gun.

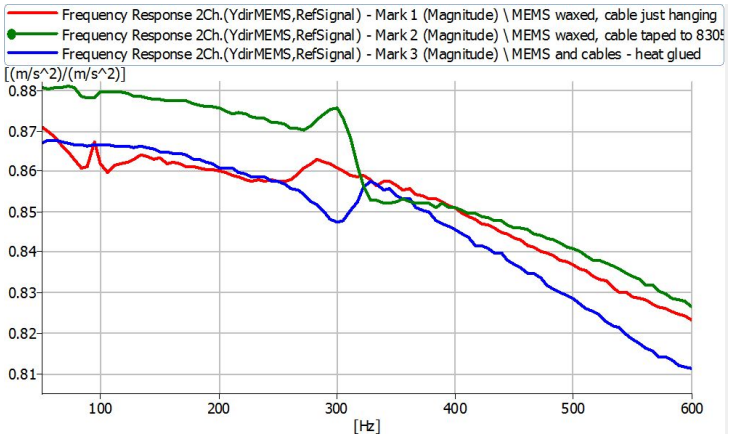

Fig. 7.21: Resultant FRFs for all three analysed cases. Colour plots online.

7.5.1 Shaker's location

In most of the calibrations performed thus far, some non-ideal behaviours were observed at around 280 Hz and the cause of it must be investigated. Therefore, two cases were compared here: (a) a shaker located on top of a concrete block laying on air-springs, which in principle was supposed to eliminate the environmental vibration and (b) the shaker being place directly on the laboratory floor. The results are shown in Fig. 7.22d. Based on those results, it is recommended not to use a concrete block on air springs, but rather just to put the shaker directly on the rigid concrete floor. Possible rocking motion is then not emphasised, which can be the case when locating the shaker on the concrete block.

7.5.2 Shaker used

At AAU's laboratory, two shakers were available at the time of the measurements. As it can be seen in Fig. 7.23, the two responses are not equivalent. One shaker experiences an "additional resonance", even though the same set-up and boundary conditions (cable fixations) were used. After contacting B&K regarding this issue, their response on shakers' comparison was the following (Plechinger, P.L., 2011):

```
The response from our expert team to your shaker comparison is the following:
This resonance is due to the combination of the table head mass and the stiffness
of the spring suspending the mass. If the spring and the table (which are circular)
were fully symmetrical without any eccentricity, there would theoretically be
a single resonance peak. Because of non-symmetry in the production process,
this is to be expected. However, if one was using a
control loop, this would not make any difference.
```

Thus no other action was taken at this stage and the difference was taken as an inherent problem, a feedback loop control being recommended if possible.

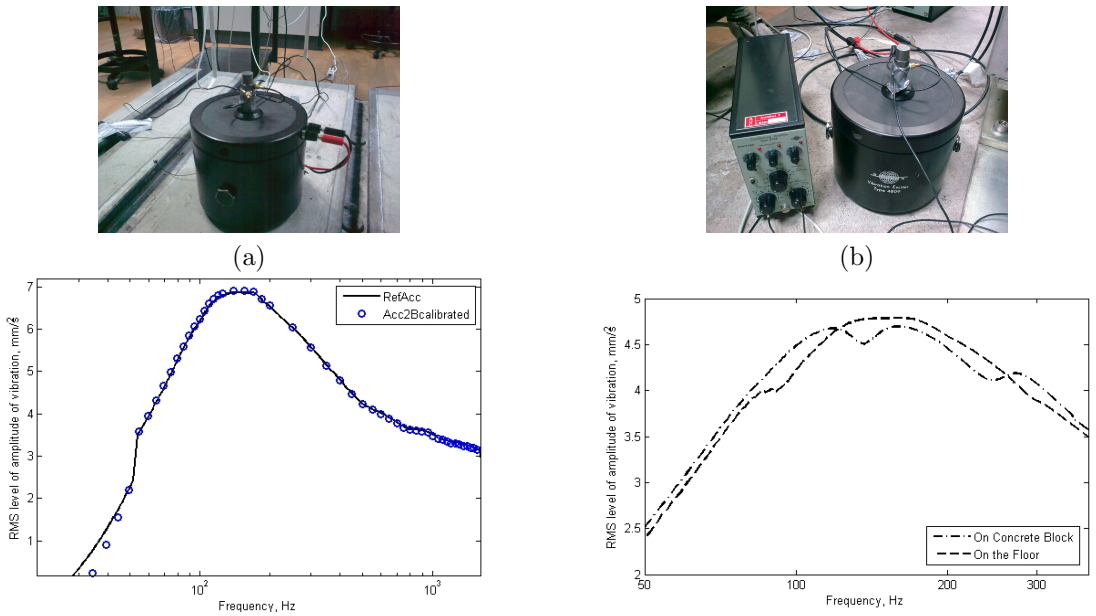

Fig. 7.22: Location of the shaker (a) on the concrete block; (b) on the floor; (c) first results from shaker calibration test located on the table (Section 6.1); (d) comparison of shaker calibration tests located on a concrete block and floor.

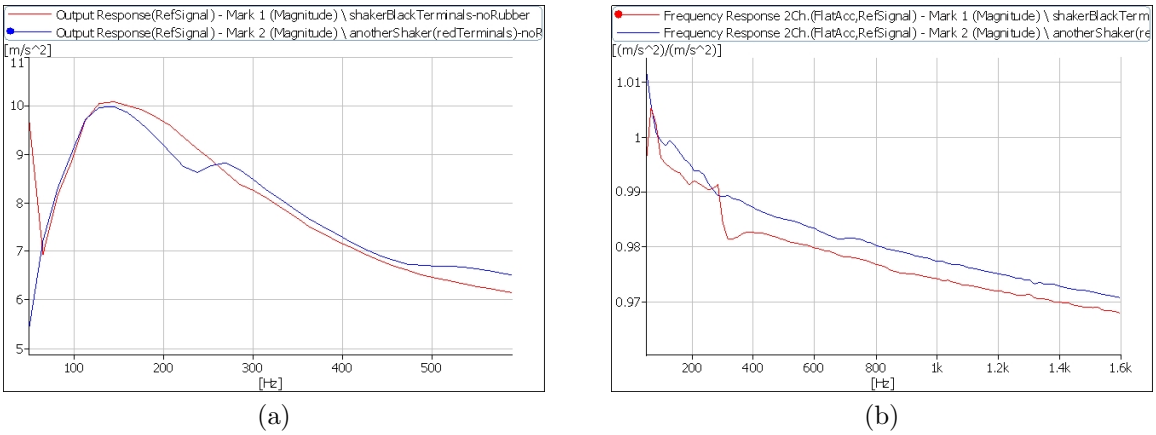

Fig. 7.23: Comparisons of responses measured at two different shakers. Colour plots online.

7.6 Signal clipping

It was also observed that at amplitudes above approximately 8 m/s^2, the time signal is "clipped" at the top (Fig. 7.24a). On the other hand, for low acceleration levels (Fig. 7.24b) clipping does not occur. The latter could be caused by the fact that the amplitude of static and dynamic components exceed the maximum voltage to be sent to PULSE. However, PULSE is capable to accept 7.071 V_{peak} (Bruel & Kjær, 2008) and the clipping 43.323 m/s^2 corresponds to 4.4195 V_{peak}, which is way below the PULSE limit input peak voltage. The reason for the latter issue could be that the accelerometer no.40 has a measurement range only up to 1.7 g (cf. Table 3.1), and since we measure in the horizontal direction, the signal to be measured is superimposed over the constant acceleration due to gravity (of value 1 g). Thus, in the next tests, the accelerometer no.40 was not used and only the one with lower sensitivity (no.8) was tested so as to lessen this effect.

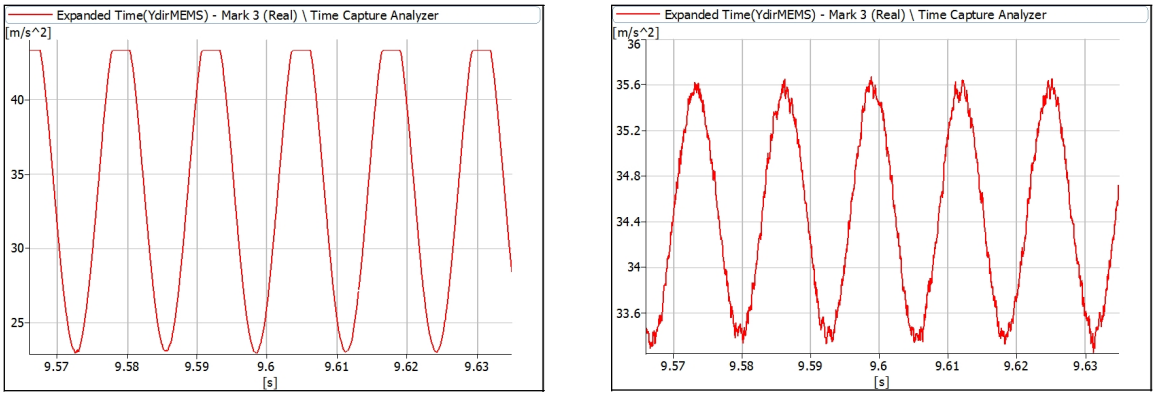

(a) (b)

Fig. 7.24: Time capture of the non-filtered time signal from the MEMS accelerometer for excitation level: (a) 10 m/s^2 and (b) 1 m/s^2.

7.7 Linearity of the MEMS transducer

After figuring out that the MEMS accelerometer no.40 experiences some clipping at higher accelerations, the MEMS accelerometer no.8 was employed instead (the one with no clipping observed). Then, the linearity in terms of response at different amplitudes of acceleration was re-analysed[2]. The MEMS was directly glued onto the shaker (hot glue being used) and the small B&K 4374 accelerometer was used as the reference (also being attached on the top of the MEMS using a hot glue gun, as shown in Fig. 7.25a). A stepped sine excitation up to 1.5 kHz was sent out from the shaker to perform the calibration.

As can be seen from Fig. 7.25b, the behaviour at different excitation levels is approximately the same. The ripples at very low level (3 m/s^2) were caused by combination of low precision of the SSR and the lower signal to noise ratio (the dynamic range was not tuned after each change of level, in order to speed up the measurements). These results are in contradiction with the tests analysed in Section 7.2.7. However, as previously pointed out in Section 7.6, the MEMS no.40 used in Section 7.2.7 exhibited some signal clipping, which could be responsible for the non-linear behaviour.

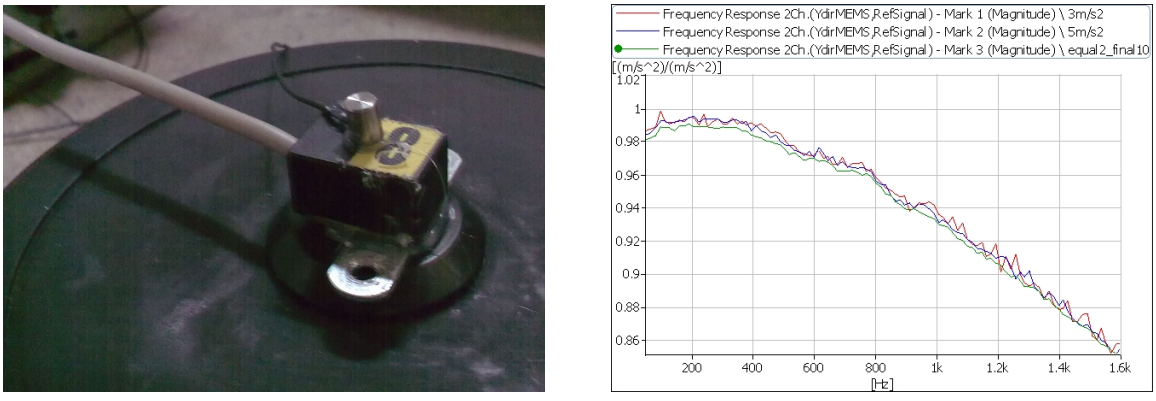

(a) (b)

Fig. 7.25: (a) Reference accelerometer B&K 4374 glued to the top of the MEMS to be calibrated; (b) FRFs measured. Colour plots online.

[2]The measurements presented in Section 7.2.7 were carried out using the transducer no.40, for which clipping occurred. Thus, the re-measurement was performed.

7.8 Reproducibility of measurements

Even when using the same set-up, the same responses had not been recorded throughout the report thus far in some cases. This points at some potential problems concerning reproducibility. Simply by playing with the position of the string support of the cable, some improvement was achieved, however still the re-measurements did not lead to the same responses (cf. Fig. 7.26). The problems could be caused by the fact that the cable is rather thick and stiff, embedded and clamped into the accelerometer's body. There were some attempts to fix the cabling as recommended (discussed in Section 7.4), but the string was too stiff and the glue too soft so it would not hold firmly. The problem with cabling, a potential cause for the resonant behaviour as well as for lack of reproducibility will be addressed later on by using a bare MEMS chip with thin and flexible cables (i.e. with no casing).

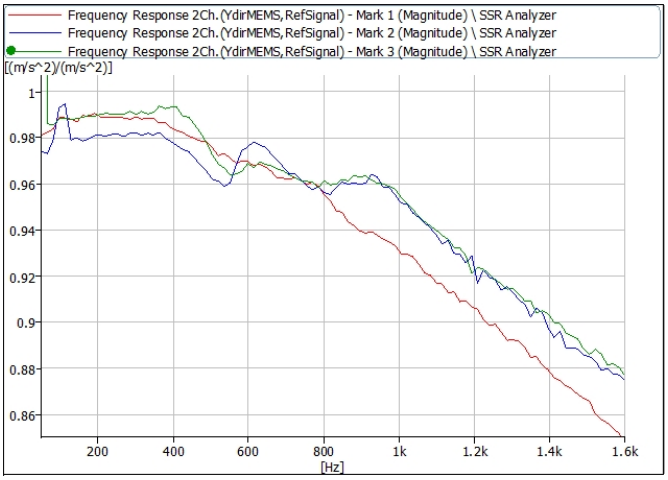

Fig. 7.26: Checking reproducibility: Mark 1 - measurements on shaker with black terminals; Mark 2 - using shaker with red terminals; Mark 3 - returning to the shaker with black terminals. Colour plots online.

7.9 Steady-state response vs. Sine sweep excitation

Further measurements comparing the SSR approach and the sine sweep one were done in order to see if the excitation method used could influence the results obtained. The tests were done with the reference accelerometer calibrated (where for the sine sweep measurements the gain was set in the post-processing, since it was forgotten to be set during measurements).

For the first set of tests done (Fig. 7.27) the responses obtained from SSR correspond with the data measured for sine sweep excitation. When the sine sweep test was re-measured, some differences were observed, as presented in Fig. 7.28. This can be caused by a pre-amplifier drift (the B&K 2635 was used) or some environmental conditions which would cause the change of calibration constant used. However, it is recommended to re-run the measurement with properly calibrated reference accelerometer (using calibrator) and/or try another pre-amplifier (e.g. more noisy but probably stable Charge-to-DeltaTrons).

7.9.1 Sine sweep settings

Using sine sweep measurements and FFT analyser recording the data into the multi-buffer for each period of time, some ripples were present in the autospectra measured. Thus, some verification was carried out as well. As shown in Fig. 7.29a-c, the effect is independent of the shakers, accelerometer or pre-amplifier used; however it was found, as presented in Fig. 7.29d, that using averaging, the problem is solved. Moreover, it was recommended to use peak averaging instead of the multi-buffer analysis for future tests.

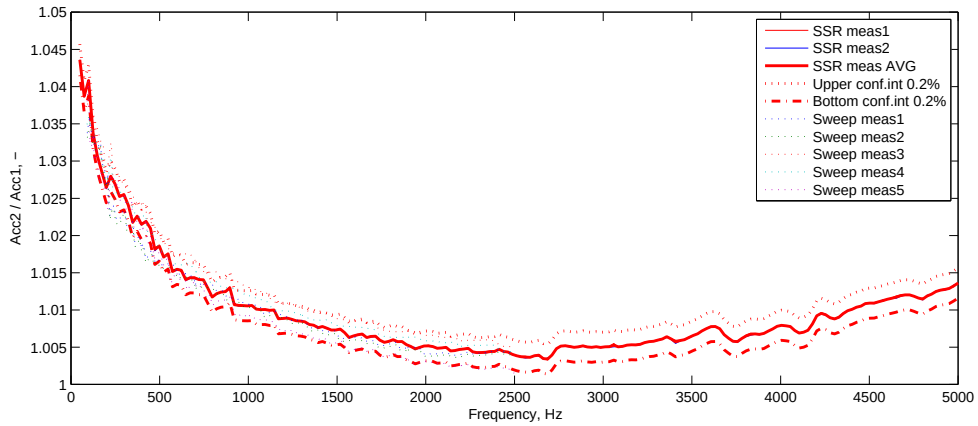

(a)

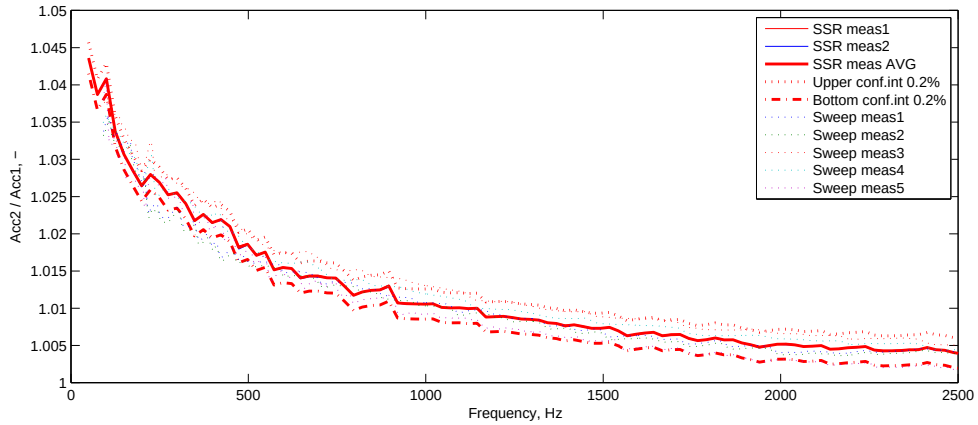

(b)

Fig. 7.27: Comparison of SSR and sweep results: (a) up to 5 kHz; (b) zoom to 2.5 kHz. Colour plots online.

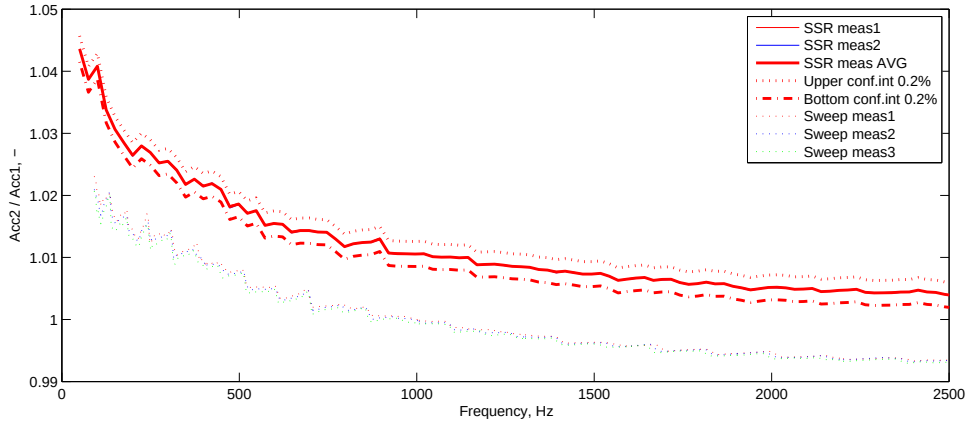

Fig. 7.28: Comparison of SSR measurements (old set) and re-measuring the sine sweep measurements (new set). Colour plots online.

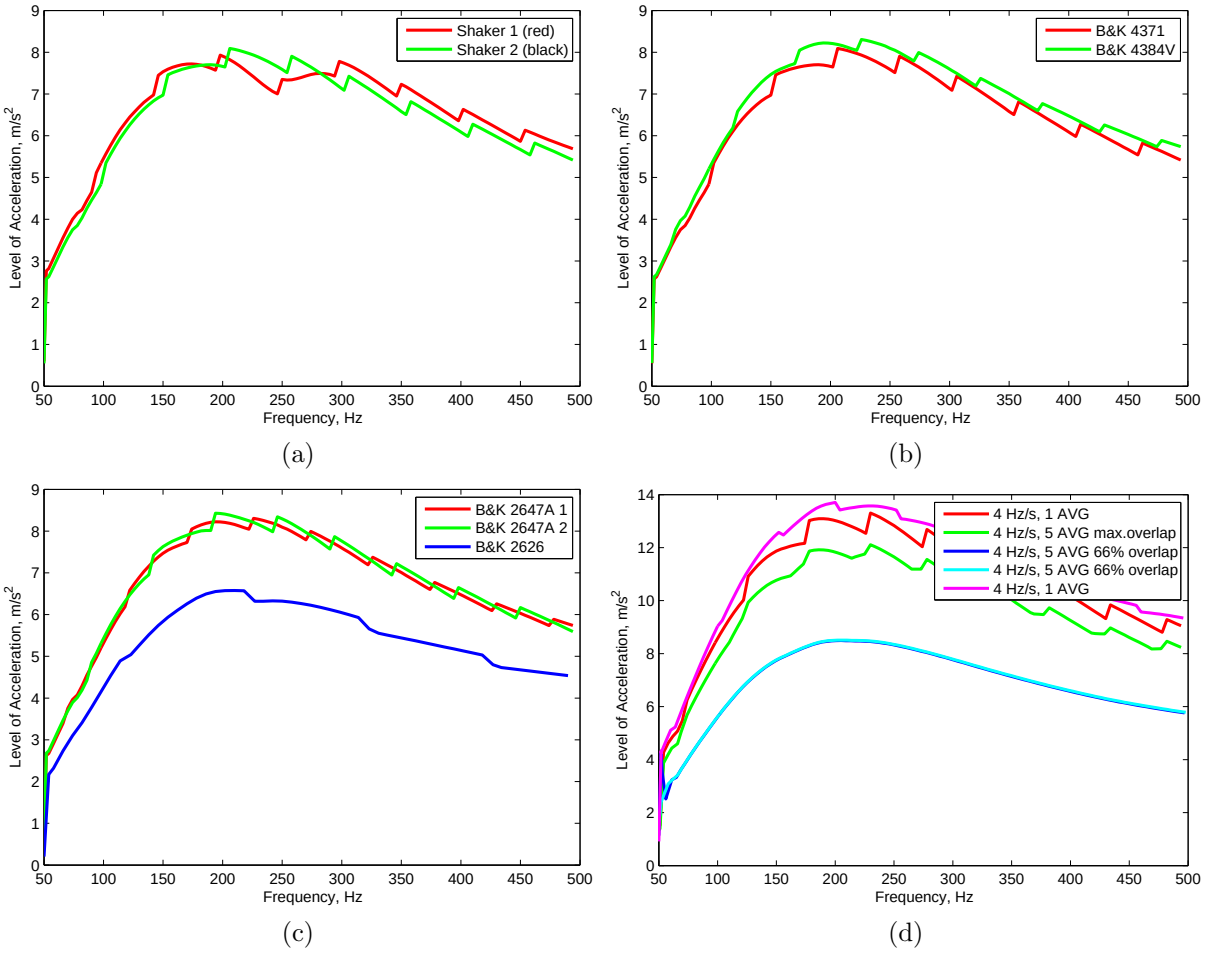

Fig. 7.29: Autospectra measured changing (a) the shaker; (b) accelerometers; (c) accelerometer's pre-amplifiers; (d) varying the averaging. Colour plots online.

7.10 Conclusions

In order to idealise the excitation, an SSR license was used. It did not ensure the full feedback loop control, yet the stepped sine excitation was providing (more or less) constant excitation level during the test. Thus, the two MEMS accelerometers were tested, the problem with the resonant response at 280 Hz being still observed and tracked when altering the position, type of fixation or even the type of reference transducer. The direct cause of this misbehaviour was not identified in this chapter; however, it was recommended to locate the shaker on the floor as well as changing the cabling for the MEMS accelerometer due to its thickness. Furthermore, the traducer no.40 should not be used due to clipping problems.

8

Sine Sweep Measurements using a vibration controller

After the purchase of the vibration controller B&K VC-LAN 7541 (Fig. 4.1c) by AAU, measurements were performed using a closed feedback loop control, which was supposed to idealise the measurement scenario and therefore improve the results. The controller is capable to adjust the amplitude of vibration on-line, which was not possible using the SSR employed in the previous chapter (it relied on the response recorded during the equalisation process). Also the measurement process is faster comparing to the SSR, since no equalisations are required. The test carried out alongside their results are presented in this chapter.

8.1 Sine sweep settings

Firstly, a set of back-to-back calibration measurements with a fixed acceleration amplitude were performed, two different types of sweep rate being compared:

- Linear sweep at a rate of 10 Hz/s and 20 Hz/s.
- Logarithmic sweep at a rate of 2.5 oct/min and 5 oct/min.

In B&K PULSE LabShop, the FFT analyser was set to Peak averaging in order to capture just the response at the excitation and thus avoiding problems with the multi-buffer discussed in Section 7.9.1. Moreover, in order to reduce the noise in the measured responses, overlap was chosen as "Max" when the curves were smooth. Zero overlap was not tested, but for 66.6% as well as for 75%, the signal was still noisy.

The FRFs (H1[1] being the one plotted) are presented in Fig. 8.1. It can be seen that except for the case `linSweep20Hz/s` (i.e. linear sweep at rate 20 Hz/s), good agreement between the FRFs is obtained. The 20 Hz/s case needs to be re-measured.

From the FRFs, it can also be noticed that there are no longer troubles at 280 Hz as observed in the previous tests. The response curve is relatively smooth for all cases. The frequency dependence of the FRF (ideally the response of the accelerometers should be independent of the frequency) can be caused by the reference accelerometer's response (B&K 4371 was used as the reference, its response being presented in Fig. 4.2c), or due to the accelerometer to be calibrated. With the reference accelerometer B&K 8305, the possible frequency dependence will be caused purely by the calibrated accelerometer.

The autospectrum is the representation of the signal's energy during the measurement period. Thus, as shown in Fig. 8.2, it is dependent on the sweep rate, since for slower sweeping more energy is "collected" within the measurement period than for the faster one. Also, the type of sweep influences the autospectrum. Using the FFT (frequency bands of constant frequency width), the logarithmic sweeping will cause exponential shape of the autospectra (it is slower at low and faster at higher frequencies)[2]. On the other hand, the FRFs are independent of the type of excitation, since it takes the ratio of the two signals which are exposed to the same excitation at each frequency (and so it does not see the sweep type).

[1] As a reminder, an FRF is defined as the ratio between the output Y(f) and input X(f) of a system in the frequency domain. In situations where the output of the system is expected to be noisier than the input, an FRF H1, defined as the ratio of the cross spectral density in the frequency domain of the input X(t) and the output Y(t) -denoted as S_{xy}- by the auto spectral density in the frequency domain of the input X(t) -denoted as S_{xx},is used instead.

[2] The peaks around 1 kHz visible in Fig. 8.2a-b are caused by some troubles with the finish of sweeping, which after reaching 2 kHz continued down to 1kHz when stopped. This problem was solved in future tests.

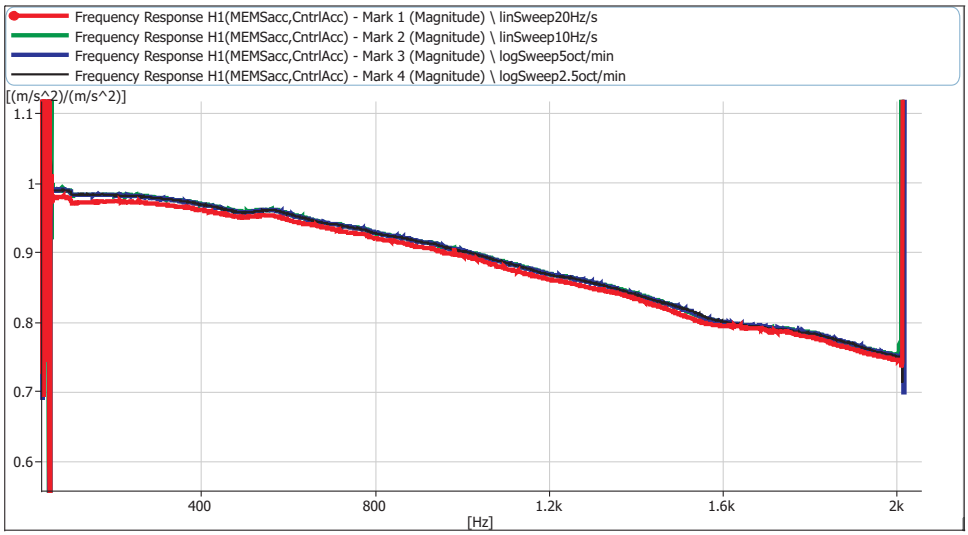

Fig. 8.1: Comparisons of all measured FRFs H1. Colour plots online.

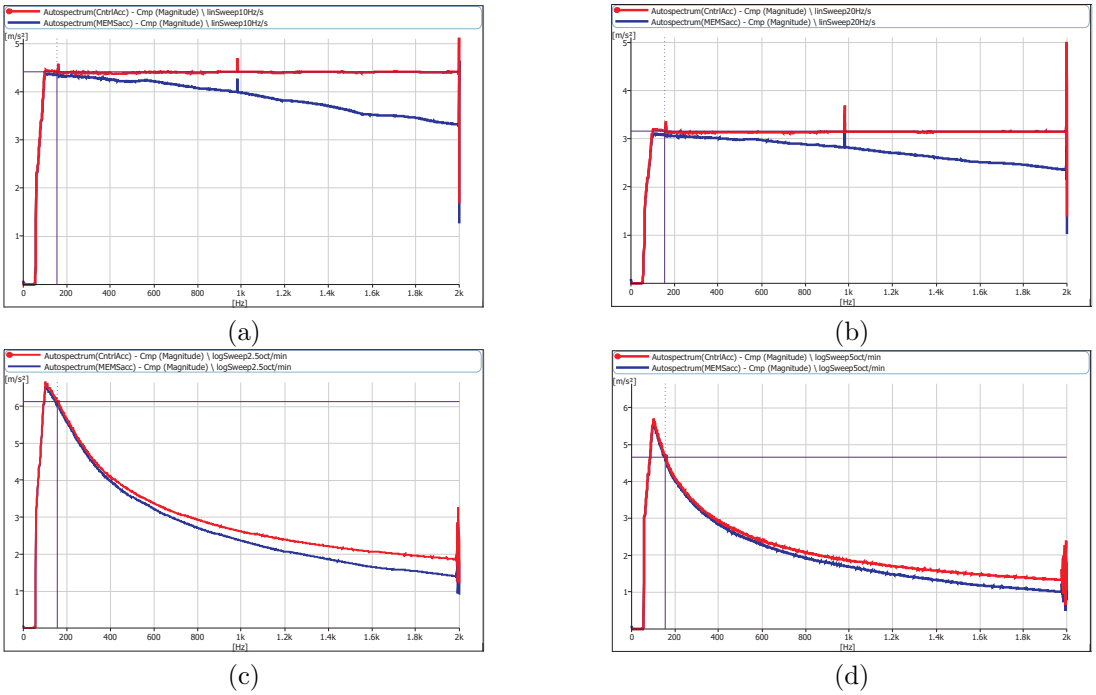

Fig. 8.2: Autospectra functions for control and MEMS accelerometers: (a) linear frequency sweep at rate 10 Hz/s; (b) linear frequency sweep at 20 Hz/s; (c) logarithmic frequency sweep at 2.5 oct/min; (d) logarithmic frequency sweep at 5 oct/min. Colour plots online.

8.2 Sine sweep vs. single sine excitation

To verify whether or not sine sweep measurements can provide the same results as single frequency measurements, and hence prove that sine sweep can be used instead of the sine excitation, four different types of sweep excitations were compared with the excitation at single frequencies. As for the sine sweep, the sweep rates as well as the sweep types (both linear and logarithmic), were varied.

As shown in Fig. 8.3, neither the sweep rate nor the sweep type affects the frequency response (FRF H1 estimate is of interest here). Also and more importantly, the responses obtained for the single frequency excitation agree with the sine sweeps, i.e. the sweep measurement can be used instead of series of pure sine excitations. In doing so, the calibration process can be markedly sped up.

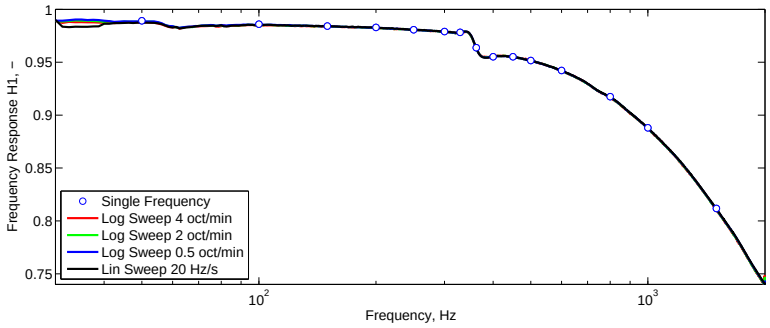

Fig. 8.3: Frequency response function H1 for the different sweeps under study (Log - logarithmic, Lin - linear) and a single frequency excitations. Colour plots online.

8.3 Conclusions

Using the vibration controller, it was proved that it can substitute (and even improve) the vibration excitation and so enhance the tests as such. From the comparison of the sine sweep and single sine excitation, a very good agreement of the two methods was obtained, so further on the controller with the electrodynamic shaker will be used for excitation.

The comparison of the linear and logarithmic sweep revealed that they excite the system in equal manner. Hence, if the constant frequency step is not required, a logarithmic one of around 5 oct/min can be used to save time of measurement, since it is faster than the linear one.

9 Sine sweep measurement at LU

In order to avoid a potential rocking motion, which could occur when using the small shaker B&K 4809 as excitation (as done during tests at AAU), new series of measurements were carried out at LU, involving here the use of bigger shakers as well as a vibration controller.

Thus, some of the measurements already performed thus far and presented in the previous chapter were re-done to look for improved results when involving a bigger shaker together with the vibration controller.

9.1 Fixation of the shaker

Before the tests with the MEMS accelerometers were performed, an investigation regarding the influence of the type of shaker employed and their fixation was done first. To that end, two different shakers (B&K 4808 and B&K 4507) were investigated. The shaker B&K 4808 was fixed in two ways: (i) mounted on top of a wooden plate and the latter being bolted to a metal table (Fig. 9.1b) or (ii) directly bolted to a heavy metal table (Fig. 9.1c); whereas the B&K 4507 was only fixed by bolting it to the metal plate (Fig. 9.1d). For each shaker, different accelerometers were placed on the shaker itself as well as around, as shown in Fig. 9.1, their response being recorded when the shaker was fed with a random noise signal (except of `B&K 4808_meas2`, which was done with a sine sweep).

The FRFs for the table-shaker and wood-shaker attachment measurements are presented in Fig. 9.2. The accelerometer denoted as "Table" was always fixed to the steel table (Fig. 9.1), whereas the one denoted as "Wood" represented either the accelerometer fixed onto the wooden support (when present for the B&K 4808, Fig 9.1b) or to the base of the shaker (for later measurements, Fig. 9.1c,d). The frequency responses between the wood and table are shown in Fig. 9.3.

As presented in Fig. 9.2 and 9.3, the shaker B&K 4808 (measurements denoted as `B&K 4808_meas1` and `B&K 4808_meas2`) does not possess any significant resonance peaks within the measured bandwidth, just some noise being measured. On the other hand, the responses from the shaker B&K 4824 (denoted as `B&K 4824_meas1` and `B&K 4824_meas2` in the plots) do present some significant high frequency responses (above 500 Hz in all measurements). The latter was actually perceived when carrying out the measurements in the lab using the B&K 4824, as some high frequency noise coming from the shaker was heard. Hence, the shaker B&K 4824 was not used in order to avoid potential problems with it,

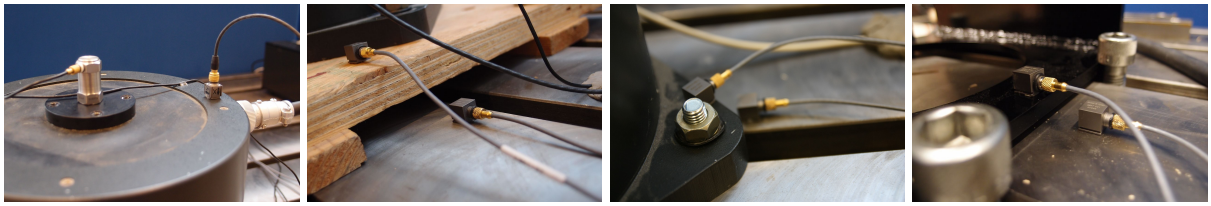

(a) (b) (c) (d)

Fig. 9.1: Location of the table, wood and shaker accelerometers: (a) top of the shaker (shaker accelerometer fixation); (b) Table and Wood accelerometers when the shaker B&K 4808 was fixed on the wooden plate; (c) Table and Wood accelerometers when the shaker B&K 4808 was fixed directly on the steel table; (d) Table and Wood accelerometers when the shaker B&K 4824 was fixed directly on the steel table.

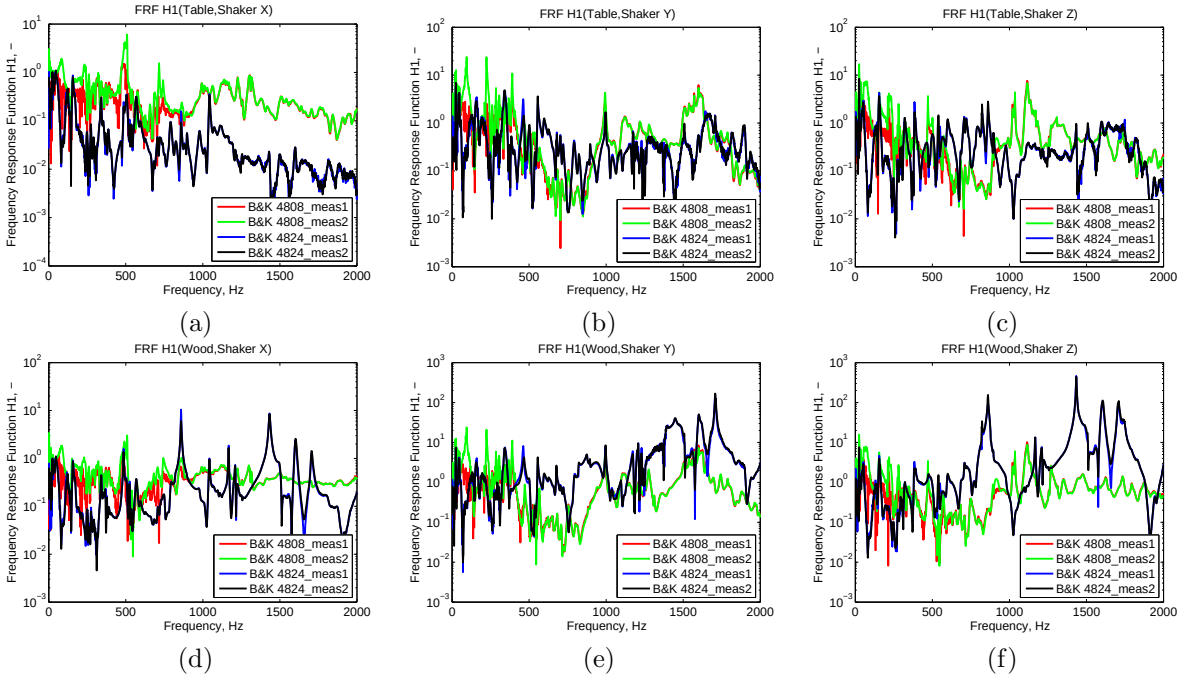

Fig. 9.2: FRFs for shaker-wood-table measurements: (a)-(c) table-shaker X,Y,Z; (d)-(f) wood-shaker X,Y,Z, for all four test measurements (the curves denoted as B&K 4808_meas1 and B&K 4808_meas2 were done using the shaker B&K 4808 and the ones named as B&K 4824_meas1 as well as B&K 4824_meas2 on the B&K 4824).

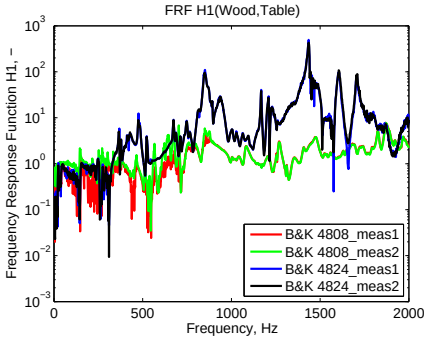

Fig. 9.3: FRFs for wood-table measurements (the curves denoted as B&K 4808_meas1 and B&K 4808_meas2 were done using the shaker B&K 4808 and the ones named as B&K 4824_meas1 as well as B&K 4824_meas2 on the B&K 4824). Colour plots online.

and thus the B&K 4808 fixed directly on the steel table (no wood plank used) was utilised in further measurements.

9.2 Sweep rate investigation

Together with the verification of the shakers' fixation, the chosen sweep rate 4 oct/min (as seen in the previous chapter, a logarithmic sweep of around 5 oct/min is recommended) was analysed if it is suitable also for the bigger shakers. The MEMS inner-chip accelerometer was fixed to the reference B&K 8305 by using wax and the FRFs recorded. A comparison with random noise as well as with a slower sweep (2 oct/min) was done, the results being presented in Fig. 9.4. Since the slower sweep rate provided exactly the same response as the one chosen 4 oct/min, a sweep rate 4 oct/min was considered as optimal for further measurements (this conclusion is coherent with the one drawn in the previous chapter, but it was considered that it should be double checked for the different shakers too). However, the results from random noise measurements presented in Fig. 9.4 do not yield to the same response as obtained for the sine sweep. Nevertheless, analysing a later set of measurements using two dual axial MEMS accelerometers (no.06 and 17), one can notice that both types of excitation are indeed equivalent (cf. Fig. 9.5). The problems depicted in Fig. 9.4 could have be caused by, for example, insufficient or wrong FFT analyser settings.

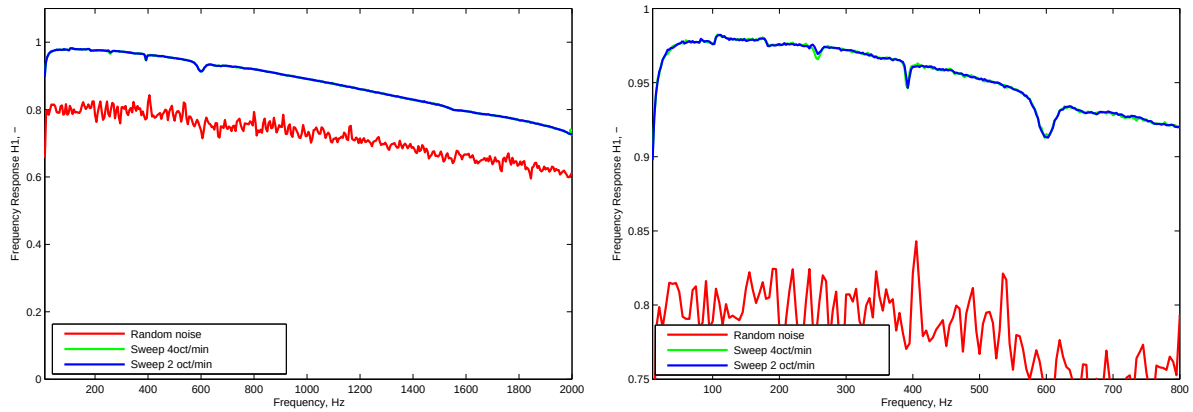

(a) (b)

Fig. 9.4: Frequency response of the sine sweep measurements with different sweep rates as well as random noise: (a) an overall view; (b) zoom to signals measured. Colour plots online.

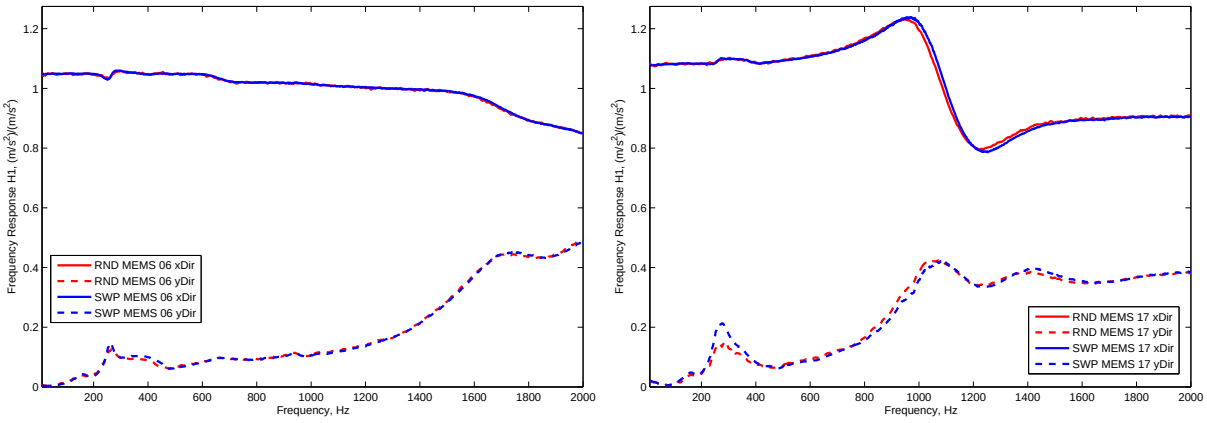

(a) (b)

Fig. 9.5: Comparison of random noise (RND) and sine sweep (SWP) excitation for dual-axial measurements on: (a) MEMS 06 and (b) MEMS 17. Colour plots online.

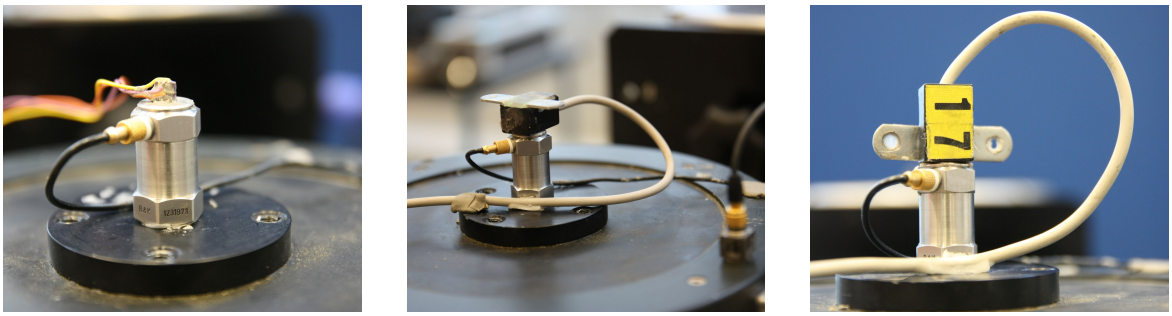

(a) (b) (c)

Fig. 9.6: Fixation of: (a) naked MEMS; (b) encapsulated MEMS, y-direction; (c) encapsulated MEMS, x-direction. The B&K 8305 is used as reference when calculating the FRFs.

9.3 Comparison of MEMS transducers

In the measurements performed in this section, five different MEMS transducers of the ones developed at LU have been used, either encapsulated or as a pure chip with thin cables (the henceforth so-called "naked MEMS", see Fig. 9.6). All of these MEMS are equipped with the chip ADXL-202 (due to the signal clipping problem present in the ADXL-203 chip mentioned in Section 7.6). The comparison of FRFs is shown in Fig. 9.7, using the accelerometer B&K 8305 as the reference for calibration. The estimated calibration constants for 159.2 Hz[1] are listed in Table 9.1. It can be seen that a quite substantial variation in calibration constants is present for the MEMS transducers tested. However, their response is relatively flat within the bandwidth up to 250 Hz, which indicates that after a correct calibration, the transducers could be potentially used for low frequency acceleration measurements as they are intended to.

To verify if the estimated calibration constants given in Table 9.1 work properly, the time data recordings previously acquired for the MEMS no.06 in its x-direction were multiplied by a reversed value of the corresponding constant listed in Tab. 9.1 (i.e. for MEMS 06 xDir by 1/1.0481), the results being plotted in Fig. 9.8. In Fig. 9.8b, it can be seen that not only the amplitude, but also a phase shift should be considered in order to achieve a precise calibration. The corresponding FRFs (before and after calibration) are compared in Fig. 9.8c, where a small difference is still present. The latter calls for further verification of the usage of the calibration constant.

Table 9.1: List of estimated calibration constants (FRF H1 at 159.2 Hz.)

	MEMS 06	MEMS 08	MEMS 17	MEMS 43	naked MEMS
xDir	1.0481	1.0069	1.0792	0.9965	0.9750
yDir	1.0190	1.0558	1.0734	0.9980	-

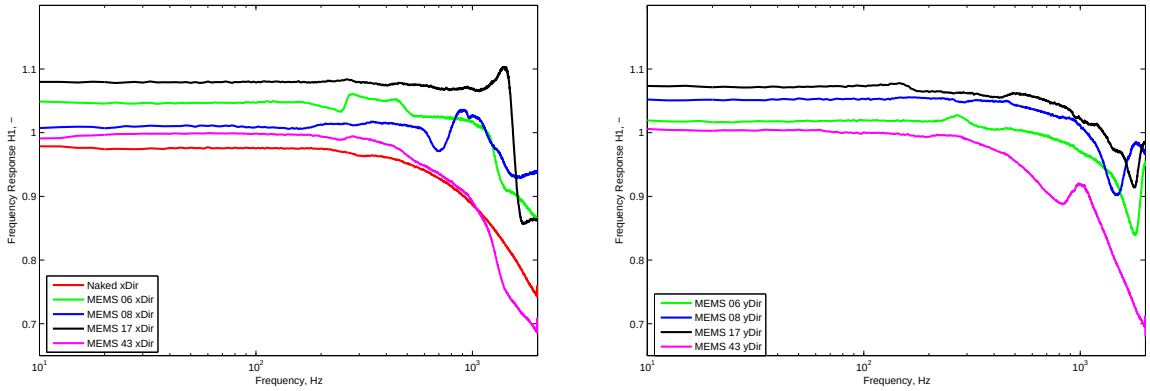

(a) (b)

Fig. 9.7: FRFs for all the MEMS transducers excited in: (a) x-direction; (b) y-direction. Colour plots online.

9.4 MEMS position onto the reference accelerometer

The relative position of the MEMS accelerometer with respect to the reference one was analysed using the SSR approach in Section 7.2.6. The offset caused by the location of the MEMS transducer could cause some transversal vibrations. Therefore, the MEMS transducer was fixed to the reference one using beeswax re-trying different positions and measured again, this time employing the bigger shaker (B&K 4808, instead of the B&K 4809 utilised in Section 7.2.6). The vibration controller was used to improve the excitation as such.

[1]The calibrator B&K 4294 provides a vibration excitation level of 10 m/s^2 at 159.2 Hz (or 1000 rad/s). To be able to compare the results from B&K 4294 with the ones gathered from the sweep calibration, the read-out at 159.2 Hz was taken.

The comparison of the FRFs for different off-set positions and cabling arrangements (shown in Fig. 9.9) is presented in Fig. 9.10. From those, it can be concluded that the off-set location is responsible for excitation of frequencies above 200 Hz. However, what is noticeable is that the response below 100 Hz seems to be unchanged, thus for low frequency measurements it can be stated that the correct alignment is not so important.

9.5 Capsule fixation onto the reference

During the previous tests, it was observed that when abundant amount of wax was used, that created a gap between the reference accelerometer and the MEMS' capsule (Fig. 9.11b). Therefore, three cases were compared in this section: a centered capsule with "normal" amount of wax (i.e. sort of an ideal condition) as well as two cases where different amounts of beeswax were used, see Fig. 9.11a. Similarly to the previous test, the low frequency content up to approximately 200 Hz seems to be unaffected. However, for frequencies above 200 Hz, both the amount of wax as well as the relative position of the MEMS on top of the reference one influences the responses significantly. All in all, the fixation during calibrations needs to be done properly.

9.6 MEMS vs. piezo accelerometer

To verify if the problem with the response at 280 Hz is only related to the MEMS transducers, or if it can be detected also using piezoelectric transducers, both types were compared. Some analysis has already been presented in Section 7.3, however the results were questionable. In the test performed

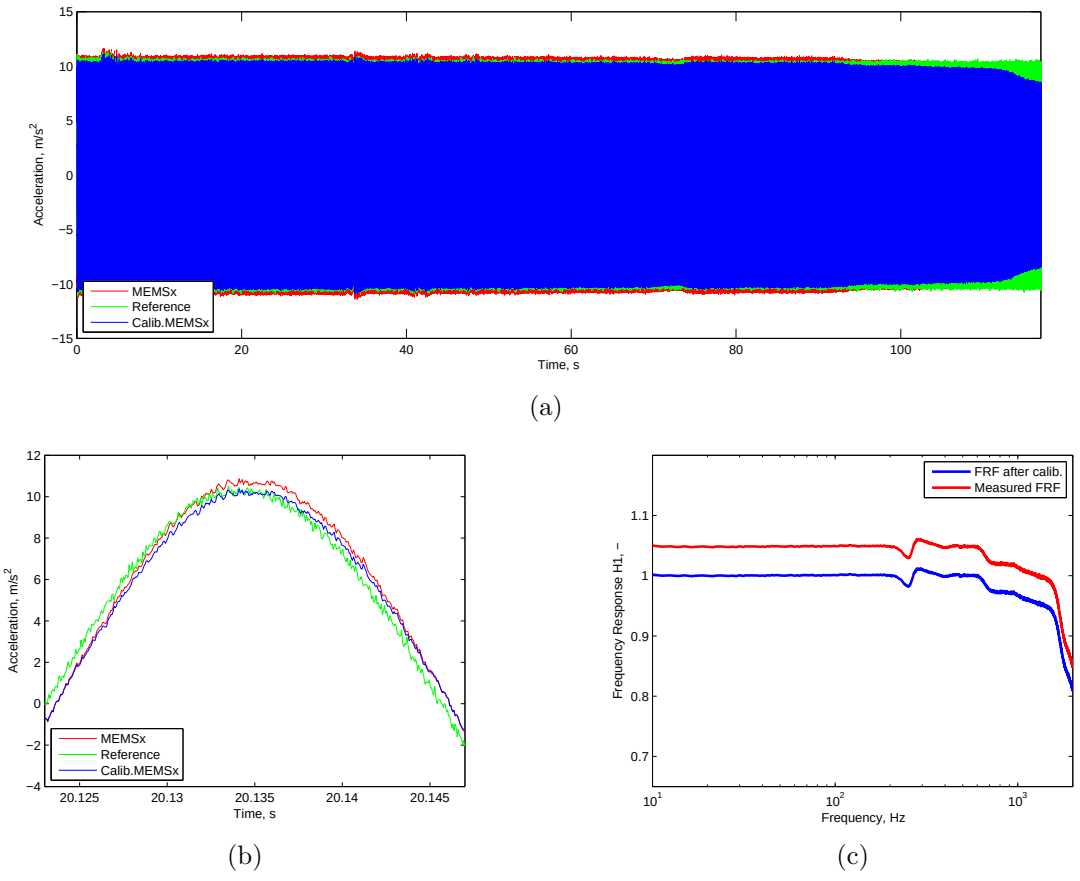

Fig. 9.8: (a) Whole time capture for MEMS 06 x-direction measurement; (b) Zoom to half-period of time capture; (c) Comparison of FRFs before and after calibration (i.e. after application of the calibration constants given in Table 9.1). Colour plots online.

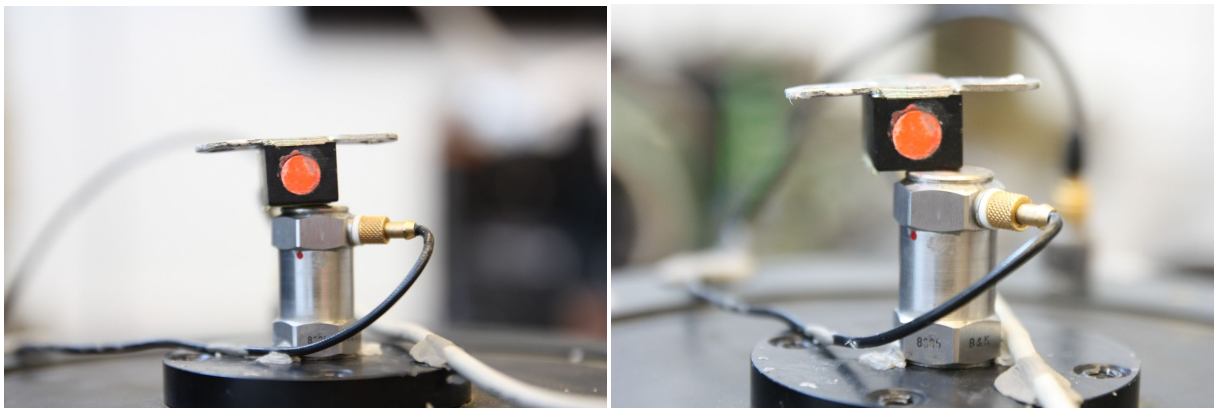

(a) (b)

Fig. 9.9: Accelerometer with MEMS chip in: (a) centered position; (b) off-set.

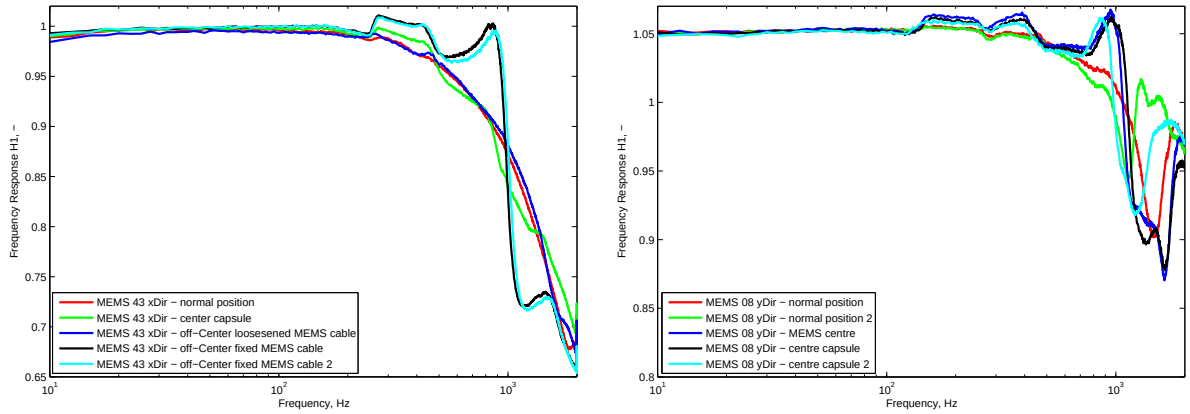

(a) (b)

Fig. 9.10: Comparison of different off-set positions of MEMS transducers for (a) x-direction measurements; (b) y-direction measurements. The normal position was the one before paying attention with a specific alignment (it was close to having capsule centered). For MEMS 43 also the cable of the MEMS transducer was either fixed to the shaker's table (as in Fig. 9.9) or not. Colour plots online.

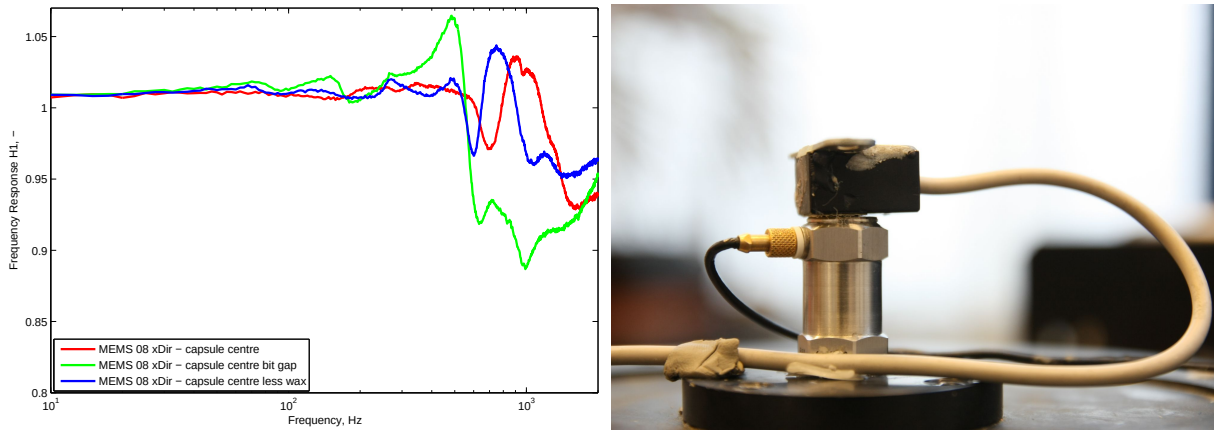

(a) (b)

Fig. 9.11: (a) Comparison of the influence of the gap and wax layer; (b) visualisation of the gap between the reference accelerometer and the MEMS capsule. Colour plots online.

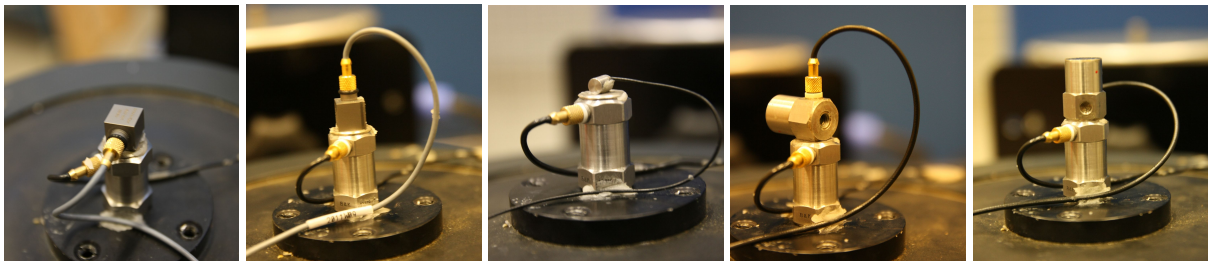

(a) (b) (c) (d) (e)

Fig. 9.12: Piezo accelerometers used: (a) B&K 4507-001, direct measurement; (b) B&K 4507 001, reverse (indirect) measurement; (c) B&K 4374, reverse (indirect) measurement; (d) B&K 4332, direct measurement; (d) B&K 4332, reverse (indirect) measurement.

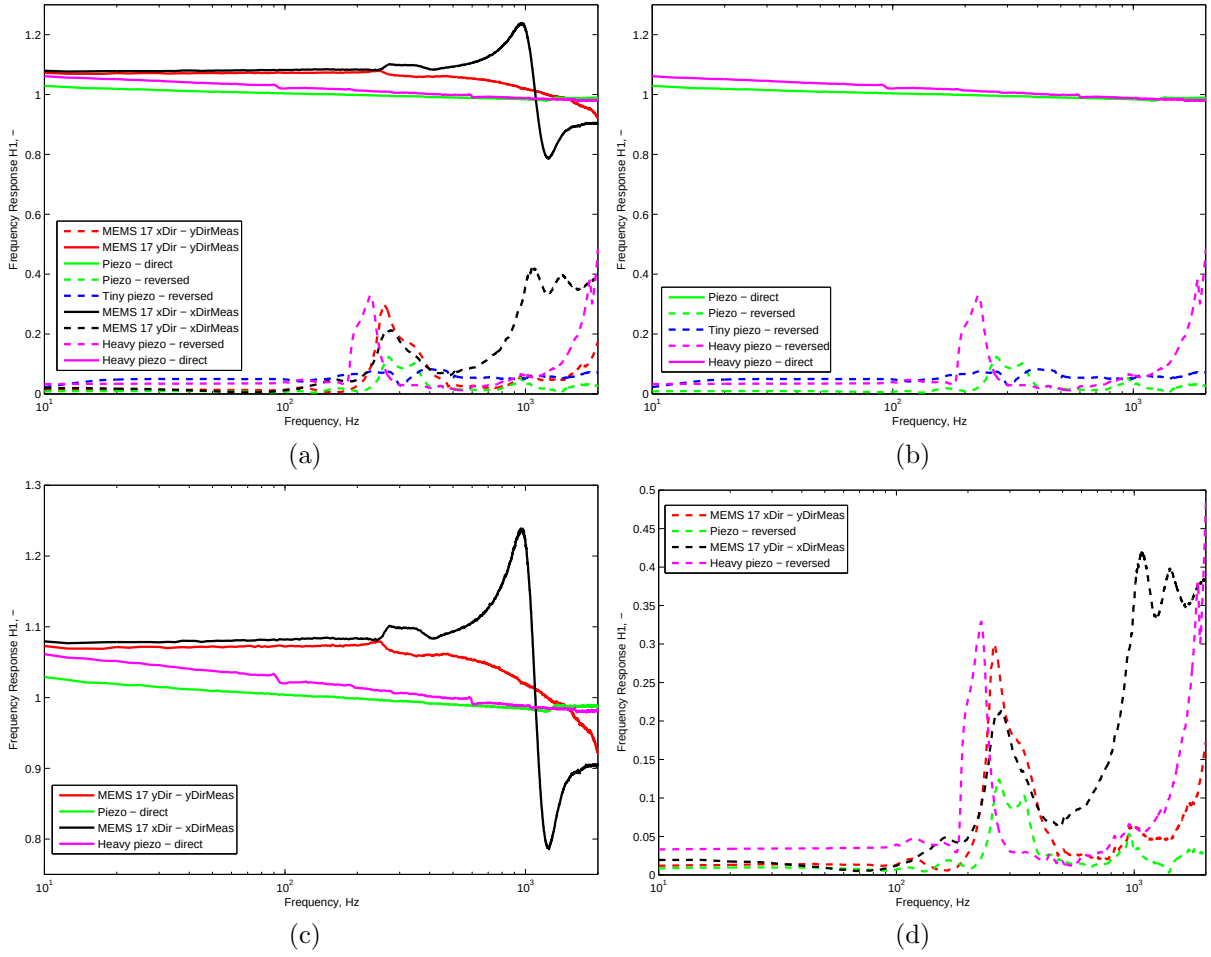

Fig. 9.13: FRFs for: (a) both piezo as well as MEMS transducers (MEMS for both measurement directions); (b) comparison for direct and reversed excitation of piezo transducers; (c) comparison of direct excitation of both piezo as well as MEMS transducers; (d) comparison of indirect (reverse) excitation of the transducers. The so-called "Tiny piezo" relates to the B&K 4374, "Piezo" denotes the B&K 4507-001 and "Heavy piezo" the B&K 4332. Colour plots online.

here, the vibration controller was hooked up to the big shaker. Furthermore, the number of piezo accelerometers tested was increased. Five piezo accelerometers arrangements shown in Fig. 9.12 were compared. The transducers B&K 4507-001 and 4374 (Fig. 9.12a-c) were fixed by means of beeswax, whereas the B&K 4332 (accelerometer in Fig. 9.12d-e) has a side thread to fix the transducer turned 90°, i.e. a stud was employed to assure a firmer fixation.

The FRFs measured are presented in Fig. 9.13. Taking only the piezo accelerometers (Fig. 9.13b), the transducers were excited also in the indirect way and some resonant response at around 250 Hz was captured. It is our belief that this could be caused by the fixation, or even by the reference transducer. A bit unclear is why the heavy piezo accelerometer B&K 4332 fixed by a stud does not provide a firm fixation and also transverse motion is detected. Thus, even when using a big shaker and a vibration controller, no definite results using piezo transducers were obtained and they should be checked further.

9.7 Two channel recordings

In the case of the two-axial MEMS accelerometers, the two signals (for each direction) are logged simultaneously. Therefore, to see how (and if) the responses are interconnected, various excitation directions (either $x-$ or $y-$direction) were applied. The responses recorded are presented in Fig. 9.14. It can be observed that some response is measured also indirectly (in the transversal direction). It is also noticeable that the frequencies excited indirectly (around 300 Hz and 1 kHz) are the frequencies where the problematic response in the directly excited direction is observed, i.e. they are linked each other. This can point out that the alignment of the chip can contribute to the response at 280 Hz.

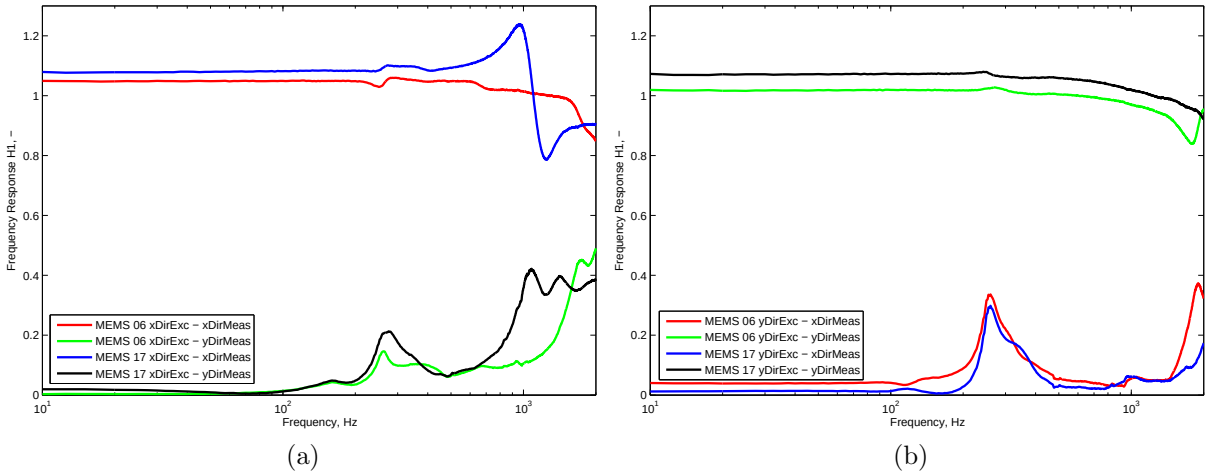

Fig. 9.14: Comparison of measurements with both channels logged for MEMS 06 and 17 excited in: (a) x-direction; (b) y-direction. Colour plots online.

9.8 Conclusions

To eliminate the possible transversal vibration which can occur on the smaller shaker, bigger shakers were tested together with the vibration controller in a way creating a more ideal excitation. Some of the previous tests were re-measured, but the cause of the resonant response at 280 Hz could still not been identified. Yet using smaller amount of wax and centering the capsule, the FRFs obtained were less distorted than the ones obtained in previous chapters (i.e. using a smaller shaker and SSR excitation method). Thus, a bigger shaker together with the vibration controller are recommended for calibration.

10 Additional characterisations

As seen in previous chapters, the chip alignment could be a potential cause of the resonant behaviour observed at 280 Hz. Thus, the last set of measurements performed with the chip set-up and thin cables (i.e. naked MEMS) focused on checking the influence of the chip alignment within the capsule. Moreover, focus was put into the measurement bandwidth and the calibration methodology as such.

10.1 Gain evaluation

Up to now, it was assumed that during the measurements performed, the noise is present at the output signal (in our case, the signal from the accelerometer to be calibrated). Thus, the FRF H1 estimate was used. However, to verify that this assumption is correct, all three types of FRFs which can be found in the B&K PULSE software to evaluate the results, namely the FRFs H1, H2 and H3, were compared in Fig. 10.1. From the figures, it can be noted that the FRFs for all three types are identical, i.e. they overlap each other, the latter implying that no influence in the results is observed regardless of

Table 10.1: Comparison of FRFs values at 159.2 Hz and corresponding gain value extracted from sweep sine measurements.

Measurement name	FRF H1	FRF H2	FRF H3	Gain (1/FRF)
Calibration using B&K 4294	-	-	-	**0.9116**
20120401piezoCalibTest1_withCalibConst_with159.2Hz	1.0019	1.0019	1.0019	0.998104≈**1**
20120401piezoCalibTest1_withNoCalibConst_with159.2Hz	1.0992	1.0992	1.0992	**0.909753**

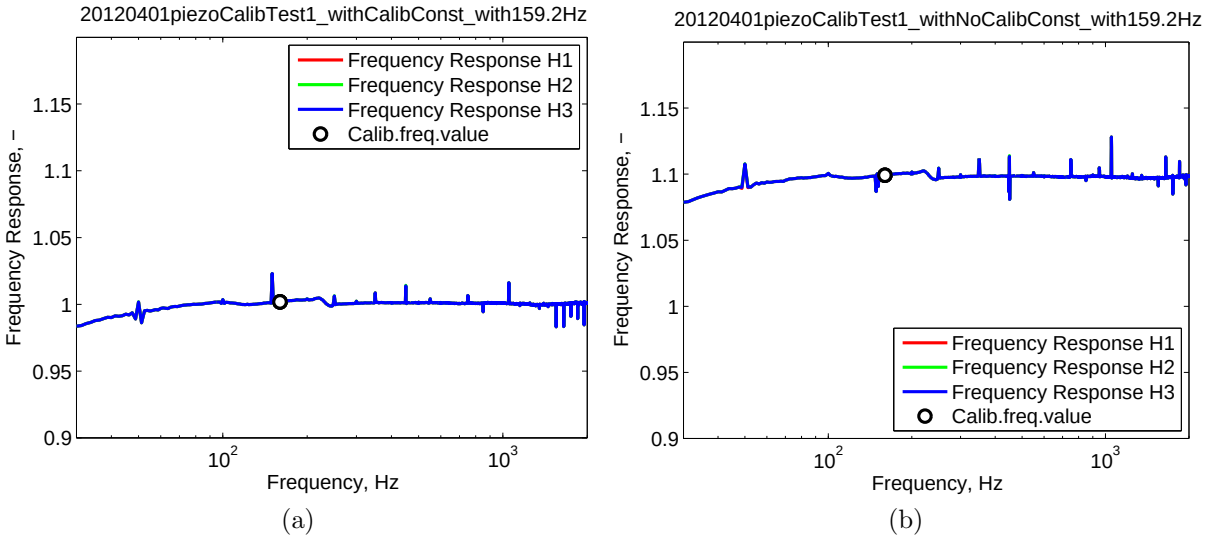

Fig. 10.1: Comparison of the frequency response functions H1, H2, H3 for the two measurements listed in Table 10.1. Colour plots online.

the function chosen for evaluation.[1]

Firstly, the calibration of the piezo transducer (for the test, a B&K 4332 was taken) was done with the B&K 4294, a gain of 0.9116 (Table 10.1) being found. Subsequently, this factor was used in PULSE to calibrate the accelerometer signal. Performing the sine-sweep measurements, the FRFs are plotted in Fig. 10.1a. Reading the value of the FRF at 159.2 Hz, the gain was found to be very close to 1 (Tab. 10.1).

The sine-sweep test were performed again, this time with no gain inserted in the PUSLE system (i.e. just the sensor sensitivity is used), the FRFs obtained being plotted in Fig. 10.1b. Reading-out the value at 159.2 Hz, the gain was found as 0.9097, which is close to the one found using the calibrator B&K 4294, i.e. close to 0.9116. Thus, the calibration procedure using a reference accelerometer and a sine-sweep control approach of the shaker seems to be sufficiently precise for the purposes under investigation here.

10.2 Tilting of the MEMS' chip using a rubber isolator

Due to the fact that the MEMS' chips are glued to the sensor's casing in a way that the alignment is not necessarily ideal, i.e. x-, y- and z-axis do not necessarily coincide with the edges of the casing, the influence of the chip's tilting (i.e. deviation from the ideal position, as shown in Fig. 10.2) was investigated here. As shown in Fig. 10.3, seven different tilting angles were assessed. Furthermore, the influence of a rubber isolator being placed between the shaker and the reference accelerometer was also analysed, which should help to avoid transversal motion on the calibration, as discussed in (Licht and Salbøl, 2010). Another parameter investigated in this set of measurements was also the influence of amount of beeswax, just to prove that the measurements carried out are not influenced by that factor. The coordinate system of the MEMS transducer is shown in Fig. 10.2. For measurements, a logarithmic sine sweep (4 oct/min) with a closed feedback control was chosen. As concluded in Chapter 8, the linear and logarithmic control strategies with the parameters used yielded to similar results and since logarithmic seeps are faster, they were used in these tests.

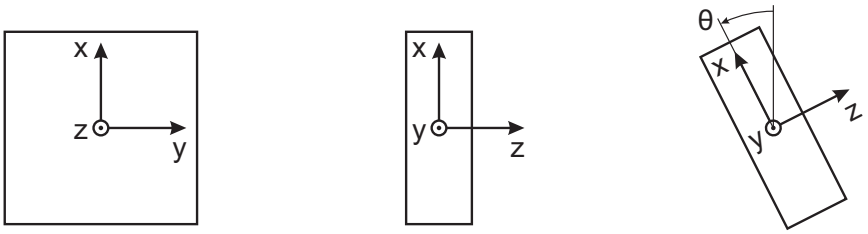

Fig. 10.2: Sketch of a naked MEMS accelerometer ADXL-202/ADXL-203. θ indicates the tilting angle.

10.2.1 Influence of tilting

As shown in Fig. 10.4, the orientation of the transducer has a significant influence on its dynamic response. Even the problematic response around 200 Hz seems to be caused by tilting the transducer. When the chip is correctly installed (i.e. at zero tilting angle), the FRF is smooth and close to 1. However, as the chip is tilted, the response lies below 1 and some local resonance around 200 Hz starts to emerge[2].

Even when comparing the responses at 159.2 Hz (i.e. the calibration frequency) for various tilting angles, one can see from Fig. 10.5 that there is some tendency, which can be properly fitted with a second order polynomial function. Thus it can be concluded, that the tilting (caused by improper alignment

[1] In Fig. 10.1 some peaks occur. The source of those peaks have not been identified, but it is assumed that combination of the sweep and single sine control strategy used could have caused it. However, at the frequency of interest (i.e. 159.2 Hz) the FRFs are smooth, i.e. the evaluation of the gain is unaffected.

[2] Note that the local resonance has shifted down from the previous value of 280 Hz to 200 Hz. This could be due to the fact that e.g. the MEMS' capsule is not present. All in all and regardless of the frequency value, the local resonance is still present and must therefore be addressed properly so as to properly calibrate the MEMS.

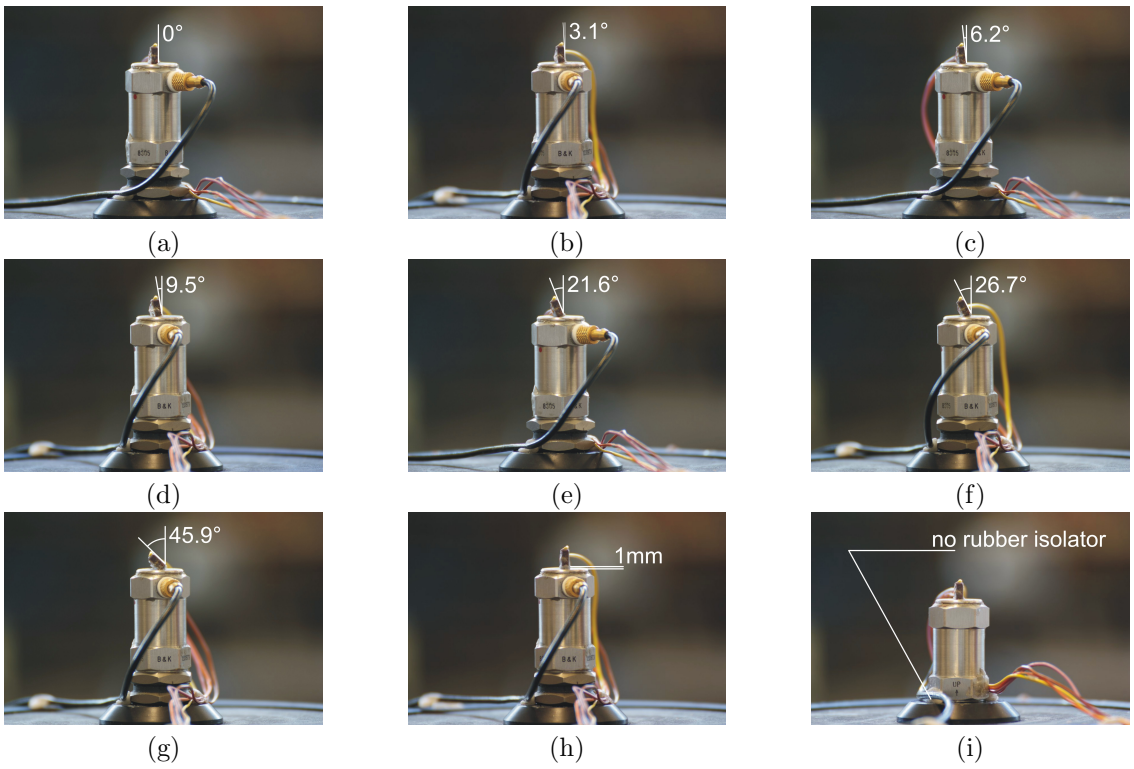

Fig. 10.3: Fixation of the naked MEMS accelerometer on a top of the reference accelerometer B&K 8305; (a) - (g) variation in tilting angle (rubber isolator present); (h) increasing the amount of beeswax (rubber isolator present); (i) removing the rubber isolator between the shaker table and reference accelerometer.

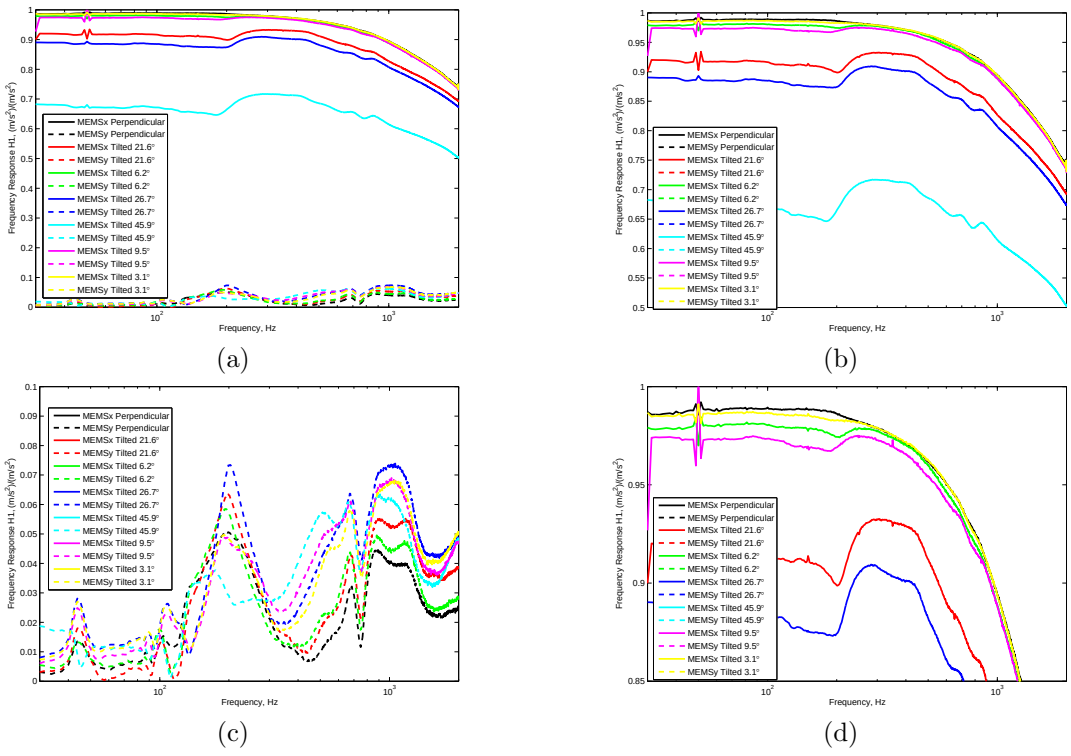

Fig. 10.4: FRFs for different tilting angles: (a) both x- and y-direction measurements; (b) zoom to x-direction measurements; (c) zoom to y-direction measurements; (d) zoom to x-direction measurements with focus on the "correct" response curve (i.e. for perpendicular, 0° tilting angle). Colour plots online.

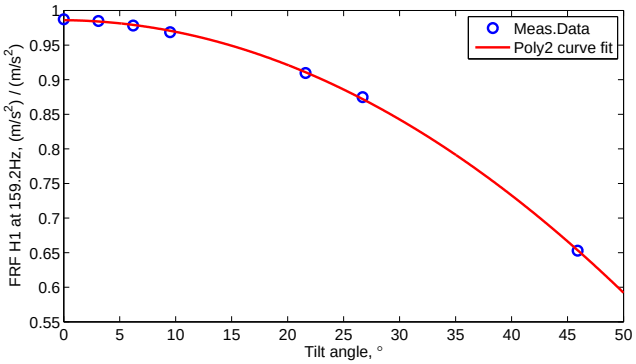

Fig. 10.5: Frequency response at 159.2 Hz (calibration frequency) for different tilting angles. The points were fitted with a second order polynomial function.

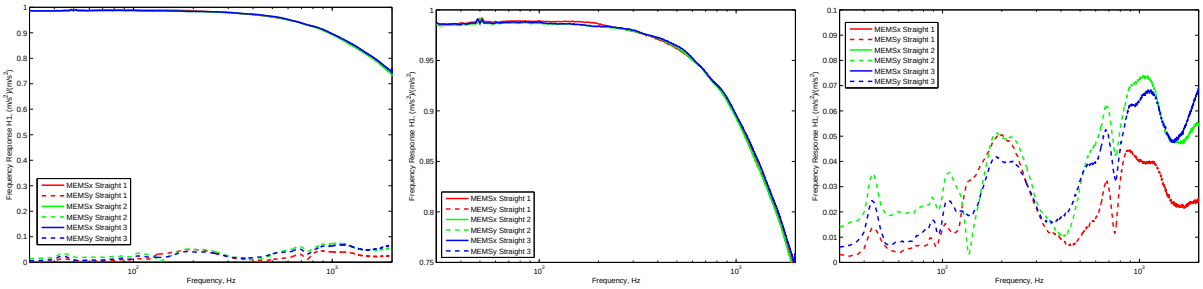

(a) (b) (c)

Fig. 10.6: Repeatability test: FRFs for the three measurements considering a straight position of MEMS accelerometer: (a) all measurements; (b) zoom to x-direction; (c) zoom to y-direction. Colour plots online.

inside of the casing) can cause the erroneous results with problematic response around 200 Hz, which was observed from the beginning of the project.

To check if the same responses could be reproduced for the straight position, the MEMS transducer was removed, re-installed and remeasured three times. As summarised in Fig. 10.6, a good reproducibility was achieved.

10.2.2 Using a rubber isolator

The influence of transversal vibration on the calibration process is discussed in (Licht and Salbøl, 2010). In there, they managed to reduce the transversal vibration of the accelerometer to be calibrated at higher frequencies (around 4 and 21 kHz) by using a mechanical filter B&K UA-0559 between the shaker and the reference accelerometer. In the investigations presented here, a different rubber isolator was found in the accelerometer set B&K 4370 and installed between the shaker and the reference accelerometer (instead of a B&K UA-0559 as they did in the previous reference), cf. Fig. 10.3.

When no isolator is used (Fig. 10.3i), some problems at 280 Hz are still present (cf. Fig. 10.7). On the other hand, using the isolator, however, the response is improved and the unwanted response around 280 Hz reduced. Hence, it seems that the use of an isolator can improve the quality of the measurements performed.

10.2.3 Influence of beeswax layer

The third parameter that was checked was the amount of beeswax applied for fixation (the wax B&K YJ-0216 was used). As presented in Fig. 10.9, the thickness of the beeswax layer does not significantly affect the FRFs. The problems around 200 Hz are not present, since the rubber isolator is used and the MEMS sensor was placed in the theoretically ideal straight position.

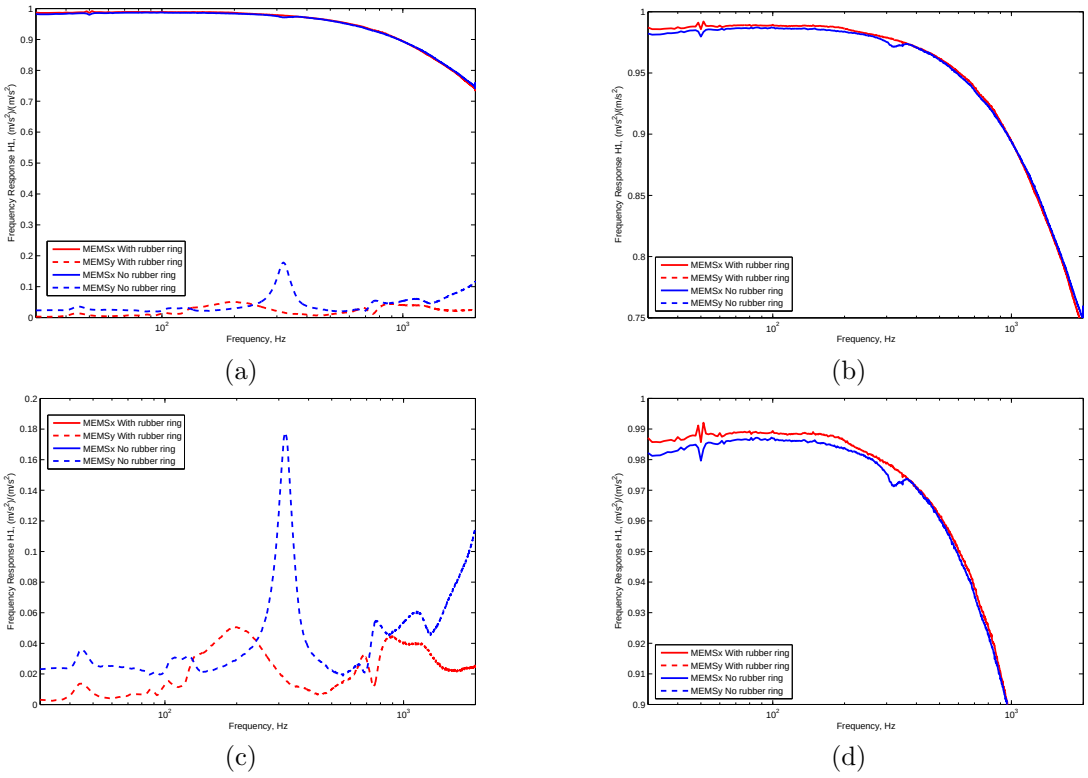

Fig. 10.7: FRFs for the cases with and without a rubber ring (Fig. 10.3a and Fig. 10.3i, respectively): (a) both x- and y-direction measurements; (b) zoom to x-direction measurements; (c) zoom to y-direction measurements; (d) zoom to x-direction measurements with focus problem on the non-smooth part of the curve around 200 Hz. Colour plots online.

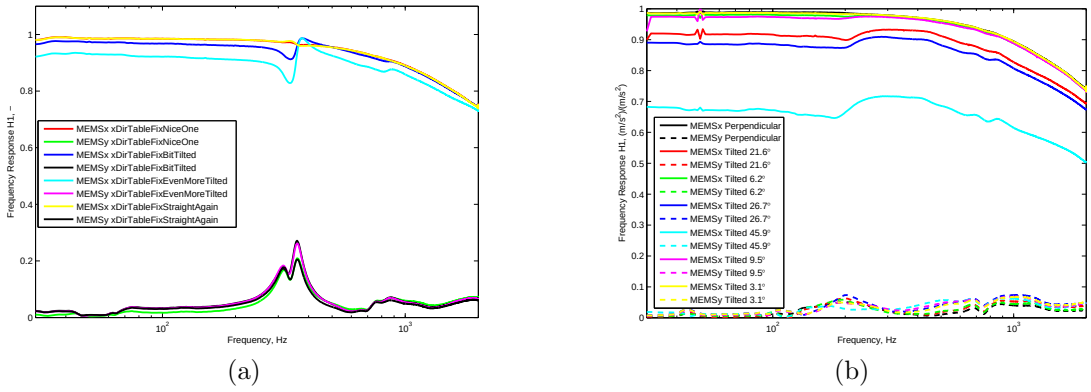

Fig. 10.8: FRFs for different tilting angles: (a) old measurements with no rubber isolator (Darula, 2013); (b) measurements with the rubber isolator used. Colour plots online.

10.3 Bandwidth settings by a capacitance value

According to the MEMS accelerometers' data sheets (Analog Devices, 2010), the bandwidth of the transducer can be controlled by the value of the capacitance used, where the limit values are 0.002 μF and 10 μF. Its exact value is then calculated from (Analog Devices, 2010):

$$F_{-3dB} = \frac{5\ \mu F}{C_{(X,Y)}} = \frac{1}{2\pi(32\ \text{k}\Omega) \times C_{(X,Y)}} \tag{10.1}$$

which leads to bandwidths (at -3 dB) from 0.5 Hz to 2.5 kHz.

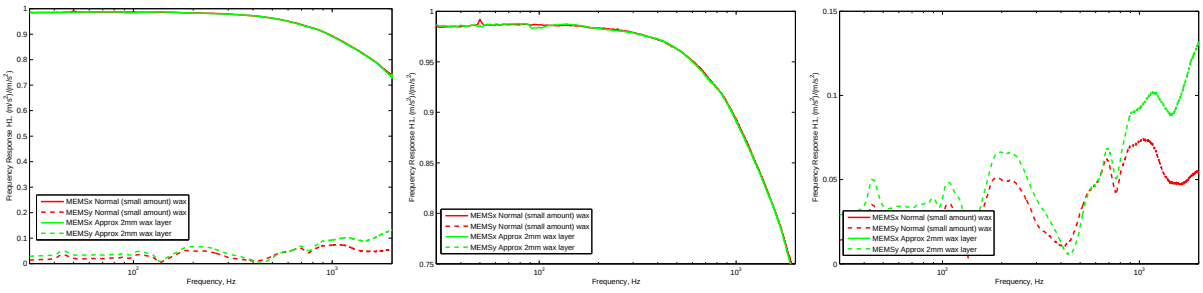

(a) (b) (c)

Fig. 10.9: FRF for the straight position of the MEMS accelerometer with "normal" (i.e. small amount) of wax layer (Fig. 10.3a) and approximately 2 mm layer wax (Fig. 10.3h): (a) all measurements; (b) zoom to x-direction; (c) zoom to y-direction. Colour plots online.

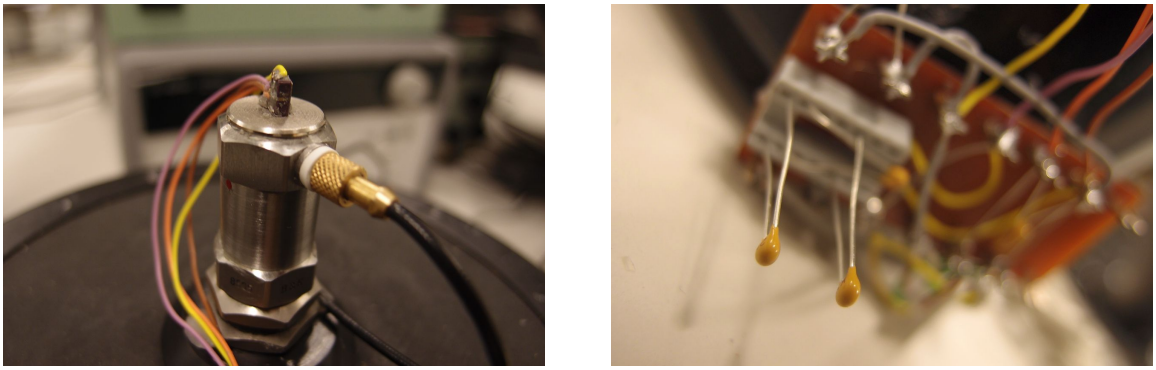

(a) (b)

Fig. 10.10: (a) A naked MEMS fixed to the reference accelerometer by means of beeswax. The reference accelerometer is isolated from the shaker using a rubber element to improve the performance at 300 Hz. (b) fixation of two additional capacitors into the compartment (all together three capacitors C_x were used at that measurement).

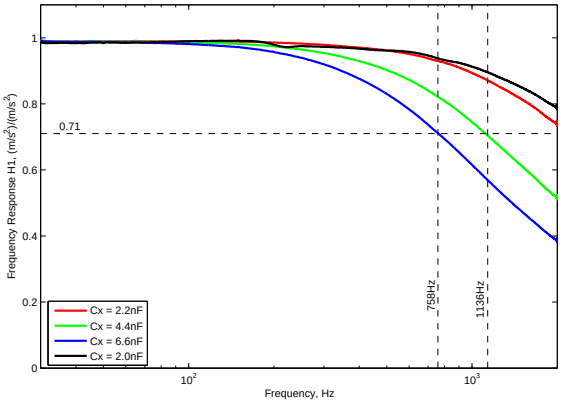

Fig. 10.11: FRFs for different values of the capacitance C_x. Colour plots online.

Table 10.2: Bandwidth values for different capacitances.

Capacitance C_x	Bandwidth
2.0 nF	2500 Hz
2.2 nF	2273 Hz
4.4 nF	1136 Hz
6.6 nF	758 Hz

To verify the latter, the MEMS transducer was fitted to the reference one (the B&K 8305) as straight as possible (following Fig. 10.10a) and equipped with a board, where the capacitance can be varied (Fig. 10.10b). The FRFs for different values of the capacitance used and their corresponding bandwidths marked are shown in Fig. 10.11, the resultant upper limits being listed in Table 10.2. As expected from Eq.(10.1), by increasing the capacitance C_x, the bandwidth is reduced. Thus, the choice of capacitance

can be effectively used to optimise the performance of the transducers. Moreover, it needs to be kept in mind that the capacitance affects the calibration curve (FRF) to an extent where the transducer can be just used within the limits governed by the $C_{(X,Y)}$ value.

On the other hand, as can be noticed from the Fig. 10.11, the change of capacitance does not influence the response in low frequencies. Thus, if that region is of interest (as it is the case for us), the choice of capacitance is not so important.

10.4 Sweep parameters

The sine sweep was assessed in Chapter 8, i.e. when the vibration controller was firstly used for tests. However, and ultimately aiming at sorting out the problem with the response around 280 Hz to obtain the correct smooth calibration curves using a naked MEMS; the potential influence of the sweep settings on the calibration results was re-tested.

Different sine-sweep types (linear and logarithmic) are here assessed comparing the autospectra measured (Fig. 10.12-10.13). As seen in Fig. 10.12, the FRFs obtained are independent of the type of sine sweep used. Furthermore, as can also be seen in Fig. 10.13, different sweep rates excite the transducer at different levels in the frequency domain. However, using the vibration controller implies that the level of the acceleration applied during the sweep is preserved constant (Fig. 10.14), i.e. 10 m/s^2 (except of some deviations caused by a sudden change of the system). Also, as proved in the previous section (and as it is shown in Fig. 8.3 as well as in Fig. 10.12), using the FRF, the frequency responses are similar. The latter means that within the levels analysed, the MEMS transducers can be treated as linear, i.e. independent of the excitation.

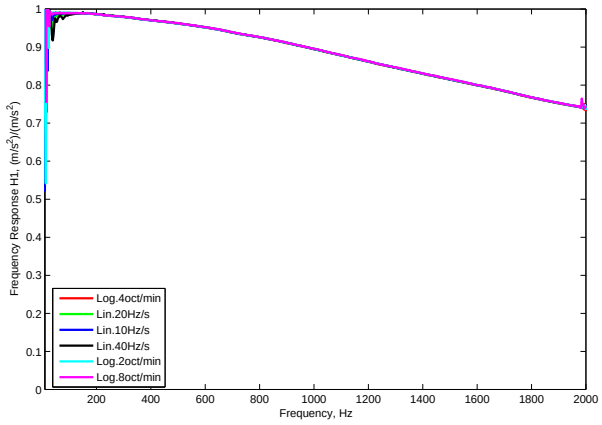

Fig. 10.12: FRFs for all types of sine sweeps compared. Colour plots online.

10.5 Conclusions

In the final set of measurements, only the inner chip with thin cables was investigated so as to eliminate the influence of the thick cable used with capsules. The assessment of the chip tilting revealed that a correct (straight) arrangement leads to the smooth FRFs, i.e. the problematic response around 280 Hz is not present. Thus, it is recommended to align the chip in the capsule as straight as possible.

Also it was observed that a rubber isolator between the reference accelerometer and the shaker helps to suppress the unwanted response around 280 Hz as well. Therefore it should be used also in further calibrations.

In this chapter, the influence of the capacitors controlling the measurement bandwidth was also assessed, the results obtained coinciding with the manufacturer's data provided. Moreover, it was shown that any of the capacitors used in the test influenced the low frequency response.

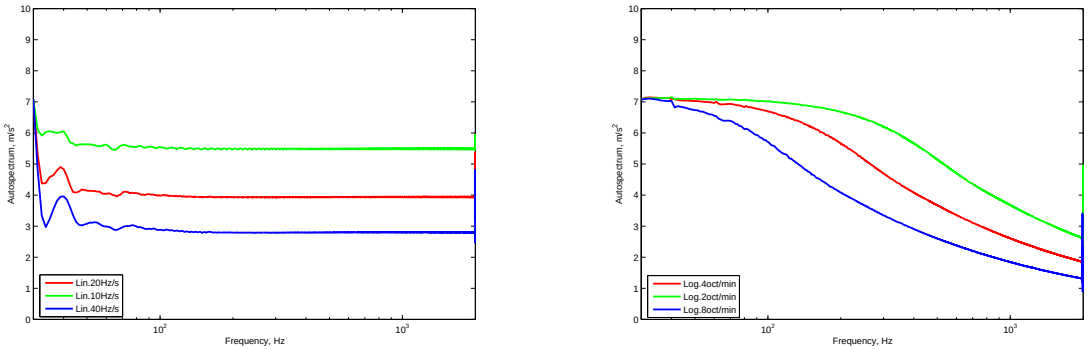

(a) (b)

Fig. 10.13: Measured autospectra for different sine sweeps (a) linear; (b) logarithmic. Colour plots online.

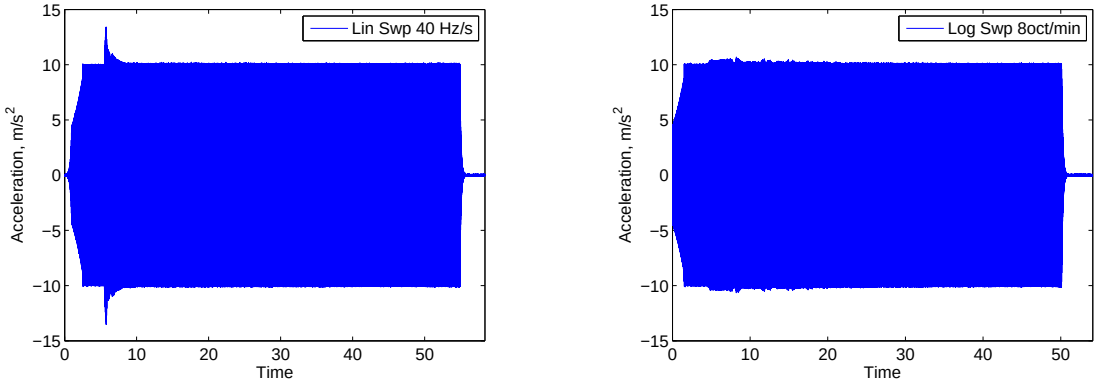

(a) (b)

Fig. 10.14: Time captures (a) linear; (b) logarithmic.

11 Conclusions

The report summarises the construction as well as calibration of MEMS-based vibration transducers. The MEMS chips are placed within the capsules together with the corresponding PCBs, capacitors and operational amplifiers. The sensitivity of the constructed transducers was assumed using the chip manufacturers' data-sheets, but also a more precise method was searched. More specifically, the latter was investigated through performing back-to-back calibration tests, using the transducer B&K 8305 as reference and several electrodynamic shakers. Firstly, a set of simple tests (using the MTS machine, and an open-loop shaker set-up) proved the feasibility of the method. Later on, using the SSR license, the excitation was more idealised (constant in the frequency domain). However, an unwanted response of the MEMS transducers around 280 Hz was observed. One of the ways to identify the problem was to substitute the SSR license with a proper feedback loop control and so to idealise the excitation even more. However, it did not solve the problems with the unwanted resonant responses. With further series of test and changing the elements in the measurement chain, it was finally found, using a set-up with a naked MEMS (i.e. no casing involved), that the alignment of the inner-chip needs to be set properly, since it strongly affects the sensitivity of the transducers. Moreover, the cables should not be too stiff to avoid transverse motion of the casing.

It was also found that the MTS method can potentially be used, since the FRFs are constant in the lower frequency region. However, it is too time consuming due to the calibration procedure being based on single frequencies, and also because of the need of performing filtering after the signals are acquired, due to the noise present. Furthermore, it can only be used (due to MTS limitations) up to 50 Hz, and the plate the accelerometers are attached to must be analysed dynamically prior to the calibration so as to avoid excitation of its modes of vibration within the frequency range analysed.

11.1 Guidelines for development of MEMS accelerometers

All in all, it was also shown that the MEMS accelerometers developed are suitable for the applications dealt with in our research (i.e. vibrations of small amplitude and up to approximately 300 Hz). This will enable acquisition of rich data as input for calibration and development of vibroacoustic computer prediction tools of wooden buildings.

However, for the accelerometers to be reliable and accurate, several aspects must be kept in mind when constructing and calibrating these transducers:

1. Initially and during their construction and mounting, special attention must be paid to the following aspects:
   - When introducing and assuring the chip into the casing, if a misalignment of the chip respect to the edges takes place, non-smooth FRFs (i.e. resonant behaviours) in the frequency range of interest for us could occur. The mounting should, hence, be as straight as possible.
   - The cables of the accelerometers should be compliant enough not to cause transversal motion of the accelerometers, which could lead to erroneous readings.
   - The MEMS chip ADXL-203 should be used with care (i.e. with lower excitation levels), due to possible signal clipping taking place. It is desired, hence, to use the ADXL-202, with lower sensitivity, to avoid those problems. If higher sensitivity is required for the problem at hand, saturation issues of the ADXL-203 should be addressed thoroughly beforehand.
2. Calibration using the MTS machine, despite of it being accurate, should be, when possible, avoided, since no calibration above 50 Hz is possible.

3. A back-to-back calibration method proved to be accurate and fairly simple to perform calibrations. The following aspects were found:
    - Use of an electrodynamic shaker (the big one B&K 4808 tried being the preferred one) together with a vibration controller (proper feedback loop control) is the recommended method to be used.
    - The shaker should preferably be placed, when measuring, on the lab floor or solid object fixed to the floor. In this manner, possible rocking motion which could be present when putting the shaker, e.g. on top of a concrete block on air cushions, is avoided.
    - Regarding the shaker excitation, a logarithmic sweep could be employed when no constant frequency step is required, since it is faster. Moreover, a rate of around 5 oct/min could be used to further speed up the process, since it was proved that it yielded the same FRFs than slower rates.
    - For fixation of the MEMS accelerometer onto the reference one (B&K 8305 behaving good to that end), it is sufficient to use a beeswax for the frequencies of interest here (i.e. up to a couple of hundred Hertz).
    - Likewise, it is recommended to use a rubber isolator between the reference transducer and the shaker to reduce potential small transversal vibrations.

The report presents the results obtained during the course of the project. However there are still fields of potential continuation, e.g.:

- Long-term stability with respect to calibration.
- Compensation of the misalignment of the chip inside of the capsule (to be able to use current transducers with some possible inherent misalignments).
- Automation or further simplification and speeding-up of the calibration procedure.

Bibliography

Analog Devices (2000). *Low-Cost ± 2g Dual-Axis Accelerometer with Duty Cycle Output.* Norwood, USA: Analog Devices.

Analog Devices (2010). *Precision ± 1.7g Single-/Dual-Axis iMEMS Accelerometer ADXL103/ADXL203.* Norwood, USA: Analog Devices.

Badri, A., J. K. Sinha, and A. Albarbar (2010). A method to calibrate the measured responses by mems accelerometers. *Strain 47*(Supplement s2), 242–257.

BIPM (2008). International vocabulary of metrology (VIM) – Basic and general concepts and associated terms.

Bishop, R. H. (2002). *The Mechatronics Handbook* (1 ed.). Boca Raton, USA: CRC Press.

Bruel & Kjær (2008). IDAe Hardware Configurations for PULSE - Types 3560-B, 3560-C, 3560-D and 3560-E. System Data. Available online: `http://www.bksv.jp/doc/bu0228.pdf` (last access: 8.12.2015).

Bruel&Kjaer (1972). *PM Vibration Exciter Type 4809. Instruction Manual.* Naerum, DK: Bruel&Kjaer.

Bruel&Kjaer (1978). *Piezoelectric Accelerometers and Vibration Preamplifiers. Theory and Application Handbook.* Naerum, DK: Bruel&Kjaer.

Bruel&Kjaer (1982). *Measuring Vibration. Primer.* Naerum, DK: Bruel&Kjaer.

Bruel&Kjaer (2015). *PULSE Electroacoustics Type 7907-S1. PULSE Basic Electroacoustics Type 7797. Product data.* Naerum, DK: Bruel&Kjaer.

Carver, R. and M. Looney (2008). Calibrate accelerometers for industrial apps. *EE Times-Asia March 16-31*, 1–4.

Darula, R. (2013). Mems calibration - check influence of tilting. report from measurements (18.3.2013). Aalborg, DK: DMME AAU.

Hopkins, C. (2007). *Sound Insulation.* Oxford, UK: Elsevier / Butterworth-Heinemann.

IEEE (1999). IEEE 1293-1998: IEEE Standard Specification Format Guide and Test Procedure for Linear, Single-Axis, Non-gyroscopic Accelerometers. The Institute of Electrical and Electronics Engineers, New York, USA. i.

IEEE (2008). IEEE 1293-1998/Cor 1-2008: IEEE Standard Specification Format Guide and Test Procedure for Linear, Single-Axis, Nongyroscopic Accelerometers Corrigendum 1: Changes to Annex K and Annex L. (Corrigendum to IEEE 1293-1998). The Institute of Electrical and Electronics Engineers, New York, USA. C1 -3.

ISO (1998). ISO 5348: Mechanical vibration and shock – Mechanical mounting of accelerometers. International Organization for Standardisation, Geneva, CH.

ISO (2003). ISO 16063-21: Methods for the calibration of vibration and shock transducers - part 21: Vibration calibration by comparison to a reference transducer. International Organization for Standardisation, Geneva, CH.

ISO (2013a). ISO 717-1: Acoustics – Rating of sound insulation in buildings and of building elements – Part 1: Airborne sound insulation. International Organization for Standardisation, Geneva, CH.

ISO (2013b). ISO 717-2: Acoustics – Rating of sound insulation in buildings and of building elements – Part 2: Impact sound insulation. International Organization for Standardisation, Geneva, CH.

Larsen, J.B. (2011). Personal communication, 2011.

Licht, T. and S. Salbøl (2010). ISO 16063-11: Uncertainities in Primary Vibration Calibration by laser Interferometry - Reference Planes and Transverse Motion. Bruel & Kjær Technical Review, No.1/2010. Naerum, DK: Bruel&Kjaer.

Ljunggren, F., C. Simmons, and K. Hagberg (2014). Correlation between sound insulation and occupants perception – proposal of alternative single number rating of impact sound. *Applied Acoustics 85*, 57 – 68.

Lyshevski, S. (2002). *MEMS and NEMS – Systems, Devices, and Structures.* CRC Press LLC.

MathWorks (2010). Matlab r2010b help.

MTS (2006). *MTS 810 & 858 Material Testing Systems.* Eden Prairie, USA: MTS SYSTEMS CORPORATION.

Negreira, J. (2013). *Vibrations in Lightweight Buildings – Perception and Prediction.* Department of Construction Sciences, Division of Engineering Acoustics, Lund University, Sweden.

Plechinger, P.L. (2011). Personal communication, november 2011.

Quach, Q. (2011). Matlab - windowing part 1. `http://blinkdagger.com/matlab/matlab-windowing-part-1/` (last access: 13.7.2011).

Randall, R. B. (2011). *Vibration-based Condition Monitoring: Industrial, Aerospace and Automotive Applications* (1 ed.). Chichester, UK: Wiley.

Sørensen, T. (2011). Personal communication.

Spectrum (2015). *SBench 6.2.12 Data Acquisition Software for Windows and Linux.* Spectrum Systementwicklung Microelectronic GmbH. Manual. Available online: `http://spectrum-instrumentation.com/sites/default/files/download/sbench6_manual_english.pdf` (last access: 10.12.2015).

Stein, G., R. Chmurny, and V. Rosik (2007). Measurement and analysis of low frequency vibration. *Measurement Science Review 7.3*(3), 47 – 50.

A
Laboratory journals

To track the whole process of the measurements reported on this technical publication, solving the partial problems and verifying how some apparatus/parameters influenced the responses of the MEMS sensors, a number of small reports (laboratory journals) were prepared, their being listed below together with a small description of their content.

Each laboratory journal related to the measurements contains a list of apparatus (with serial numbers of the items used), description of the measurement parameters envolved as well as a list of the measurements themselves, in order to be able to replicate the measurements, if ever needed.

All the journals are archived and they are available upon request at the authors.

Calibration of MEMS accelerometers (9.5.2011)
The report presents a brief literature review on MEMS calibration, lists of available apparatus which can be used for calibration and presents the preliminary measurements done at AAU on June 2nd, 2011.

MEMS Calibration (18.7.2011)
The report summarises the first results from the MEMS calibration and points out at some questionable areas, which should eventually be investigated. Calibration was executed AAU on June 29th, 2011. The additional measurements were done at AAU afterwards (1-3.7.2011).

MEMS Calibration #2 (27.7.2011)
The report presents a quick analysis of results done on the MEMS set-up until July 27th, 2011. The main attention is paid on eliminating the non-ideal behaviour of the MEMS accelerometer's response at around 280 Hz observed during the previous measurements.

MEMS Calibration #3 (2.8.2011)
The report summarises a comparison of the two shakers available at AAU and discusses linearity of the MEMS accelerometers as well as the reproducibility of the measurements performed.

MEMS Calibration #4 (30.8.2011)
Comparison of two methods; an SSR (steady state response) and sweep (rate 4 Hz/s) are presented and discussed. The reference accelerometer B&K 8503 and piezo accelerometer B&K 4331 with the pre-amplifier B&K 2635, borrowed from LU were used in the test.

Sine Sweep and Ripples (28.9.2011)
The report summarises a quick discussion on the setting of the sweep function in B&K PULSE LabShop. Especially focus is paid on ripple phenomena observed when the shaker was run immediately after one run was terminated.

Add-on Measurements / Calibrations (23.2.2012)
A discussion on add-on measurements for the MEMS calibration is summarised.

MEMS calibration with Bruel&Kjaer PULSE and Bruel&Kjaer VC-LAN (22.1.2013)
Test the MEMS calibration using a constant amplitude at sine sweep excitation. To that end, the shaker control strategy using the vibration controller B&K VC-LAN. To make more advance signal processing of the transducer signals, they are recorded and processed in B&K PULSE (LabShop v17 was used).

MEMS calibration – Big shaker (7.3.2013)
The aim of the measurements was to do additional MEMS calibration using a bigger shaker(s) and thus avoid possible rocking motion of the shaker's table. During the measurements, also piezo accelerometers were used in order to compare directly the responses of the MEMS and piezos.

MEMS calibration – Check influence of tilting (18.3.2013)
The aim of the quick check was to find if also "naked" MEMS accelerometers have a response in the non-directly excited direction with a peak around 300 Hz. It was observed that the tilting around the non-excited axis introduces some non-smooth behaviour.

MEMS calibration – Sine Sweep Test (24.3.2013)
The aim of the measurements performed was to compare different sine sweep rates as well as single frequency excitation to prove that the chosen 4 oct/min is safe and that no transients occur.

MEMS calibration – Check the Gain evaluation (1.4.2013)
The main aim was to check if the FRF H1 can be used to extract the calibration constant at 159.2 Hz. The "real" calibration in PULSE LabShop is done first, and then also using a controller sweep and a pure sine excitation to double check the procedure. Moreover, three different FRF estimates (H1, H2 and H3) are compared.

MEMS calibration – Check the influence of tilting and modify the shaker fixation (13.4.2013)
The main purpose of the measurements carried out was to see the behaviour of the FRF curves for different tilting angles of the naked MEMS accelerometer. Furthermore, a rubber isolator was used to improve contact between the shaker and the reference accelerometer, similarly as it was done in B&K Tech.Rev. (Licht and Salbøl, 2010) using mechanical filters (B&K UA-0559). A comparison of the case with and without the isolator is provided as well.

MEMS calibration – Bandwidth and Sine Sweep Test (17.4.2013)
Measurements performed so as to test the capacitance C_X (used to set the bandwidth of the x-direction measured signal). Also, the linear and logarithmic sweep rates are compared from autospectra plots.

B

MATLAB GUI for data comparison

To speed up comparisons of the measured data and easily generate figures for the reports, a graphical user interface (GUI) function was created in MATLAB. Its main window is shown in Fig. B.1.

B.1 Features

- The main feature of the GUI is to load data and to sort them into a table on the left. There is an option to load the "MAT data" (stored under `\auxFiles\MathDataFile.mat`), or the PULSE ASCII files stored under `\data`.
- To identify the measurement number, additional information is loaded from the PULSE ASCII file and listed into the table (using the bottom slider under the table, additional information can be accessed).
- From the left table, the measurements can be plotted and compared with one another.
- To tweak the legend, it is allowed to change the name of the measurement, by just clicking the field in the table. The same holds for the transducer, channel name as well as for the type of analyser.
- In the bottom left, it is allowed to choose what will be listed in the legend (transducer, channel name, analyser and/or name of the measurement).
- Also the plot ranges and plot scales (linear/logarithmic) can be adjusted to get the best visualisation.
- If a specific data are to be plotted all, the "plot all" box can be ticked.
- Choosing the top menu `File` one can reset the plots (un-tick all ticked plots), re-load data (re-set all the names), or close the GUI.
- Choosing the top menu `Evaluate->Calib.constant`, a window with calibration constants evaluated at 159.2 Hz for all chosen (plotted) measurements appears (Fig. B.1b).
- Choosing the top menu `Export->Export Fig`, the window for figure export appears (Fig. B.1c).

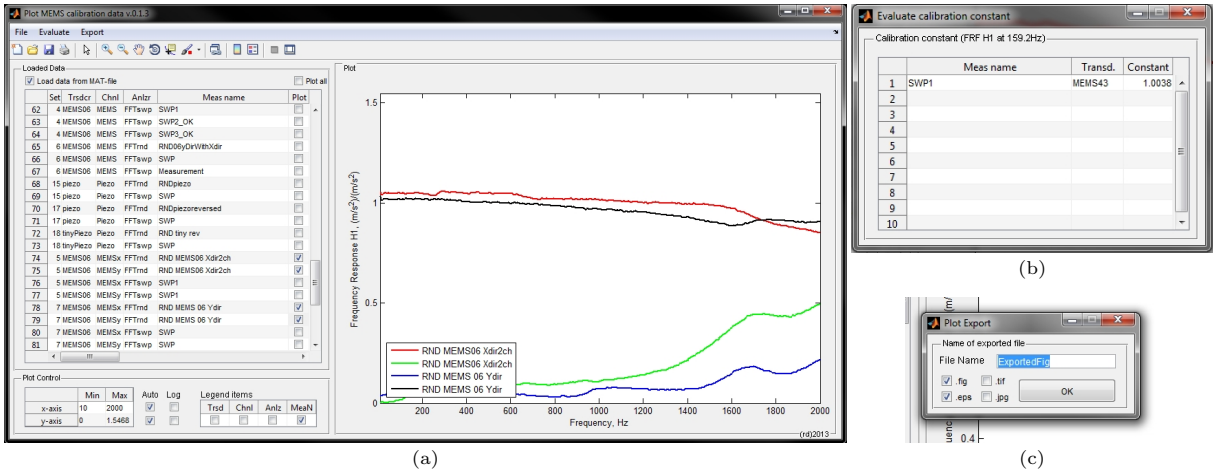

(a) (b) (c)

Fig. B.1: MATLAB GUI v.0.1.3: (a) overview on the main window; (b) window with evaluation of the calibration constant; (c) export window.

One can choose what type is to be saved (.fig, .eps, .jpg, .tif) and the name can be changed as well. The figures are saved by default to the folder `\figs`.

B.2 Restrictions

- Due to the loading of the PULSE ASCII file and using the B&K file `GetPulseAsciiFile.dll` to process them, the 32-bit version of MATLAB needs to be used. At this stage, no .uff file support has been added.
- No double y-axis feature has been implemented yet. The latter means that only one physical quantity can be compared, either FRFs or Autospectra, not FRF with Autospectra.
- No size of the exported plot can be defined yet, just a fixed default one is used.